Master's thesis

NTNU
Norwegian University of Science and Technology
Faculty of Natural Sciences
Department of Materials Science and Engineering

Fredrik Oftedal Forr

# The effect of bird droppings on the corrosion of structural materials used in offshore applications

Master's thesis in Materials Science and Engineering
Supervisor: Jan Halvor Nordlien
Co-supervisor: Andreas Erbe & Håvard Wilson
June 2022

NTNU
Norwegian University of
Science and Technology

Fredrik Oftedal Forr

# The effect of bird droppings on the corrosion of structural materials used in offshore applications

Master's thesis in Materials Science and Engineering
Supervisor: Jan Halvor Nordlien
Co-supervisor: Andreas Erbe & Håvard Wilson
June 2022

Norwegian University of Science and Technology
Faculty of Natural Sciences
Department of Materials Science and Engineering

NTNU
Norwegian University of
Science and Technology

# Preface

This master's thesis is for the completion of a master's degree in Material Science and Engineering at the Department of Materials Science and Engineering (IMA) at the Norwegian University of Science and Technology (NTNU) in Trondheim, Norway.

The initiators of the thesis was Shell Norway and MainTech AS.

I would like to thank Jan Halvor Norlien as supervisor together with Andreas Erbe and Håvard Wilson as co-supervisors for guidance and discussions throughout the semester when needed.

I would also thank Anita Storsve and Marthe Folstad for their great help regarding the laboratory work, and for helping out with the ordering of chemicals and sample preparation. I would also thank various persons that have been in the corrosion lab that helped with various questions.

A special appreciation is for Ørjan Ellingsen and Vegard Schøyen at Shell for discussing the goal of the experiments and for finding sample material. Kurt Ekrem and Darko Petkovic at Randaberg Coating AS deserve attention for providing sample materials and coating these with thermally sprayed aluminium. Thanks to Espen Strandheim at Aker Solutions ASA, for the discussion around the issue.

My family and friends have my appreciation for giving motivation and support in various ways throughout the semester.

# Abstract

The current trend in the oil and gas industry is the desire for building automated platforms that are either "normally unmanned" or "unmanned". This introduces an extreme demand for the design, which must be able to perform for long periods without inspections and maintenance. These platforms are planned to be operational for up to 40 years. The design and material choice must be top-notch for all aspects of the installation to be able to achieve this. In addition, the absence of personnel substantiates more bird life on the platforms.

Others have investigated mitigation and deterrent methods for bird life on platforms, along with mapping of how selected birds move around in the North Sea. The corrosion behaviour due to bird droppings is not studied. This is where this thesis come in, as the bird droppings' effect on corrosion for steels and aluminium is not described in the literature.

By increasing the knowledge of this issue, preventive measures could be made to increase the lifetime of unmanned platforms. To do this there has been conducted two parallel tests. The first was to expose the selected materials to a salt-spray chamber, with and without bird droppings. This has given both a visual presentation of how the bird droppings affect the corrosion of the materials, as well as mass loss measurements that give a measure of the amount of corroded metal. These samples were then analysed using FTIR and Raman spectroscopy to search for traces of substances that had adhered to the surface of the selected materials.

The same selected materials were analyzed using electrochemical experiments. Specifically polarization curves and polarization resistance. To be able to do electrochemical experiments with bird droppings on the surface, an unconventional cell setup was used. This consisted of a syringe that housed the reference and counter electrode along with the electrolyte. Bird droppings could then be put into the tip of the syringe. The electrochemical experiments showed that most materials tested, benefited from the presence of bird droppings, e.g. passivation, increase in pitting potential, and decreased corrosion current density was observed changes.

# Sammendrag

Den nåværende trenden i olje- og gassindustrien er at flere aktører ønsker å bygge automatiserte plattformer som er enten normalt ubemannet, eller ubemannet. Dette gir økte krav for design, som må kunne yte for lange perioder uten hverken inspeksjoner eller vedlikehold. Disse plattformene er planlagt å kunne være operative opp til 40 år. Design og materialvalg må være fra øverste hylle, for alle deler av installasjonen for å kunne oppnå dette. I tillegg, vil fravær av personell føre til økt fugleliv på plattformene.

Andre har undersøkt begrensning og avskrekkende virkemidler for fugleliv på plattformer, sammen med kartlegging over hvordan enkelte fugler beveger seg i Nordsjøen. Korrosjonsadferden forårsaket av fugleavføring ble ikke undersøkt. Det er her denne avhandlingen kommer inn da effekten fugleavføring har på korrosjon av stål og aluminium ikke er kjent i litteraturen.

Ved å øke kunnskapen om dette temaet, kan forebyggende tiltak bli utarbeidet for å forlenge levetiden til de ubemannede plattformene. For å gjøre dette har det blitt gjennomført to parallelle tester. Den ene var å utsette utvalgte materialer for et salttåkekammer, med og uten fugleavføring. Dette gir både en visuell presentasjon av hvordan fugleavføringen påvirket korrosjonen, samt et målbart vekttap som sier hvor mye av metallet som har korrodert. Disse prøvene ble så analysert med FTIR og Raman spektroskopi for å lete etter substanser som har festet seg til overflaten av prøvene.

De samme utvalgte materialene ble testet med elektrokjemiske eksperiment. Nærmere bestemt polariserinskurver og polariseringsmotstand. For å kunne gjennomføre elektrokjemiske eksperiment med fugleavføring på overflaten, ble det brukt en ukonvensjonell metode. Denne besto av en sprøyte som inneholdte referanseelektrode og motelektrode sammen med elektrolytten. Fugleavføring kunne da bli ført inn i tuppen på sprøyten. Resultatene fra de elektrokjemiske eksperimentene sto i kontrast mot resultatene fra salttåkekammeret. Dog, verdifull informasjon om korrosjonsadferden ble oppnådd. De elektrokjemiske eksperimentene viste at mange av de testede materialene dro nytte av tilstedeværelsen av fugleavføring. For eksempel passivering, økt pitting-potensial og redusert korrosjonsstrømtetthet ble observert med fugleavføring på overflaten.

# Table of Contents

**1 Introduction** **1**

**2 Background** **2**

2.1 Bird droppings . . . . . 2

2.2 Common offshore materials . . . . . 2

2.2.1 Carbon steel . . . . . 3

2.2.2 AISI 316 . . . . . 3

2.2.3 Duplex stainless steels . . . . . 3

2.2.4 Thermally sprayed aluminium . . . . . 4

2.2.5 EN AW 6082 . . . . . 4

2.3 Corrosion mechanisms . . . . . 4

2.3.1 Pitting corrosion . . . . . 5

2.3.2 Crevice corrosion . . . . . 5

2.4 Electrochemical measurements . . . . . 6

2.4.1 Corrosion current density . . . . . 6

2.4.2 Pitting potential . . . . . 7

2.5 Vibrational spectroscopy . . . . . 7

2.5.1 Expected vibration bands . . . . . 8

**3 Materials and methods** **9**

3.1 Bird droppings . . . . . 9

3.2 Materials and apparatus . . . . . 9

3.3 Salt spray test . . . . . 10

3.3.1 Raman/FTIR analysis . . . . . 12

3.3.2 Mass loss . . . . . 12

3.4 Electrochemical experiments . . . . . 13

3.4.1 Procedure . . . . . 14

**4 Results** **16**

4.1 Salt spray test . . . . . 16

4.1.1 Pictures of exposed samples . . . 20
4.1.2 Mass loss . . . 22
4.2 FTIR and Raman Spectroscopy . . . 24
4.3 Electrochemical experiments . . . 27
4.3.1 Carbon steel . . . 27
4.3.2 AISI 316 . . . 28
4.3.3 22% Cr DSS . . . 29
4.3.4 25% Cr SDSS . . . 30
4.3.5 Thermally sprayed Aluminium . . . 31
4.3.6 EN AW 6082 . . . 32
4.3.7 Variables achieved from measurements . . . 33

**5 Discussion** **34**

5.1 Salt spray test . . . 34
5.1.1 Carbon steel . . . 34
5.1.2 AISI 316 . . . 35
5.1.3 22% Cr DSS . . . 35
5.1.4 25% Cr SDSS . . . 36
5.1.5 Thermally sprayed aluminium . . . 36
5.1.6 EN AW 6082 . . . 37
5.2 Vibrational spectroscopy . . . 38
5.2.1 FTIR spectra . . . 39
5.2.2 Raman spectra . . . 40
5.3 Electrochemical experiments . . . 40
5.3.1 Carbon steel . . . 41
5.3.2 AISI 316 . . . 42
5.3.3 22% Cr DSS . . . 42
5.3.4 25% Cr SDSS . . . 44
5.3.5 Thermally sprayed aluminium . . . 45
5.3.6 EN AW 6082 . . . 47
5.4 Summary . . . 47

5.5 Review of methods . . . . . 48
5.5.1 Review of salt-spray method . . . . . 48
5.5.2 Review of electrochemical method . . . . . 49

**6 Conclusion & further work** **52**

**A Appendix** **ii**

A.1 Spectra from FTIR spectroscopy . . . . . ii
A.2 Spectra from Raman spectroscopy . . . . . vi
A.3 Raw data for mass loss . . . . . xii
A.4 Test certificate EN AW 1050 . . . . . xiii

# List of Symbols and Abbreviations

| | |
|---|---|
| $i$ | Current density |
| $i_{corr}$ | Corrosion current density |
| $E_{corr}$ | Corrosion potential |
| $R_p$ | Polarization resistance |
| $b_a$ | Anodic Tafel slope |
| $b_c$ | Cathodic Tafel slope |
| $CR$ | Corrosion rate |
| **AISI** | American Iron and Steel Institute |
| **BD** | Bird droppings |
| **CE** | Counter electrode |
| **DSS** | Duplex stainless steel |
| **EN AW** | European standard |
| **OCP** | Open circuit potential |
| **PREN** | Pitting resistance equivalent number |
| **RE** | Reference electrode |
| **SDSS** | Super duplex stainless steel |
| **TSA** | Thermal sprayed aluminum |
| **WE** | Working electrode |

# 1 Introduction

Most people in today's society have most likely had experience with bird droppings. Either if it is hitting the bonnet of their car, or jacket, or creating a coating on the local statue. In any case, the bird droppings are unpleasant and associated with being an aggressive substance. Several studies have been done on how bird droppings affect different areas. Car paint [1][2][3], copper and bronze [4][5], and highway structures [6], are some of the areas that has been studied. Where the clear coat of the car paint was found to be degraded by the bird droppings, the copper and bronze suffered from significant chemical damage, and e.g. concrete proved to be broken down by the bird droppings. The stones used for building old churches, and other cultural heritage, are also found to be broken down by the droppings [7][8]. Hence, bird droppings can compromise the lifetime of several materials in the urban environment.

For offshore installation, a certain performance is expected for the materials that are used. It could for example be strength, toughness, weight, or ductility. But, one of the most important parameters for reducing cost is the lifetime of the materials. Thus, a long lifetime is desired for upcoming installations. The trend at the time is that the oil and gas industry will create unmanned- and normally unmanned installations, which most likely introduces a greater presence of birds on the installations [9]. Also, the ability to remove the bird droppings from the installations, e.g. water, will not be possible as there will not be any people present to do this task. Helidecks must maintain their integrity, allowing personnel to travel to and from the installations. This must then always be operative, especially in the event of an evacuation. Some of the planned platforms are not designed with a helideck, as ships are planned to be the main transport [9].

The effects of bird droppings on concrete is the only investigation done on performance materials. Thus, the effect on the various materials that are conventionally used on offshore installations is unknown. Many of the materials used are metals, which means that corrosion is the main degradation mechanism that is occurring on the installations. The purpose of this thesis was to investigate how bird droppings affect the corrosion behaviour of conventionally used materials. Selected here were carbon steel, AISI 316, duplex stainless steel, super duplex stainless steel, thermally sprayed aluminium, and EN AW 6082.

To contribute to understanding the bird droppings' effect on these materials, there has been done two parallel testing methods. One is salt-spray testing where samples were exposed with and without bird droppings in the salt-spray chamber. Following this test, the samples were examined in FTIR/Raman spectroscopy to see if there was any organic compound that could affect the corrosion behaviour on the sample surface. Ultimately, the samples were weighed before and after the salt-spray test, to determine the mass loss of the various samples. Corrosion products were also removed and samples were weighed after removing these. The other testing method was with electrochemical experiments consisting of polarization curves and polarization resistance. The goal of these experiments was to establish quantifiable results of the pitting potentials and corrosion current densities of the materials. To be able to do this, a new method was prepared which made it possible to do measurements with bird droppings on the surface of the respective material.

# 2 Background

In the following chapter, different background for the thesis will be given to better discuss the effects seen in the results.

## 2.1 Bird droppings

Bird droppings are an important variable in this study, which means a certain understanding of this is required. The composition of bird droppings is not well known, with deviations between different studies. One study state that uric acid, protein, ammonia, and nitrite make up about 20% of the seabird dropping composition [10]. Another study was conducted where bird droppings of urban pigeons proved to contain chemical elements not found for pigeons held at farms [6], concluding that the diet plays a role in bird dropping composition [11][12]. The farm-grown pigeon showed to contain C, N, O, P, Cl, S, Si, and F, which were not found in the urban pigeons to the same extent. How much of each element, and in which molecules they exist, are not described. A different study discovered that the amount of soluble salts in bird droppings from urban pigeons is 4%, where the anions present are sulfate, chloride, phosphate, fluoride, bromide, and nitrate ranging from highest concentration to lowest [8].

Guano is a word used to describe dried and solidified excrement [13]. The term is used in combination with several species, e.g. bird- and bat guano. Fresh bat excrement has proved to have a pH that is close to neutral (5.1-7.3)[14]. However, when the excrement dries and solidifies (i.e. bat guano), the pH drops to more acidic (2.7-4.1). How the effect is on bird droppings is not known, but others have assumed similar behaviour [9]. The pH of the chicken excrement used for this thesis is believed to be slightly acidic as it contains uric acid [4]. Bacterial respiration occurring in the bird droppings can produce products that lower the pH of the droppings additionally [13].

Areas where bird droppings have been studied, are largely the car industry where its effect on clear coat is found to be harmful [2][1][3]. Bird droppings is also suspected to degrade building stones [7]. The corrosion behaviour of copper and brass was also altered, were substances in the bird droppings reacted with the copper and brass to produce corrosion product not expected for atmospheric corrosion [4]. More roughness led to the conclusion that bird droppings could degrade concrete and stone [6][15].

## 2.2 Common offshore materials

The different materials used in the experiment are materials that are often used in the offshore industry. As different applications need different characteristics the materials are designed to cover different needs. Carbon steel, stainless steels, and aluminium, along with a metallic coating, thermal sprayed aluminium (TSA), will be used. Based on NORSOK standard M-001 [16], which describes the material selection of steels, the carbon steel, and 316 stainless steel is typically used for topside structures, piping, and vessels. Carbon steel is also recommended to be coated to mitigate corrosion. For applications with higher demand for corrosion resistance, duplex stainless steels are recommended. These applications could be piping and vessels with corrosive fluids. In addition, these may also be used in pumps, and valve internals. Aluminium EN AW 6082 is recommended for "structural sections and components", in the NORSOK standard M-121 [17].

Aluminium does not have the same mechanical properties as steels, but inherits a good corrosion resistance in marine environments [17]. Anodizing is often done to these alloys to increase the corrosion resistance further. TSA is a metallic coating that is often used on top of steel because of its excellent corrosion properties. In the event of a coating breakdown, exposing a small area of the base steel, the steel will be cathodically protected by the aluminium [18].

To increase the corrosion resistance of the steels, certain alloying elements are added [19]. For the respective steels, the alloying elements that increase the corrosion resistance are mainly chromium and molybdenum [19]. Increasing the amount of these alloying elements will increase the corrosion resistance, along with compromising other properties of the steel, e.g. increased carbide formation [20]. What makes the steel more corrosion resistant is that the chromium or molybdenum contributes to forming a protective oxide film [19][21]. The iron in the bulk material is not directly exposed to the environment, which protects it from dissolving. The pitting resistance equivalent number (PREN) could give an idea of the localized corrosion resistance of the stainless steels. There are several types of equations for calculating this number, one of which are

$$PREN = \text{wt\%Cr} + 3.3(\text{wt\%Mo}) + 16(\text{wt\%N}). \tag{1}$$

This equation relates the amount of alloying elements that raise the pitting resistance. A higher number means higher pitting resistance. In many cases, this number could also give an idea of the resistance against crevice corrosion, which is explained in the chapter (2.3.2).

Another measure of the pitting resistance of a material is the critical pitting temperature (CPT), which highlights the temperature that is needed for pitting to be observed at rates sufficient for material damage[19]. The CPT is closely related to the PREN for stainless steel, where a high PREN gives a higher CPT [19]. For 316 the CPT is below room temperature, while both duplex steels have CPT above room temperature [19]. The CPT of aluminium is between 30 and 40°C [22].

### 2.2.1 Carbon steel

Carbon steel is one of the least alloyed materials that is used in the experiments, which gives a low corrosion resistance. However, its low price and metallic properties make it frequently used for offshore applications [23][16]. The coatings used on carbon steel are often organic coatings [16], but thermally sprayed coatings are also frequently used [18]. The carbon steel without coating will therefore be expected to corrode due to its low corrosion resistance.

### 2.2.2 AISI 316

AISI 316 is an austenitic stainless steel with a face-centred cubic (FCC) type structure [20]. The steel has the least amount of chromium among the stainless steels used in the experiments. It has some molybdenum that also increases the corrosion resistance [19]. Among the stainless steels used in this thesis, it could be considered the stainless steel that is most susceptible to pitting corrosion.

### 2.2.3 Duplex stainless steels

The duplex steels have both austenite and ferrite phases in the microstructure, where the difference in duplex and super duplex is mainly the amount of chromium in the alloy [19]. The ratio between these two phases is close to 50/50, which allows the steel to achieve excellent properties, both mechanically and in terms of corrosion resistance. [23]

The ferrite has the most strength of the two phases due to its body-centred cubic (BCC) structure [24]. The austenite is arranged in a face-centred cubic (FCC) structure. Chromium and molybdenum are ferrite-forming phases while nitrogen is austenite forming. This result in a higher concentration of chromium in the ferrite phase and less in the austenite phase. In terms of pitting resistance, an increased amount of nitrogen in the alloy could lead to higher pitting resistance in the austenite phase. Ultimately leading to ferrite being more susceptible to pitting despite its higher concentration of chromium and molybdenum [24][23]. Therefore, in the event of pitting in these steels, this will most likely occur on grain boundaries, or impurities before growing into the ferrite phase due to the lower pitting resistance [24].

The 22% Cr duplex stainless steel (DSS) has the least amount of chromium among the duplex steels. Despite it having lower chromium, the corrosion resistance of this alloy is still significantly higher than of 316 stainless steel [19].

Like DSS, 25% Cr super duplex stainless steel (SDSS) utilize austenite and ferrite phase to obtain desired mechanical properties and corrosion resistance. The SDSS is defined as duplex steel where the PREN $\geq 40$ [19]. The strong oxide layer protects the steel from localized corrosion [23].

### 2.2.4 Thermally sprayed aluminium

For deposition of TSA, an aluminium wire is utilized as feeding stock to a thermal spray gun. Because of the way these coatings are applied, the coating will be porous [25]. It is also normal that the coatings possess a lamellar grain structure as the coating is applied layer by layer. If the coating is applied in layers it is also a possibility that there will form an oxide layer before the next layer is applied [25]. Thus, inclusions of metal oxides could be in the coating.

### 2.2.5 EN AW 6082

Similar to the stainless steels, aluminium forms a passive oxide film on the surface to prevent corrosion. This oxide layer are often $Al_2O_3$ [26], but other oxides may also be on the surface, e.g. gibbsite ($Al(OH)_3$) and boehmite (AlO(OH)) [27]. Chlorides and other halides may break down the oxide film along with other effects caused by grain boundaries, impurity inclusions, vacancies, etc. The aluminium alloy EN AW 6082 is commonly used in applications where corrosion resistance of the aluminium is needed along with good mechanical properties.

## 2.3 Corrosion mechanisms

The materials used in this thesis have different characteristics and could therefore corrode with different mechanisms. For most corrosion mechanisms the metal is oxidized, where metal ions of higher oxidation number are created, e.g. from 0 to 2. This is generally written as half cell reactions as [28]

$$M_{(s)} \rightarrow M^{z+}_{(aq)} + ze^- \tag{2}$$

To balance the charge present in the system, another half cell reaction is required. Usual reduction reactions are hydrogen evolution reaction (HER), and oxygen reduction reaction (ORR), given in neutral to alkaline environment, respectively [29]:

$$2H_2O + 2e^- \rightarrow H_2 + 2OH^- \tag{3}$$

$$O_2 + 2H_2O + 4e^- \rightarrow 4OH^- \tag{4}$$

This leads to a very general reaction equation that, in simple terms, shows a corrosion reaction with HER.

$$M_{(s)} + zH_2O_{(l)} \rightarrow M^{z+}_{(aq)} + \frac{z}{2}H_{2(g)} + zOH^-_{(aq)} \tag{5}$$

When the corrosion of the metal happens uniformly across the exposed area, the corrosion is categorized as active uniform corrosion. Localized corrosion could also occur, most common among these are crevice and pitting corrosion. It is required that the material has a passive oxide film for localized corrosion to occur [29].

### 2.3.1 Pitting corrosion

Pitting corrosion is often explained by two separate mechanisms, pit initiation and pit propagation [29]. For the materials used in experiments for this thesis, the pit initiation is believed to start with ions, such as chlorides, that break down the passive film. This often happens in the areas of the oxide film that has impaired strength [29], i.e. grain boundaries or inclusions in the material. The process following the oxide film breakdown is not fully understood, but a suggestion is that the oxide film absorbs ions from the solution which allows metal ions to migrate through the oxide film and dissolve. The dissolving of metal ions will then make an immersion in the substrate, i.e. start of a pit. At this point, the pit could either become stable and start pit growth, or it could repassivate to stop further growth of the pit. For the latter, there will then be no significant pitting.

In the event of stable pit growth, the corrosion will continue in an autocatalytic manner. The dissolving of metal ions from the initiation phase continues, mainly at the bottom of the pit. These ions will hydrolyze, resulting in a local lowering of the pH in the pit. As the dissolved metal is cations, anions (e.g. chloride anions) will be attracted into the pit to maintain charge balance. Thus, the solution within the pit will become more acidic than the bulk solution, in addition to higher chloride concentration compared to the bulk solution. The dissolved metal ions will be transported out of the pit where they react with hydroxides in the bulk solution and metal hydroxides are deposited around the pit. This could make the mouth of the pit smaller, which then will lessen the solution flow inside the pit and the aggressive solution is kept in the pit. [19][21][29]

### 2.3.2 Crevice corrosion

Similar to pitting corrosion, crevice corrosion can also be divided into initiation and propagation. First of all, a crevice is required for this corrosion to occur, i.e. a thin slit with metal-metal interfaces or metal-nonmetal interfaces. A frequent example of this is a flange connection. A crucial parameter for crevice corrosion to occur is that the opening should be wide enough for a solution to enter the crevice while being narrow enough to ensure low circulation of the solution [19]. In the initial phase, the metal inside the crevice corrodes in a way described by equation (2) and (4). During these reactions oxygen present in the crevice will slowly be consumed, due to the consumption of oxygen being faster than the diffusion of oxygen into the crevice. When the oxygen is consumed, there will no longer be produced hydroxides to balance the charge caused by dissolved metal cations. Hence, anions will migrate into the crevice to maintain the charge balance. For seawater solutions, these anions will mainly be chloride ions. Metal chlorides will be produced, which again hydrolyses and produces metal hydroxide and hydrochloric acid. Resulting in a lowering of the pH inside the crevice. This proceeds in a steady state until the solution reaches a critical state where the pH is low enough, and the $Cl^-$ concentration is high enough

for the passive film of the passive material to break down. The substrate metal is then exposed directly to the aggressive solution. [29][19]

The mechanism accelerates further through an increased amount of chloride ions migrating into the crevice, which again lowers the pH further and more chloride ions are needed, resulting in an autocatalytic process similar to that of pitting.

Another similar mechanism that is relevant for this thesis is a phenomenon that occurs when thermal sprayed aluminium is covered by paint, a so-called duplex coating. These duplex coatings have been shown to degrade much faster than presumed. The suggestion of why this is the case is because the paint that covers the TSA creates a seal. In the event of coating damage, the TSA gets exposed to the surrounding environment. The TSA will then corrode underneath the paint until a crevice is formed. The initiation will be similar to the mechanism for crevice corrosion. Then, the dissolved aluminium ions will, together with the chloride that is transported under the paint, form aluminium chloride. Aluminium chloride will hydrolyze and lower the pH under the paint. Lowering of pH will cause the TSA to become unstable and corrode actively. Hydrogen evolution reaction will be an effective cathodic reaction due to the increased $H^+$ concentration which facilitates oxidation of the aluminium. The actively corroded aluminium will also react with the chlorides and form aluminium chloride. I.e. two reactions produce aluminium chloride which accelerates the corrosion. Resulting in an autocatalytic corrosion mechanism that causes the TSA to dissolve rapidly. [30]

## 2.4 Electrochemical measurements

Electrochemical measurements are a method that is widely used for assessing the corrosion behaviour of different metals. Usual techniques are creating polarization curves through potentiodynamic scans and measuring polarization resistance.

### 2.4.1 Corrosion current density

The corrosion current density ($i_{corr}$) is a measure that is closely related to the corrosion rate of a material. There are several ways of finding this, one of which being Tafel extrapolation of polarization curves similar to an Evans diagram [21]. To achieve this diagram, a potentiodynamic scan has to be done in the anodic and the cathodic direction. When the measurements are done, the data is plotted in a semi-log space. Tafel extrapolation could be done on the areas of the curves that follow the Tafel law, at least 50-70mV away from the OCP [21]. This is done by adding tangents to the curves where the lines show a linear behaviour. The point where the extrapolation for the anodic and cathodic curve intersects gives the corrosion current density, and the corrosion potential ($E_{corr}$). In some cases, the Tafel extrapolation could be difficult to fit, where a possible solution could be to use the corrosion potential as a constant horizontal line and find where anodic or cathodic Tafel lines intersect.

From the corrosion current density, the corrosion rate in mm/year could be estimated. This is done through a small derivation, ending up with the following equation

$$CR = i_{corr} \frac{Mt}{\rho z F} \tag{6}$$

Where CR is corrosion rate, M is molar mass, $\rho$ is density, F is Faraday's constant, and t is time.

### 2.4.2 Pitting potential

When exposing passive materials to a potentiodynamic scan, a pitting potential can be determined. This is the potential above which stable pitting is observed, and the current density increases rapidly. Several relevant variables could alter the pitting potential of a material. One of which is the pH, where a low pH has shown to lower the pitting potential of both steel and aluminium [19][31]. From the description of the propagation of the pitting corrosion, the hydrolysis occurring in the pit will lower the pH of the solution inside the pit. Thus, the bulk concentration will not have a large effect on the pit growth. In other words, low pH could help initiate pitting, but it is not so significant for propagation. Similar effect is seen on the chloride concentration of the solution, where high concentration of chloride anions will lower the pitting potential for steels and aluminium [19][32][33].

The surface roughness will also affect the pitting initiation. A surface with already existing pits due to roughness could have a stagnant solution in these pits. This will help the pits in the initiation/propagation transition. If there are smooth surfaces, the transition from initiation to propagation will be less probable as the solution is in constant movement around the initiation sites. Sendriks underlines the importance of having similar surface roughness when comparing samples [19]. The surface condition of the laboratory sample should be similar to the piece in service when the pitting behaviour of the piece in service is to be predicted [19].

The scanning rate of potentiodynamic measurements could also influence the pitting potential of 316 stainless steel [34]. Thus, it is of great importance to have the same scanning rate for creating comparable results.

## 2.5 Vibrational spectroscopy

Vibrational spectroscopy is a technique that is used for initiating and detecting vibrations in bonds and groups that are present on a sample surface. Relevant to this thesis are Fourier transform infrared (FTIR) and Raman spectroscopy.

Raman spectroscopy utilizes a laser as a light source that excites molecules present on the surface of the samples [35]. The emitted light travels through a lens and to a detector. Resulting in a spectrum with bands that represent vibrations occurring on the sample. This spectrum can be compared to a fingerprint, where a certain substance has a designated spectrum [35]. This makes it possible to find which substances that are present on the surface of the sample. Due to this excitation, some species could emit fluorescence that could mask peaks in the spectrum, e.g. iron [35]. The Raman spectroscope is often combined with a light microscope which is used to select a suitable area for measurements and for taking pictures of the surfaces.

The FTIR is closely related to the Raman spectroscopy, but there are some differences in the way the spectrum is measured. For FTIR there is a series of electromagnetic waves emitted from a source, the sample molecules resonent with some of the waves which are then absorbed and does not reach the detector [36]. Depending on preference, this will give either a spectrum with peaks or minima, i.e. absorption or transmittance spectrum. The FTIR does not suffer from fluorescence.

### 2.5.1 Expected vibration bands

The samples that will be used in this thesis have some corrosion products that are expected to be seen on the Raman and FTIR spectroscopy. These are manly species expected to be found. Organic compounds that are found are also included. The positions of these peaks are gathered from various studies [27][37][38]

Table 1: Table of different Raman shifts. Numbers are given in [$cm^{-1}$]

| Compound | Comoposition | $\nu_1$ | $\nu_2$ | $\nu_3$ | $\nu_4$ | $\nu_5$ | $\nu_6$ |
|---|---|---|---|---|---|---|---|
| Goethite | FeO(OH) | 244 | 299 | 385 | 480 | 548 | 681 |
| Magnetite | $Fe_3O_4$ | 310 | 540 | 670 | - | - | - |
| Maghmite | $Fe_3O_4$ | 350 | 512 | 665 | 730 | - | - |
| Makinawite | FeS | 200 | 253 | 287 | - | - | - |
| Bayerite/Gibbsite | $Al(OH)_3$ | 1020 | 806 | - | - | - | - |
| Aluminium oxide | $Al_2O_3$ | 968 | 760 | - | - | - | - |

# 3 Materials and methods

In this chapter, the experimental method and materials used will be described in detail. Both a salt-spray test and electrochemical experiments were conducted for this thesis. These have a section each where the inbound process will be described.

## 3.1 Bird droppings

The bird droppings used were provided by chickens from a local owner. These were stored in an air-tight container in a fridge. Feathers and straws were removed with the best effort before use. For both the salt-spray test and the electrochemical experiments, the bird droppings were mixed with water to create a slurry. The amount of water used to create the slurry was not constant as the consistency of the bird droppings varied.

## 3.2 Materials and apparatus

To be able to understand how the bird droppings affect the offshore installations, the experiments for this thesis is done with conventional metals that are used in the offshore industry which are:

- Carbon steel
- AISI 316
- 22% Cr duplex stainless steel
- 25% Cr super duplex stainless steel
- Thermally sprayed aluminium (TSA)
- EN AW 6082

The TSA sprayed on the carbon steel has a thickness of 200-300$\mu$m with a 25$\mu$m silicon resin sealer. The wire used for the TSA used in the experiments was of the grade EN AW 1050A. This is an aluminium wire with high purity (>99.5% Al) which also should give a good purity of the deposited metallic coating. The composition of the coating is assumed to be close to that of the wire. The test certificate of the aluminium wire used for the application of the TSA is provided in the appendix. Table 2 lists the amount of alloying elements in each of the alloys. The chemical composition given by: [19] for the steels, A.4 for the TSA wire, [39] for the EN AW 6082.

Table 2: Table showing typical example of the amount of alloying elements in the respective materials. Values are given as wt% and single values are maximum values.

| Steel | Cr | Ni | C | Mn | Si | P | S | Mo | Fe | PREN |
|---|---|---|---|---|---|---|---|---|---|---|
| Carbon steel | - | - | 0.4 | - | - | - | - | - | balance | - |
| 316 | 16-18 | 10-14 | 0.08 | 2.0 | 1.0 | 0.045 | 0.030 | 2-3 | balance | 25.25 |
| DSS | 21-23 | 4.5-6.5 | 0.03 | 2.0 | 1.0 | 0.030 | 0.020 | 2.5-3.5 | balance | 33.18 |
| SDSS | 24-26 | 6-8 | 0.03 | 1.0 | 1.0 | 0.030 | 0.010 | 3-4 | balance | 40.55 |
| Aluminium | Mn | Fe | Mg | Si | Cu | Zn | Ti | Cr | Al | |
| EN AW 6082 | 0.40-1.00 | 0.5 | 0.60-1.20 | 0.70-1.30 | 0.10 | 0.20 | 0.10 | 0.025 | balance | |
| EN AW 1050A | 0.05 | 0.40 | 0.05 | 0.25 | 0.05 | 0.07 | 0.05 | - | >99.5 | |

### 3.3 Salt spray test

For the salt spray, three samples of each material were made. This gave the total amount of 16 samples. These samples were taken out at different exposure times during the experiment. There was always one sample from at least two material types taken out at the same time to be able to compare the two material types.

Before the testing started, the samples were cut into 4×8 cm rectangular pieces. These were then rinsed in distilled water, acetone, and ethanol to remove various glue and ink deposits which were present on the surface of some samples after shipping. All samples were then weighed individually before clear nail polish was applied on the edges of the samples to avoid edge effects. Bird-droppings slurry was spread on half the sample surface. Then the samples were placed in the Ascott CC450IP cyclic chamber. The thickness of the samples meant the standard sample holders could not be utilized. To ensure that the water would run off, and not accumulate on the surface, the samples were supported by a plastic piece. This gave the samples an angle of 23°to the horizontal plane. The setup is shown in Figure 1.

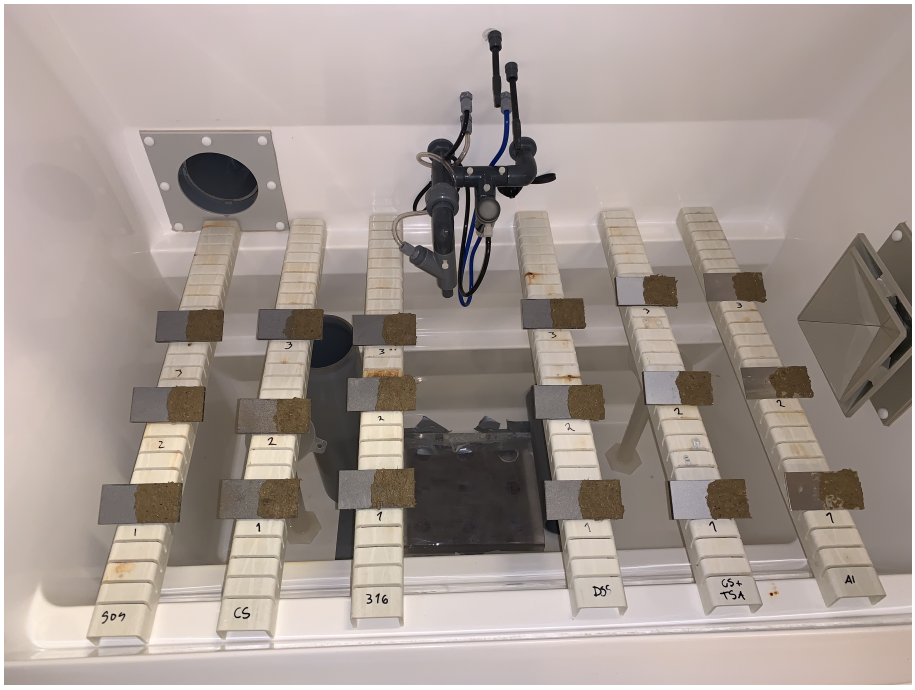


Figure 1: Photo of the samples in the chamber. Bird droppings spread on the right half of the sample. Material type and sample number is also written on each rack.

The testing was inspired by the ASTM G85-19 standard [40], which is a cyclic test that is made to simulate rain, high humidity, and sunny weather. Cycle steps are listed in Table 3. Cyclic exposure should make the materials corrode faster as the salt concentration will be high during drying and wetting.

A salt solution was made according to section 6.3 in the G85 standard, which is a solution of 5 parts NaCl solved in 95 parts drinking water. The initial pH of the solution was not adjusted to 2.8-3.0 as the standard suggests. The low pH would make the carbon steel corrode very fast, and therefore the initial pH was 6.5 for the salt solution. After two weeks of running (334 hours), the most corrosion-resistant materials showed almost no corrosion. Thus, the solution was adjusted to

Table 3: Table of cycles in the salt-fog chamber

| Cycle step | Condition | Temperature [°C] | Cycle time [h:mm] |
|---|---|---|---|
| 1 | Spray | 49 | 0:45 |
| 2 | Dry-air purge | 49 | 2:00 |
| 3 | Soak at high relative humidity | 49 | 3:15 |

reach a pH of 3.0 by using concentrated acetic acid, as suggested by the G85 standard. This was done to accelerate the corrosion process on the more corrosion-resistant materials. The experiment proceeded under these conditions for an additional 358 hours, resulting in a total exposure time of 692 hours for the materials that were left in the chamber for the whole experiment. Table 4 shows the time each sample was held in the salt-fog chamber.

Table 4: Table of the amount of time each of the samples was exposed to the salt-fog chamber

| Material | Sample | Time [h] |
|---|---|---|
| Carbon steel | 1 | 49 |
| | 2 | 334 |
| | 3 | 592 |
| AISI 316 | 1 | 49 |
| | 2 | 334 |
| | 3 | 692 |
| 22% Cr DSS | 1 | 334 |
| | 2 | 692 |
| | 3 | 692 |
| 25% Cr SDSS | 1 | 334 |
| | 2 | 592 |
| | 3 | 692 |
| TSA | 1 | 334 |
| | 2 | 592 |
| | 3 | 692 |
| EN AW 6083 | 1 | 334 |
| | 2 | 692 |
| | 3 | 692 |

After 692 hours the experiment was concluded and the remaining samples were removed from the chamber. This led to several samples of the same material being taken out at the same time stamp. When samples were removed from the chamber, they were rinsed in water to remove salt deposits and left to dry before storing them in individual plastic bags. Following the ASTM G85-19 standard.

### 3.3.1 Raman/FTIR analysis

The samples that were exposed to the salt fog chamber were then analysed using FTIR/Raman spectroscopy. The samples were not prepared in any other way than the rising with water that was done when the samples were taken out of the salt-fog chamber. The instruments used were Bruker Vertex 80v vacuum FTIR spectrometer and WITech Alpha 300R, for FTIR and Raman respectively. The measurements were done at room temperature.

Both the area with and without bird droppings were examined for the samples that were exposed for the longest time. The Raman spectra were achieved using 50x magnification and a distance of 9.1 mm. The laser emitted light with a wavelength of 532 nm, and laser power of 0.15±0.05 mW. The accumulation time was at least 60 seconds. All lights were turned off and window blinds were closed during the measurements. The number of scans for each spectrum was somewhere between 6 and 10 to minimize the amount of noise in the spectra. The samples also had a relatively rough surface which can also contribute to fluorescence in the spectra. Thus, a flat spot was desired to mitigate the fluorescence in the spectra.

FTIR spectroscopy was used to complement the Raman spectroscopy, due to the fluorescence on the steel samples. The FTIR does not suffer from fluorescence, and thus, the vibrations masked by the fluorescence in the Raman spectroscopy should be visible in the FTIR.

To analyze the samples in the FTIR instrument a grazing incidence was used to gather data on the sample surface. A gold mirror was used as background before the samples were inserted into the sample chamber to remove any background noise that originated from the instrument itself. The grazing incidence had an aperture that exposed a set area of the sample. The biggest available aperture was used for all spectra, which gave an exposure area of 1.78 $cm^2$. A big area leads to more rays hitting the sample and being reflected to the detector. This aperture was chosen based on the roughness of the samples, where a bigger area would increase the chances of a ray being scattered to the detector. The side of the samples that had no bird droppings applied during the salt spray test was also used as background to easily visualize the differences between the two surfaces. Both FTIR and Raman spectra will be presented in the results (4.2) or in the appendix (A.1 & A.2). The spectral resolution was set to 4 and 100 scans for the measurements.

### 3.3.2 Mass loss

After the spectroscopy analysis, the samples were weighed again to analyze the mass loss during exposure in the salt-spray chamber. For comparison of the corrosion rates between the side with and without bird droppings, the samples needed to be cut. They were cut across the middle of the sample, creating samples close to 4x4cm. This meant that one sample gave now two individual pieces where one was the side that had bird droppings on the surface, and the other was plain. These pieces were then weighed before and after the removal of the corrosion products. The corrosion products were removed chemically according to the ASTM G01 standard [41]. This standard provides information on how different metals should be cleaned for the best removal of corrosion products without damaging the base material. Chemical cleaning consists of different acids and chemicals used to soak the materials for some time. Table 5 shows the solution, temperature, and time used to remove the corrosion products for the different base materials.

Table 5: Table showing the different cleaning procedures for removing corrosion products of the different base materials.

| Base Material | Solution composition | Temperature [°C] | Exposure time [min] |
|---|---|---|---|
| Carbon steel | 500 mL hydrocloric acid (HCl)<br>3.5 g hexametylene tetramine<br>Reagent water to make 1000mL | 23 | 10 |
| Stainless steel | 100 mL Nitric acid ($HNO_3$)<br>Reagent water to make 1000mL | 60 | 20 |
| Aluminium | 50 mL Phosphoric acid ($H_3PO_4$)<br>20 g chromium trioxide ($CrO_3$)<br>Reagent water to make 1000mL | 90 | 5-10 |

## 3.4 Electrochemical experiments

Electrochemical experiments were completed along with the salt spray test. The method used is rather unconventional and should be considered as an attempt to create a method that would simulate a layer of bird droppings on the given material, to get the experiments as close to the real-world conditions as possible.

A syringe was modified to fit a reference electrode and a platinum wire through the rubber gasket of the syringe. The reference electrode was an Ag/AgCl with a saturated KCl solution. The platinum wire was turned around the reference electrode to have the largest surface area possible as this will later be used as the counter electrode (CE). Approximately 115 mm of platinum wire with a diameter of 0.5mm was submerged in the electrolyte. With an average area of 0.2 $mm^2$ for the working electrode (WE), this yields a CE to WE area ratio of 900. The shell of the syringe is then filled with an electrolyte, which in this case is synthetic seawater prepared with inspiration from the ASTM standard D1141 [42]. The chemicals used for the preparation were the salts with <0.5 g/L, which in decreasing amount is NaCl, $MgCl_2$, $Na_2SO_4$, $CaCl_2$, and KCl mixed into type 2 distilled water. These chemicals had a purity of at least 98%. Table 6 shows the targeted values of the chemicals used for mixing the synthetic seawater. In addition to these chemicals, 0.1 M NaOH solution was used to increase the pH of the solution to 8.9. Measurement of the pH of the solution was done with PHM-210 by MeterLab.

Table 6: Table of the targeted values for mixing of the synthetic seawater solution

| Chemical | Concentration [g/L] |
|---|---|
| NaCl | 24.53 |
| $MgCl_2$ | 5.20 |
| $Na_2SO_4$ | 4.09 |
| $CaCl_2$ | 1.16 |
| KCl | 0.695 |

The standard suggests a pH of 8.2, but the pH of the solution used ended up at 8.9 due to the overuse of sodium hydroxide.

The upper part of the syringe, consisting of a gasket, reference electrode, and counter electrode, was then inserted into the shell to create a seal, as shown in Figure 2. The assembled syringe is a movable device that could be set on top of the desired flat metal surface for testing, allowing a sample to be examined in several areas. This setup allows the tip of the syringe to be filled

with bird droppings to perform measurements on the metal when covered by bird droppings. The bird droppings must have the right consistency which is adjusted using distilled water. Too much water will lead to a flowing mass that will run out of the syringe, while too little water and the droppings will plug the syringe and the electronic contact could be lost during the experiment. The consistency of the bird droppings was varying, resulting in different amounts of water in the mixture. Thus, a cement-like consistency should be pursued. The setup was always installed inside a fume hood, regardless of whether the experiment was run with or without bird droppings. There was no other preparation done for the bird droppings.

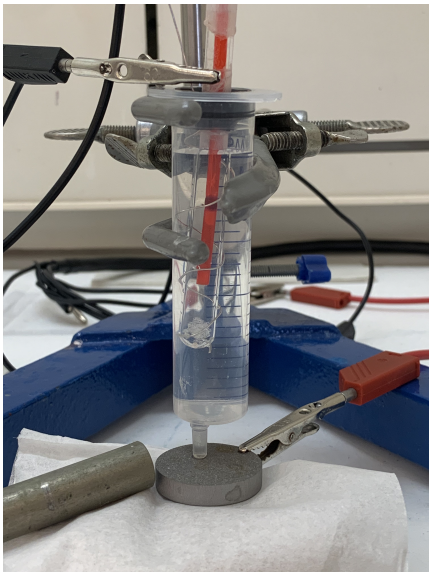

Figure 2: The setup used in the electrochemical experiments, including a Ag/AgCl reference electrode along with platinum wire as counter electrode and electrolyte inside the syringe.

The syringe setup was also tested with bird droppings deposited on top of the sample rather than inside the syringe. However, the bird droppings showed to act as a sponge in contact with the electrolyte and absorb a large amount of water, resulting in an exposed area that was both inconsistent and difficult to determine. There were also some challenges related to filling the tip of the syringe, e.g the consistency of the droppings. However, these possible problems are considered more manageable than an inconsistent reaction area.

### 3.4.1 Procedure

The samples were rinsed with ethanol, acetone, and distilled water before drying with pressurized air. The samples were not polished to a smooth surface. The potentiostat was calibrated weekly. The top of the syringe must be properly sealed so there is no leakage from the syringe. If the measurement was supposed to be run with bird droppings, the bird droppings would be added to the syringe at this point by using a spatula.

To avoid leakage, any unnecessary stress to the reference electrode or the connection of the counter electrode should be avoided. To mitigate the stress of the counter electrode the counter- and counter sense connections were joined at the end of the black wire seen in Figure 2. The same action was done for the working electrode, which has working- and working sense connections joined at the red wire. The reference electrode has only one connection for the potentiostat. The potentiostat used for the measurements was a Gamry 750 potentiostat.

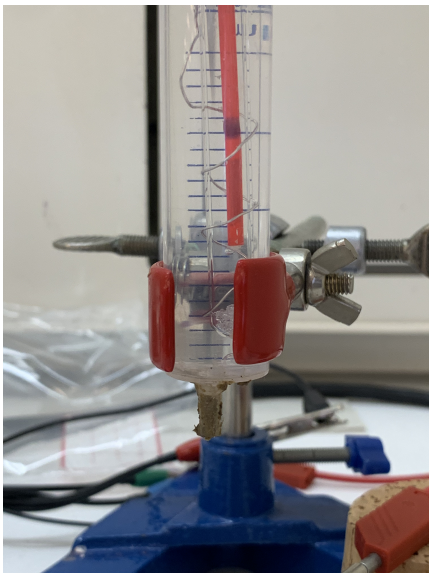

Figure 3: Picture of the syringe with bird droppings inside the syringe tip.

Polarization resistance, cathodic polarization curve, or the anodic polarization curve was measured with this setup. Before any of these measurements were done, the open circuit potential (OCP) was measured for 15 minutes. The polarization resistance was measured by applying a potential 20mV below the OCP and increasing the potential with a rate of 1.25 mV/s until a potential of 20mV above OCP was reached. The anodic polarization curve was measured by increasing the potential with a rate of 2.5 mV/s from OCP until the potential was in the range 1.0-1.3V above the OCP depending on the material to be measured. The cathodic curve was measured with the same parameters as the anodic curve but ended up at a potential of 1.0V below the OCP. The sequence of the measurements could vary, but to ensure similar conditions, all measurements were made on an unused, clean, spot of the sample.

# 4 Results

The results of the samples used in the salt spray test and the electrochemical experiments will be presented separately in dedicated chapters.

## 4.1 Salt spray test

The results from the salt spray test will be presented in this chapter. The visual condition of the samples will be discussed later. Thus, pictures of the samples in the salt-spray chamber will be presented for each of the timestamps the samples were removed. Close-up pictures of the samples after they were removed from the chamber will be given in the next chapter. The first two samples, carbon steel and 316 were removed after 49h. Figure 4 shows the condition of all samples after 49 hours.

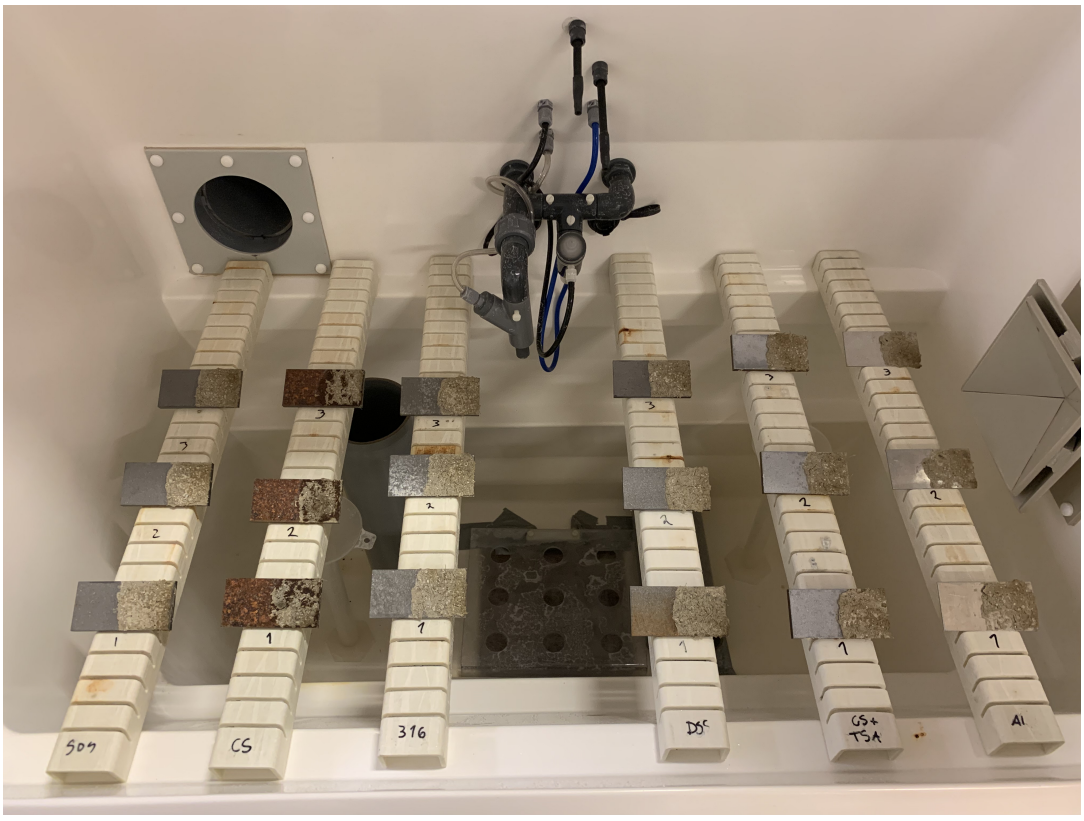


Figure 4: Picture of the samples after 49 hours of exposure in the salt-spray chamber.

The stainless steel samples show only some small discolouring on their surfaces, while the TSA and 6082 do not show any discolouring on the pictures in Figure 4. The carbon steel has discolouring on the whole surface visible in the picture. The first samples of carbon steel and 316 were removed from the chamber after this picture was taken.

From then on the samples were left for exposure for a longer time before any samples were removed. After 334h (14 days) the next set of samples was removed from the chamber. The condition of the samples is shown in Figure 5.


Figure 5: Picture of the samples after 334 hours of exposure in the salt-spray chamber.

Figure 5 show some development of corrosion of the carbon steel, indicated by the darker colour around the edges and corrosion product on the sample holder. There is a slight increase in the discolouring for DSS sample 1. Salt deposits have accumulated around the edges of the TSA, along with some salt deposits on the 316 stainless steel. After the picture was taken, one sample of each material was removed and the solution was acidified.

Acidified solution led to high amounts of corrosion on the carbon steel, resulting in a short stint from 334 to 592 hours. Figure 6 shows the condition after 592 hours (25 days).


Figure 6: Picture of the samples after 592 hours of exposure in the salt-spray chamber.

The picture in Figure 6 does not show much difference in the condition for the carbon steel other than darker colour on the sample holder. 316 show some more discolouring, both on the plain side and in the bottom right corner. The 6082 has become somewhat more matte on the plain side, indicating some corrosion. The TSA has even more salt deposits on the surface. Carbon steel, TSA, and SDSS were removed after the picture was taken.

Figure 7 shows the condition of the samples after 692 hours (29 days).

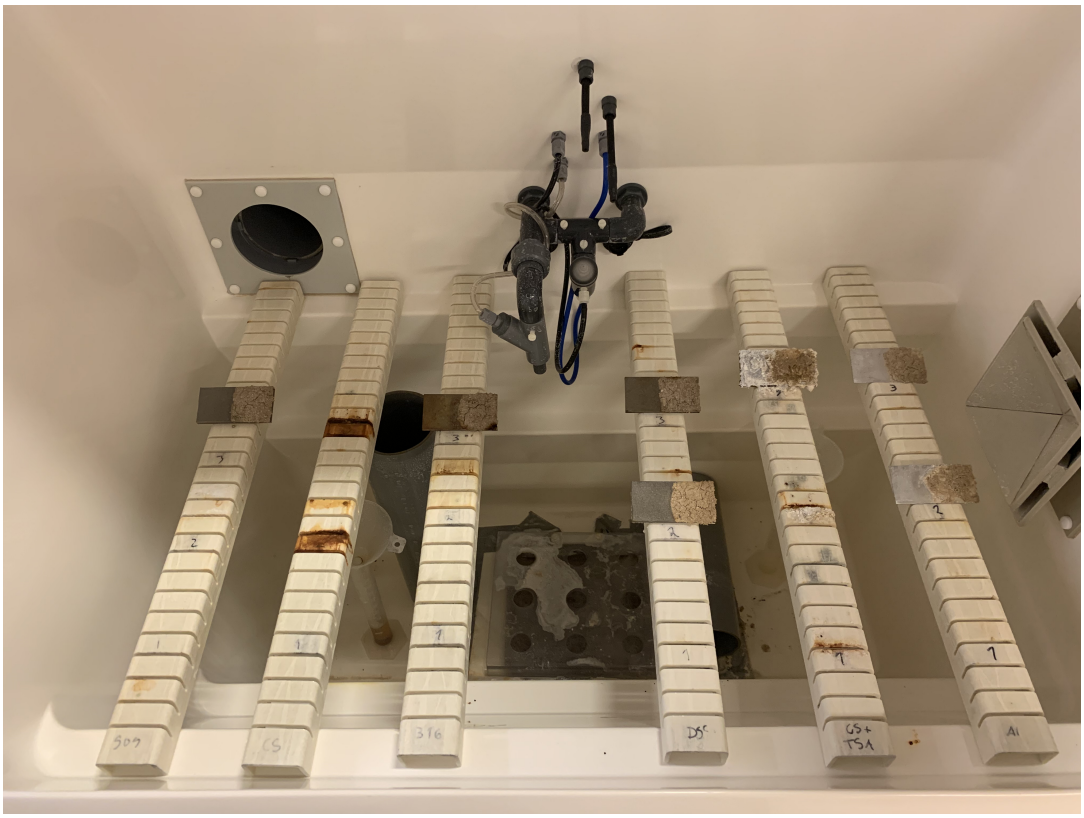


Figure 7: Picture of the samples after 692 hours of exposure in the salt-spray chamber.

in Figure 7, the TSA had more salt deposits on the surface at this point, and the 6082 showed some corrosion product on the side without bird droppings. The DSS and SDSS however, showed almost no signs of corrosion, only minor discolouring on the surface. 316 shows more or less the same amount of discolouring as in Figure 6

### 4.1.1 Pictures of exposed samples

This chapter shows pictures of the samples after they were cut. For all pictures, the right piece is the side with bird droppings. Figure 8 show pictures of the carbon steel.

(a) 49 hours (b) 334 hours (c) 592 hours

Figure 8: Carbon steel samples with different exposure times.

The pictures in Figure 8 show corrosion craters on the side of the sample that was without bird droppings. The side with bird droppings has a more homogeneous topography. There is also a colour difference between the two sides.

Figure 9 show pictures of AISI 316.

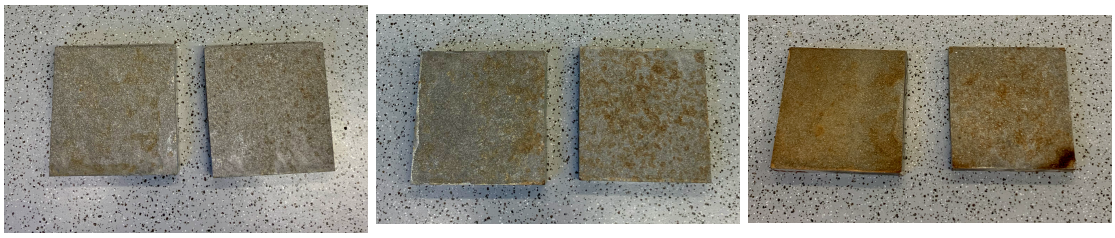

(a) 49 hours (b) 334 hours (c) 692 hours

Figure 9: AISI 316 samples with different exposure times.

For all samples seen in Figure 9, there is a spotted pattern for the side with bird droppings. The left side shows a gradual increase in discolouring for increased exposure time.

Figure 10 show pictures of the 22% Cr DSS.

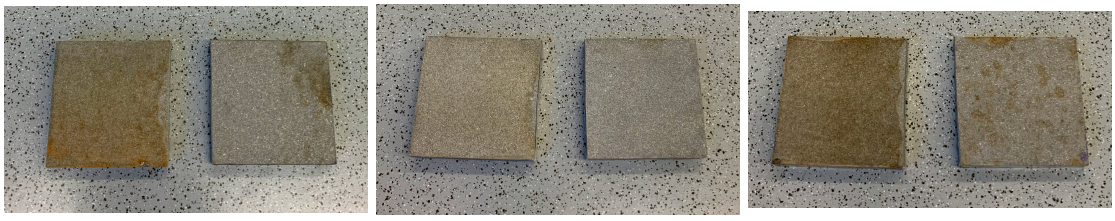

(a) 334 hours (b) 692 hours (c) 692 hours

Figure 10: 22% Cr DSS samples with different exposure times.

Pictures (a) and (c), in Figure 10, show more uniform corrosion on the side that was without bird droppings during exposure as well as a spotted pattern where bird droppings were present. Figure 10b show less discolouring than the other two samples and no spotted pattern for the right side.

Figure 11 show the 25% Cr SDSS samples after exposure.

(a) 334 hours (b) 592 hours (c) 592 hours

Figure 11: 25% Cr DSS samples with different exposure times.

For the SDSS in Figure 11, it is very little corrosion visible for any exposure time. Most corrosion is visible on the plain side of (c).

Figure 12 show pictures of the TSA samples.

(a) 334 hours (b) 592 hours (c) 692 hours

Figure 12: TSA samples with different exposure times.

On the samples shown in Figure 12, there is a deposit around the edge of all samples. Picture (a) show more corrosion on the side with bird droppings. Pictures (b) and (c) show corrosion on both sides.

Pictures of the aluminium samples are shown in Figure 13.

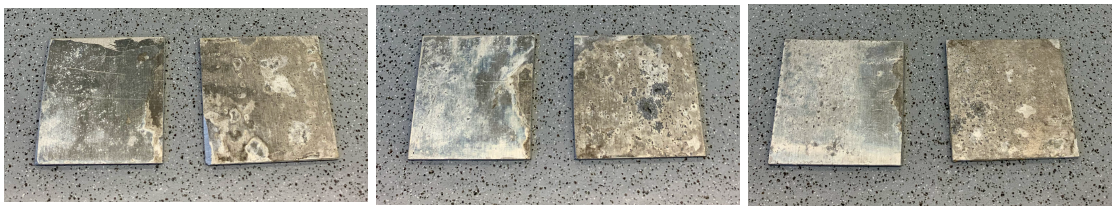

(a) 334 hours (b) 692 hours (c) 692 hours

Figure 13: EN AW 6082 samples with different exposure times.

For all pictures in Figure 13, it is more pitting corrosion on the side with bird droppings. The left side of (b) and (c) show more pitting corrosion compared to (a).

### 4.1.2 Mass loss

The samples were weighed before the salt-spray test. The weights for the samples were converted into area density to be able to compare the wight before and after the salt-spray test for both sides of the sample. In Table 7, the area densities for the plain side of the sample before cleaning is listed. The initial area density is noted $\rho_{A,0}$. The raw data, which were used to calculate the area density, are presented in the appendix (A.3).

Table 7: Table showing the area density for the samples *before* removal of corrosion products. $\rho_{A,plain}$ and $\rho_{A,BD}$ shows the area density for the plain side and bird dropping side respectively.

| Material | Sample | $\rho_{A,0}$ [g/cm$^2$] | $\rho_{A,plain}$ [g/cm$^2$] | $\rho_{A,BD}$ [g/cm$^2$] |
|---|---|---|---|---|
| Carbon steel | 1 | 4.47 | 4.37 | 4.46 |
| | 2 | 4.42 | 4.42 | 4.41 |
| | 3 | 4.40 | 4.44 | 4.53 |
| AISI 316 | 1 | 4.47 | 4.47 | 4.46 |
| | 2 | 4.48 | 4.44 | 4.46 |
| | 3 | 4.47 | 4.46 | 4.42 |
| 22% Cr DSS | 1 | 4.63 | 4.59 | 4.59 |
| | 2 | 4.67 | 4.68 | 4.64 |
| | 3 | 4.61 | 4.60 | 4.57 |
| 25% Cr SDSS | 1 | 5.18 | 5.14 | 5.14 |
| | 2 | 5.23 | 5.19 | 5.21 |
| | 3 | 5.18 | 5.15 | 5.15 |
| TSA | 1 | 4.62 | 4.60 | 4.57 |
| | 2 | 4.64 | 4.63 | 4.57 |
| | 3 | 4.55 | 4.51 | 4.48 |
| EN AW 6082 | 1 | 0.40 | 0.39 | 0.39 |
| | 2 | 0.39 | 0.41 | 0.42 |
| | 3 | 0.39 | 0.41 | 0.41 |

For these measurements, the nail polish was also present along with the corrosion product on the samples. These variables could cause the area density to increase for some samples.

The area density for the samples after removal of corrosion products is listed in Table 8. As the previous table, $\rho_{A,0}$ denotes the initial area density.

Table 8: Table showing the area density for the samples *after* removal of corrosion products. $\rho_{A,plain}$ and $\rho_{A,BD}$ shows the area density for the plain side and bird dropping side respectively.

| Material | Sample | $\rho_{A,0}$ [g/cm$^2$] | $\rho_{A,plain}$ [g/cm$^2$] | $\rho_{A,BD}$ [g/cm$^2$] |
|---|---|---|---|---|
| Carbon steel | 1 | 4.47 | 4.35 | 4.44 |
| | 2 | 4.42 | 4.16 | 4.20 |
| | 3 | 4.40 | 3.74 | 4.08 |
| AISI 316 | 1 | 4.47 | 4.47 | 4.45 |
| | 2 | 4.48 | 4.44 | 4.46 |
| | 3 | 4.47 | 4.46 | 4.41 |
| 22% Cr DSS | 1 | 4.63 | 4.59 | 4.59 |
| | 2 | 4.67 | 4.65 | 4.65 |
| | 3 | 4.61 | 4.60 | 4.57 |
| 25% Cr SDSS | 1 | 5.18 | 5.14 | 5.14 |
| | 2 | 5.23 | 5.18 | 5.21 |
| | 3 | 5.18 | 5.13 | 5.13 |
| TSA | 1 | 4.62 | 4.60 | 4.57 |
| | 2 | 4.64 | 4.62 | 4.57 |
| | 3 | 4.55 | 4.48 | 4.45 |
| EN AW 6082 | 1 | 0.40 | 0.39 | 0.39 |
| | 2 | 0.39 | 0.39 | 0.40 |
| | 3 | 0.39 | 0.39 | 0.39 |

This table shows that the samples have lost mass rather than an increased mass in the previous table. Note that the area densities of the EN AW 6082 samples are somewhat identical.

## 4.2 FTIR and Raman Spectroscopy

Before the salt spray test, and before the removal of the corrosion products, the samples were analyzed using FTIR/Raman spectroscopy. Some of the spectra will be presented in this section, and those not included are given in the appendix (A.1 & A.2). This is due to the similarity between most of the plots.

Figure 14 shows the spectra for 316 with/without bird droppings where a gold mirror is used as background.

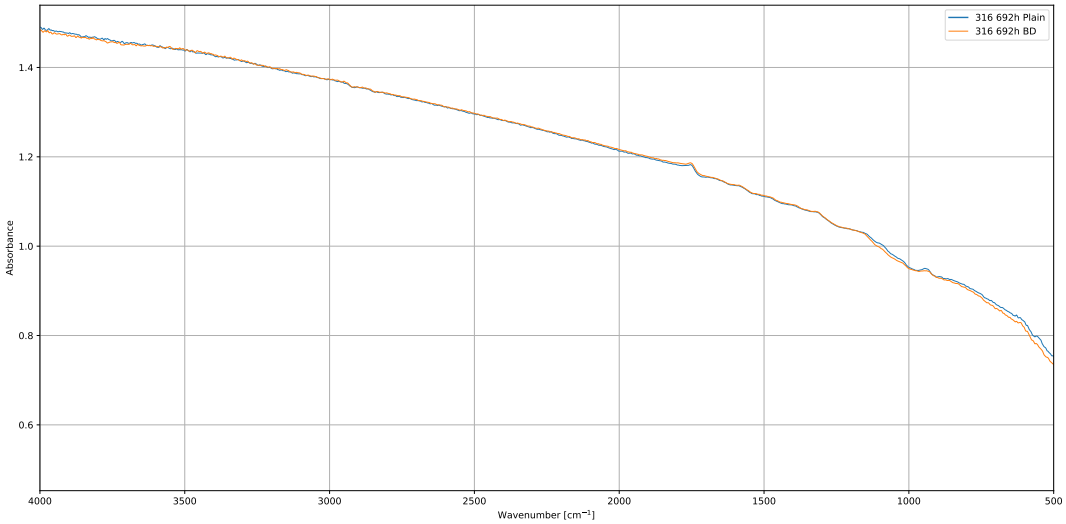


Figure 14: Comparison of the FTIR spectra for the AISI 316 sample, with and without bird droppings, that was in the salt spray test for 692h. On these spectra a gold mirror was used as background.

There is not a large difference between these two spectra. The sample was also analysed where the side of the sample without bird droppings was used as background. This produced the spectra presented in Figure 15.

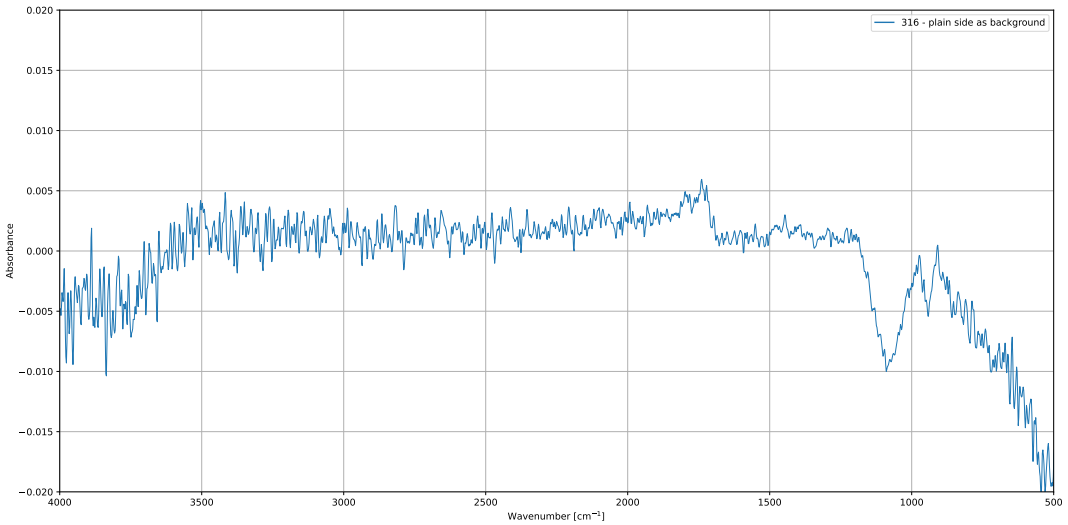


Figure 15: FTIR spectra of AISI 316 exposed to the salt spray test for 692h. Here the side without bird droppings was used as background.

This spectrum shows the differences between the two sides of the 316 alloy. The plain side is used as background, meaning peaks above zero are compounds that give more signal on the side that had bird droppings, and peaks below zero represent the plain side.

The FTIR spectra for the other steel samples given in the appendix (A.1) yield more or less the same information as the FTIR spectra given above. The plain and bird droppings side follows each other closely when a gold mirror is used, and minor differences in organic compounds when the plain side is used as background. The spectra of DSS and SDSS showed in the appendix (A.1), are the materials that show the most peaks when the plain side is used as background, Figure 35 and Figure 37 respectively.

Figure 16 shows the spectra for aluminium sample number 3, with a comparison between the sides with and without bird droppings.

There are some peaks on the plain sample that is not included in the spectrum of the side that has been exposed to bird droppings.

Most of the Raman spectra will be presented in the appendix (A.2), but as an example, the spectra of carbon steel without bird droppings are given in Figure 17.

This was the spectrum from the Raman spectroscopy that produced the clearest peaks without fluorescence. The background of this spectrum is not removed.

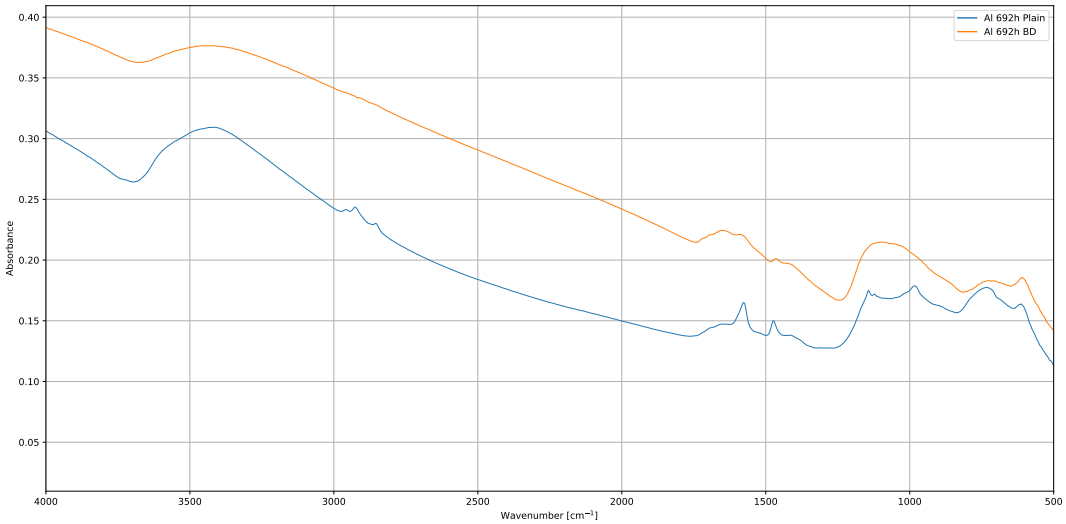


Figure 16: Comparison of the FTIR spectra for aluminium sample nr 3 with and without bird droppings that was in the salt spray test for 692h

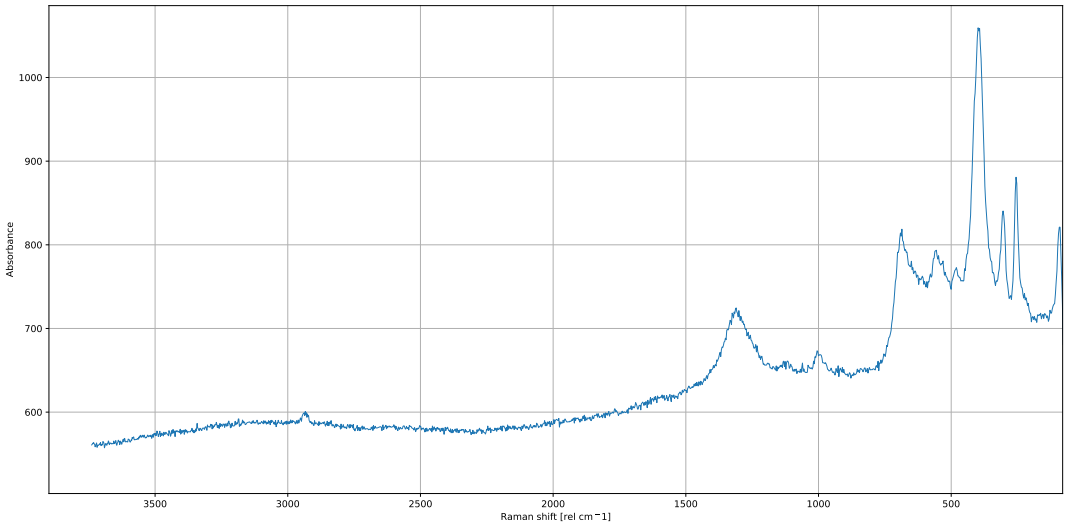


Figure 17: Plot of the Raman spectra of carbon steel without bird droppings.

## 4.3 Electrochemical experiments

In this chapter, the results of the electrochemical experiments will be presented. The scope is to compare the materials with and without bird droppings and not compare the materials directly. Thus, there will be a subsection for each of the materials used, where each of them will contain polarization curves and polarization resistance. Tables of different variables are given in chapter 4.3.7

### 4.3.1 Carbon steel

The first material tested was carbon steel.Figure 18 shows the polarization resistance for this material.

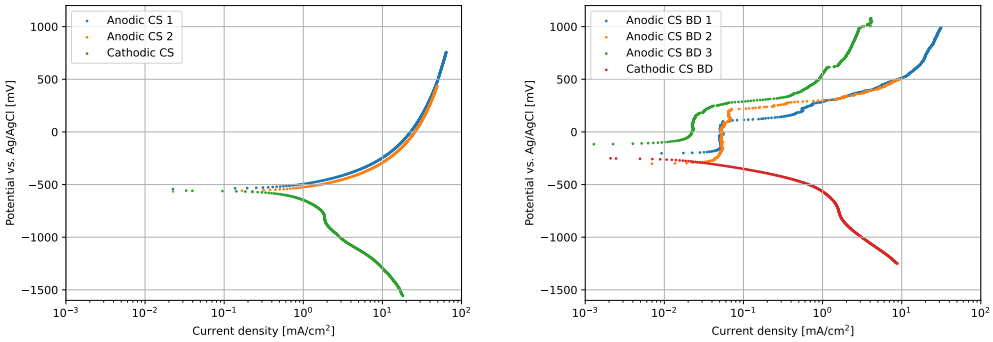


(a) (b)

Figure 18: Polarization curves for carbon steel without (a) and with (b) bird droppings.

When there are bird droppings present the measurements in Figure 18 show a passivating behaviour with pitting around 250 mV. Several measurements were done to verify the curves in Figure 18b.

Figure 19 shows the polarization resistance for the carbon steel.

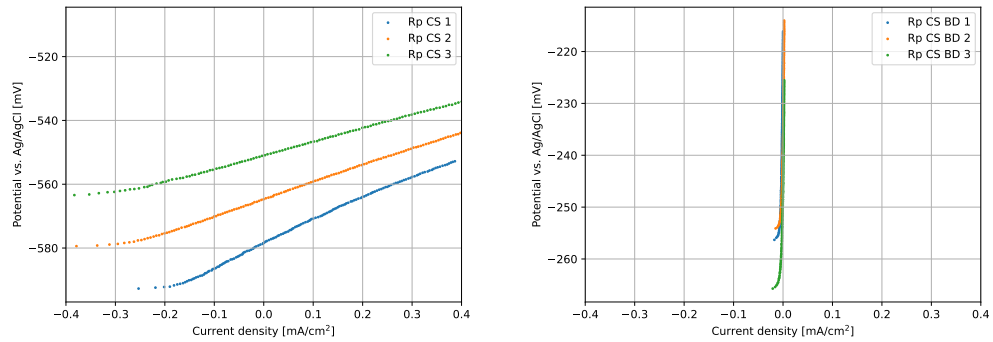


(a) (b)

Figure 19: Polarization resistance for carbon steel without (a) and with (b) bird droppings.

The curves in Figure 19 show a clear increase in polarization resistance when bird droppings are present. The $E_{corr}$ is has also increased for Figure 19b.

### 4.3.2 AISI 316

AISI 316 is the first stainless steel to be presented. The polarization curves for AISI 316 stainless steel are presented in Figure 20.

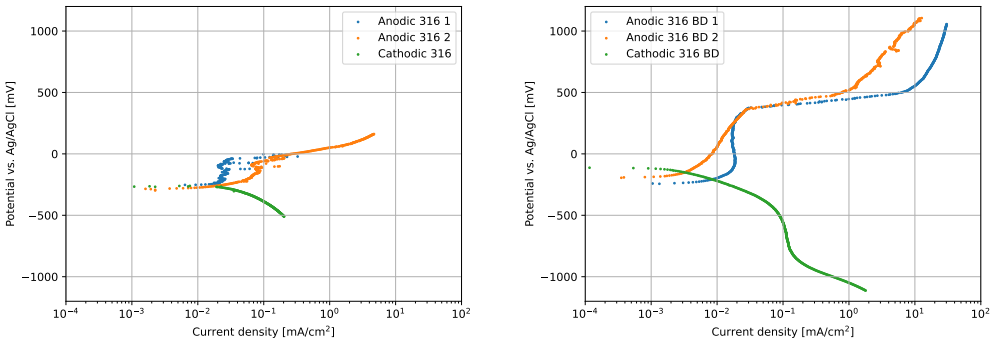


(a) (b)

Figure 20: Polarization curves for AISI 316 without (a) and with (b) bird droppings.

From the plots in Figure 20, it is clear that the pitting potential is increased for the polarization curves where bird droppings are present. The curves with bird droppings also show little to no metastable pitting before the pitting potential.

The polarization resistance measurements for AISI 316 stainless steel are presented in Figure 21.

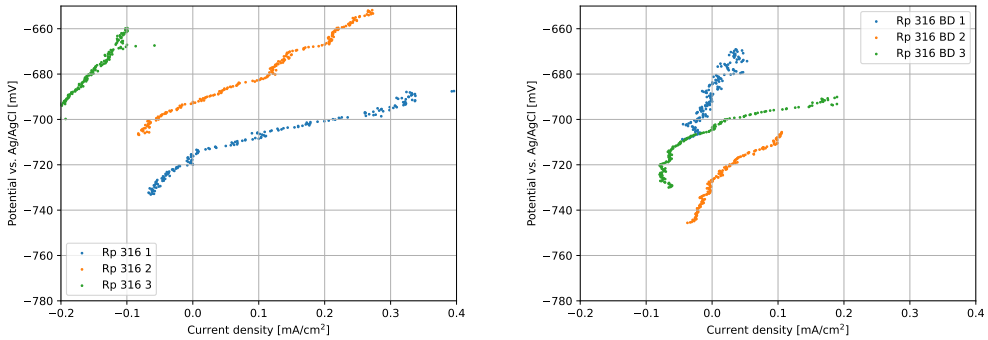


(a) (b)

Figure 21: Polarization resistance for AISI 316 without (a) and with (b) bird droppings.

The polarization resistance in Figure 21 is not that easy to comprehend from these results, as there are no clear trends in the curves.

### 4.3.3 22% Cr DSS

The duplex stainless steel proved to be a difficult material to work with, as there were a lot of fluctuations in the OCP. Consequently, many attempts were needed to get reproducible measurements.

Figure 22 shows a comparison of the polarization curves with and without bird droppings.

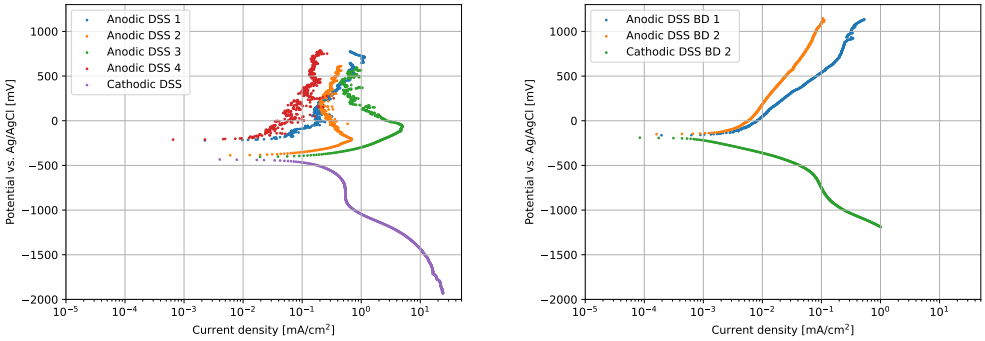


(a) (b)

Figure 22: Polarization curves for 22% Cr duplex stainless steel (DSS) without (a) and with (b) bird droppings.

In Figure 22, the DSS show less metastable pitting when there are bird droppings present in the system. There is little difference in the OCP between the systems with and without bird droppings.

Next up is the polarization resistance for DSS in Figure 23.

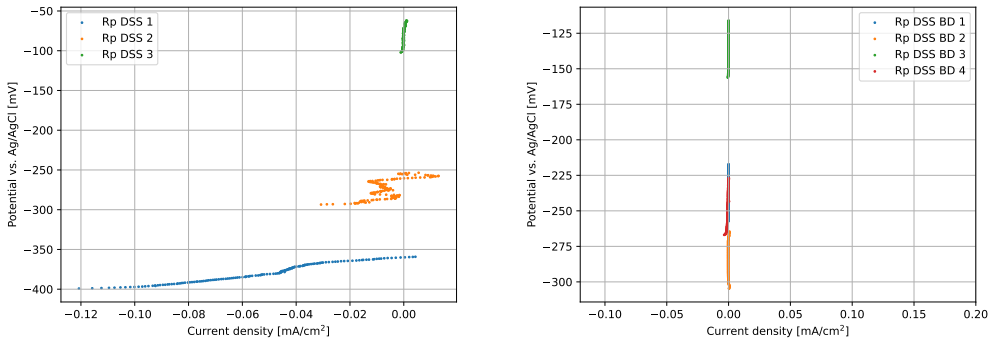


(a) (b)

Figure 23: Polarization resistance for DSS without (a) and with (b) bird droppings.

In Figure 23, it is clear that the system without bird droppings has bigger deviations than the measurements where bird droppings are present. But qualitatively, it is clear that the system with bird droppings appears to be more stable as the OCP and curves are easier to reproduce.

### 4.3.4 25% Cr SDSS

The super duplex stainless steel (SDSS) is the last stainless steel to be presented. Figure 24 shows the polarization curves for SDSS.

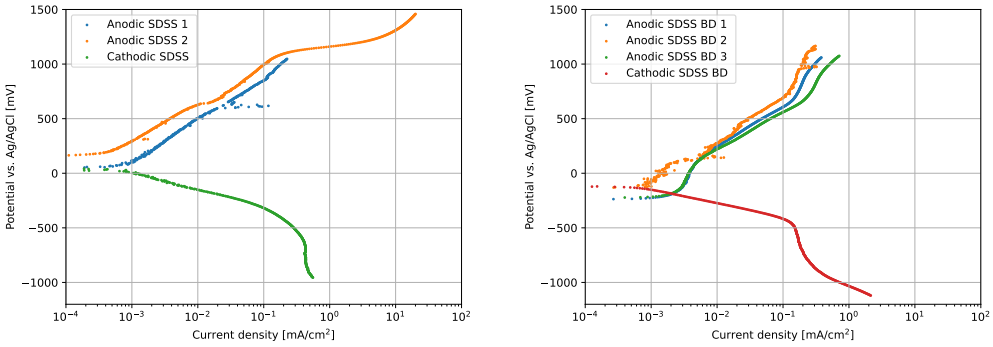


(a) (b)

Figure 24: Polarization curves for SDSS without (a) and with (b) bird droppings.

Figure 24 show little difference in the potential range that was measured. This is the material that proves the least change in the presence of bird droppings.

The polarization resistance measurements for SDSS are presented in Figure 21.

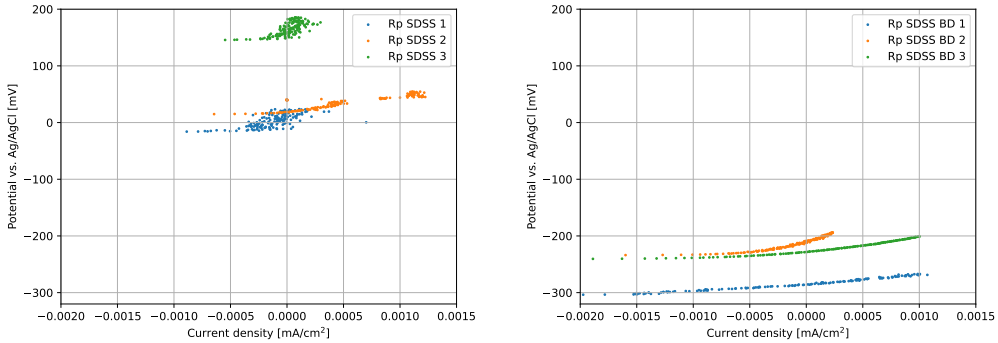


(a) (b)

Figure 25: Polarization resistance for SDSS without (a) and with (b) bird droppings.

There are more differences between the systems for these measurements than for the polarization curves presented in Figure 24. Both in terms of OCP and noise in the measurements.

### 4.3.5 Thermally sprayed Aluminium

The polarization curves for TSA is presented in Figure 26.

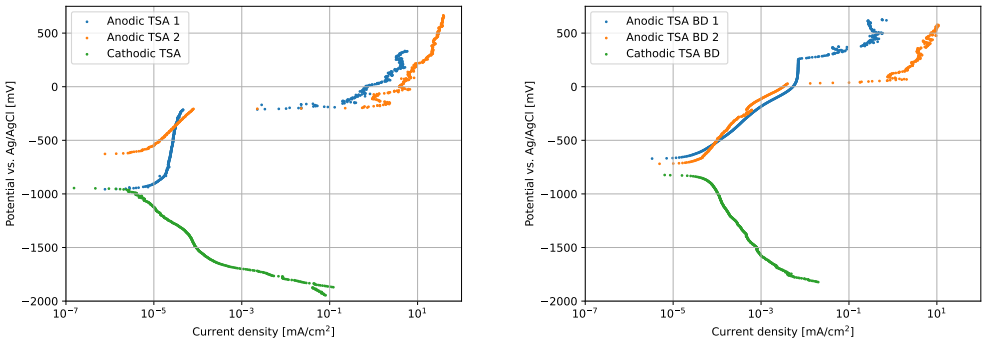


(a) (b)

Figure 26: Polarization curves for TSA without (a) and with (b) bird droppings

In Figure 26, it is clear that there is an increase in the potential where the pitting initiates when bird droppings are present.

The polarization resistance measurements for TSA are presented in Figure 27.

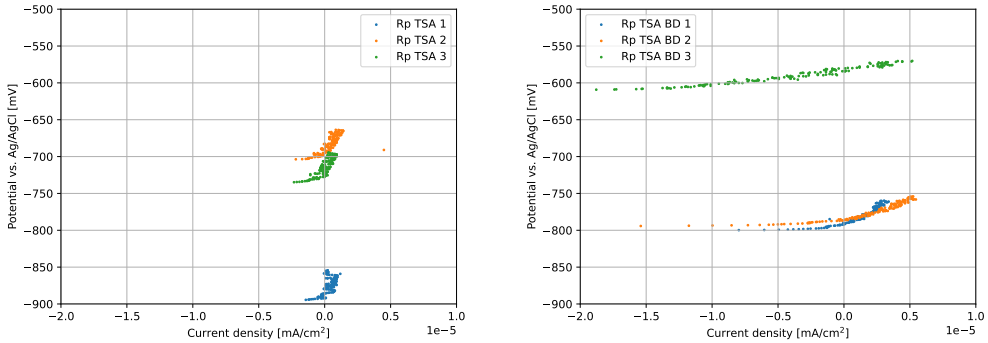


(a) (b)

Figure 27: Polarization resistance for TSA without (a) and with (b) bird droppings.

In Figure 27 it is clear that the polarization resistance for the TSA is lower for bird droppings compared to the plain surface. However, there are some deviations in the measurements.

### 4.3.6 EN AW 6082

The aluminium alloy proved to also be one of the harder materials to do measurements to. Despite this, some good polarization curves were measured which are presented in Figure 28.

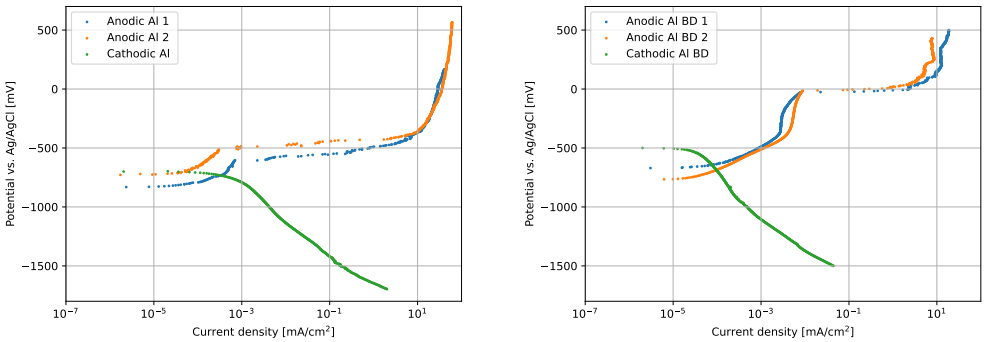


(a) (b)

Figure 28: Polarization curves for aluminium 6083 without (a) and with (b) bird droppings.

Figure 28 show a distinct difference in the pitting potential that was measured. This is the biggest difference seen in any of the materials.

Because of the nature of this material, the measurements of the polarization resistance proved to be hard when there was no bird droppings in the system. This is why Figure 29a only has two curves to show. The polarization resistance measurements is presented in Figure 21.

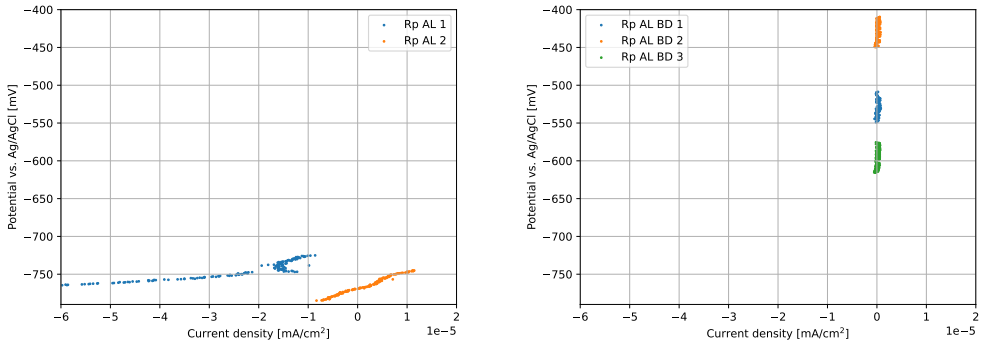


(a) (b)

Figure 29: Polarization resistance for aluminium 6083 without (a) and with (b) bird droppings.

From Figure 29 it is clear that the polarization resistance is much higher when bird droppings are present compared to the plain surface. Qualitatively, the OCP is more stable, i.e. less metastable pitting, when bird droppings are present which makes it easier to get reproducible measurements.

### 4.3.7 Variables achieved from measurements

From the polarization curves presented above, Tafel extrapolation is utilized to find the corrosion current density ($i_{corr}$) and the corrosion potential ($E_{corr}$). The point where the two Tafel slopes intersect marks both of these values which are read from the x- and y-axis. In Table 9, variables are listed where pitting potential is given for materials where this potential is clear.

Table 9: Table listing different variables achieved from the electrochemical experiments.

| Material | Without bird droppings | | | | With bird droppings | | | |
|---|---|---|---|---|---|---|---|---|
| | $i_{\text{corr}}$ [mA/cm$^2$] | $E_{\text{corr}}$ [mV] | CR [mm/year] | $E_{\text{pit}}$ [mV] | $i_{\text{corr}}$ [mA/cm$^2$] | $E_{\text{corr}}$ [mV] | CR [mm/year] | $E_{\text{pit}}$ [mV] |
| Carbon steel | $(6.7 \pm 0.5) \cdot 10^{-1}$ | $-580 \pm 28$ | 7.82 | - | $(2.2 \pm 1.5) \cdot 10^{-2}$ | $-233 \pm 76$ | 0.25 | 150±50 |
| AISI 316 | $(4.0 \pm 0.5) \cdot 10^{-2}$ | $-255 \pm 10$ | 0.47 | -50 | $(7.3 \pm 3.2) \cdot 10^{-3}$ | $-165 \pm 50$ | 0.085 | 350 |
| 22% Cr DSS | $(1.1 \pm 0.4) \cdot 10^{-1}$ | $-437 \pm 81$ | 1.28 | - | $(7.3 \pm 0.4) \cdot 10^{-4}$ | $-185 \pm 10$ | 0.085 | - |
| 25% Cr SDSS | $(3.7 \pm 2.3) \cdot 10^{-4}$ | $90 \pm 42$ | 0.0043 | - | $(8.0 \pm 2.8) \cdot 10^{-4}$ | $-155 \pm 36$ | 0.0093 | - |
| TSA | $(2.5 \pm 2.1) \cdot 10^{-6}$ | $-800 \pm 283$ | 0.00003 | -200 | $(3.3 \pm 0.4) \cdot 10^{-5}$ | $-656 \pm 50$ | 0.00036 | 125±125 |
| EN AW 6082 | $(2.0 \pm 1.4) \cdot 10^{-4}$ | $-663 \pm 53$ | 0.0022 | -550±50 | $(1.0 \pm 0.1) \cdot 10^{-4}$ | $-685 \pm 10$ | 0.0011 | 0 |

Polarization resistance gives also variables related to the corrosion behaviour. However, most of the materials show a resistance that is very high, i.e. in the magnitude of G$\Omega$cm$^2$. This is expected for some materials, but there are several orders of magnitude difference for some materials with the same system. Resulting in a large statistical uncertainty. Thus, the calculations for the corrosion current density are not included, but the figures remain in the previous sub-chapter for the sake of discussion around these.

# 5 Discussion

The experimental part of this thesis is split into two parallel experiment methods. Therefore the discussion of these parts consists of two dedicated chapters, with a summary of them both in the end.

## 5.1 Salt spray test

The salt-spray test was conducted to give a comprehensive way of learning the corrosion behaviour of the different materials and complement the electrochemical experiments. It is a method where the naked eye can give much information about how the different materials perform relative to each other. At the same time, the real-world scenario with bird droppings on the surface will be simulated.

### 5.1.1 Carbon steel

The carbon steel was, as expected, the material showing the most corrosion. Already after 49 hours, the first sample was taken out. This was to get an idea of the corrosion behaviour underneath the bird droppings in the early phases. The picture of the carbon steel in Figure 8a shows a difference in colour and topography between the sides with and without bird droppings. The mass of the samples after removing the corrosion products was presented in Table 8, where the side which had bird droppings on top showed less corrosion than that side without. This result was consistent for all samples, which could indicate that the bird dropping acts like a kind of coating and adds barrier capabilities. I.e., the bird droppings prevent the corrosion products from dissolving, and a dense iron oxide layer is formed. The corrosion rate will decrease with a growing oxide layer. This corresponds well with observations done during the removal of corrosion products, where the side with bird droppings was denser than the side without bird droppings. The dense oxide layer will then give a longer distance, for the electrons that contribute to the corrosion process, to travel into the substrate material [43]. The bird droppings are also able to absorb water, meaning there will be water present for a longer time each cycle on the side with bird droppings, compared to the plain side. But as the mass loss of the bird droppings side is lower than the plain side, the positive effects of the barrier properties are believed to trump the negative effect of water being present for more time each cycle.

After longer exposure times the surface topography between the two sides got more different, with the plain side getting bigger craters and the bird droppings side keeping a relatively homogeneous surface. The porosity of the plain side was also increased during longer exposure times. For example, after 592 hours the sample had loose flakes of corrosion product that could easily break off the sample when handled.

The side of the samples that did not have bird droppings could give an idea of how the pH in the bird droppings affects the corrosion behaviour. For samples 1 and 2 the solution in the salt chamber was near neutral, but for sample 3 the solution was acidic for the last part of the exposure time. By assuming that sample 3 had the same weight as sample 2 after 334 hours, the numbers given in Table 8 could give an estimate of mass loss per hour from 334 to 592 hours. This estimate indicates that the mass loss per hour is 2 orders of magnitude higher from 334 to 592 hours than from 0 to 334 hours. With the same calculation for the side with bird droppings, the mass loss per hour is

in the same order of magnitude throughout the whole experiment. The different corrosion rates could mean that the change of pH accelerated the corrosion of the plain side of the sample, but not for the side with bird droppings. The bird droppings' pH when dry is believed to be somewhat similar to the solution at the end of the experiment, meaning the side with bird droppings has been exposed to an acidic environment the whole experiment. The bird droppings' barrier effects are therefore believed to be more beneficial than the detrimental effects of the low pH and anions in the bird droppings.

### 5.1.2 AISI 316

AISI 316 has the least corrosion resistance among the stainless steels tested. It was removed after 49 hours along with carbon steel to have the biggest chance of having a reference sample with some weight loss. Figure 9a shows there was little corrosion on the sample at the time. Table 8 shows that there was less corrosion on the 316 samples compared to the carbon steel. The difference in mass loss underlines the poor corrosion resistance of carbon steel. The side of the 316 samples that had bird droppings, showed more mass loss than the plain side. This could be because of some small deviation in the measured geometry and the actual geometry of the sample. However, by looking at the samples exposed for longer times in Figure 9 there are differences between the two sides. For these samples, there is a spotted pattern on the surface where bird droppings were present. The experience from the carbon steel was that the bird droppings had some barrier capabilities. For a passive material like the 316, this could carry some negative effects. The barrier could make a crevice, where diffusion of oxygen into the crevice could be retarded. This could facilitate localized corrosion. The increased anion concentration and lower pH underneath the bird droppings during the drying cycle will make an aggressive environment under the bird droppings. This environment could also initiate localized corrosion by degrading the protective oxide film. Leading to more mass loss under the bird droppings. Thus, based on the spotted pattern shown in Figure 9, localized corrosion is assumed to be occurring. The combination of barrier capabilities, anion concentration, and lower pH during drying, is evaluated to be detrimental for the 316 stainless steel. This is due to the self acceleration of the localized corrosion, which leads to the suspicion that the side with bird droppings will suffer from localized corrosion after longer exposure times.

### 5.1.3 22% Cr DSS

The 22% Cr duplex stainless steel (DSS) is believed to have a better corrosion resistance than the 316. This means the behaviour of the steel in Figure 10 is unexpected. The plain side for samples 1 and 3 appear to have similar corrosion behaviour based on the colour, while sample 2 has less corrosion than the two. The mass loss of the plain side of samples 1 and 3 in Table 8 is also bigger than for sample 2, which has the least amount of mass loss. Samples 2 and 3 were removed simultaneously, which makes the behaviour of the samples suspicious. The salt-spray chamber is constructed in a way so all samples should have the same environment, and based on the mass loss of other materials, the placement of the samples is believed to be insignificant. Hence, the difference in corrosion is believed to be caused by differences in the chemical composition and microstructure of the steel across the samples. Nevertheless, based on the colour and mass loss of the samples, the DSS had less corrosion after 692 hours compared to 316.

Similar to the 316, the DSS also shows some localized corrosion on the side where bird droppings were present. Both (a) and (c) in Figure 10 show a spotted pattern in varying degree. The reasoning is believed to be the same as for 316, where barrier properties, anion concentration, and

lowering of pH due to drying are facilitating localized corrosion. The effect is not visible for (b), which could be because of the higher corrosion resistance of this sample. The chemical composition of the respective samples has not been analyzed, so which of these behaviours is expected for the DSS can not be determined. If sample 2 is the correct composition to specification, the steel should benefit from the barrier properties and withstand the negative effects. If samples 1 and 3 are the correct composition, the steel could suffer from localized corrosion underneath the bird droppings.

### 5.1.4 25% Cr SDSS

Among the stainless steels in this test, the SDSS is expected to be the most corrosion-resistant due to its high amounts of chromium. In the pictures in Figure 11 the steel shows promising corrosion resistance. There is a slight colour difference between the two sides for all samples, where the plain side shows somewhat more corrosion discolouring. This difference is most likely due to the barrier capabilities of the bird droppings. Unlike the 316, and one of the DSS samples, the SDSS does not show any spotted pattern on the side with bird droppings for any samples. This underlines the corrosion resistance of this alloy, where it seems almost unaffected by nearly 700 hours in the salt-spray chamber. Based on no signs of significant corrosion after making the solution more acidic, the alloy is believed to not show significant amounts of corrosion for longer exposures.

The mass loss shown in Figure 11 shows that there is some corrosion on the samples. It is suspicious that the mass loss indicates that the SDSS has more mass loss than the DSS, both based on expected behaviour and that there was little discolouring shown in the pictures for SDSS. One reason for this could be that the SDSS has a higher density than the other materials, so a slight error in the measurements of the geometry of the samples would affect the area density more than that of e.g. carbon steel. As the samples were not cut perfectly quadratic, the exact dimensions of the samples are difficult to get just right. Thus, the reason for the mass loss is believed to be due to errors in the dimensions of the samples.

SDSS is the stainless steel with the highest corrosion resistance. With this, the effects of the bird droppings that were visible on the other stainless steel are not visible for this alloy. The pH and anion concentration is therefore believed to not be strong enough to affect the oxide layer of the SDSS. Hence, the alloy is believed to not be significantly affected by bird droppings.

### 5.1.5 Thermally sprayed aluminium

When it comes to the TSA, the corrosion between the sides shows some differences. For sample 1 in Figure 12 it appears that the plain side of the sample is not notably affected, except for some salt deposit around the edges. The side that had bird droppings show some more dissolving of the TSA. Especially close to the edges. There could be several reasons that cause more corrosion on the side with bird droppings, which all are related to the previously discussed effects. One is that the barrier capabilities of the bird droppings create a duplex coating. It is known that a duplex coating involving TSA and organic coating is a combination that is not desired [43]. The result of this is the TSA underneath the bird droppings suffers from corrosion reminding of crevice corrosion, as explained in chapter 2.3.2. Relatively large areas of TSA are dissolved under the bird droppings, and even exposing the substrate steel where the initial coating thickness was somewhat lower, i.e. sample 3 in Figure 12c. However, the biggest difference for the TSA is seen in sample 1 (Figure 12a), where the side with bird droppings shows more corrosion than the side without.

The dry bird droppings are believed to have a pH more acidic than the initial solution. Hence, the

side with bird droppings is exposed to a net lower pH than the plain side for the first 334 hours. In Table 8, samples 1 and 2 show more mass loss for the side with bird droppings than the plain side. Sample 3 was exposed for the longest time, and show a somewhat similar mass loss for both sides. The increased mass loss of the bird droppings side for samples 1 and 2 could therefore be caused by the lower pH when the bird droppings are dry. To justify this, the mass loss of sample 3 could be of importance. The corrosion rate of the plane side of sample 3 could be assumed to have increased in the last 358 hours of the experiment, i.e. after acidification of the solution. The pH of the solution could therefore be somewhat lower than that of the dry bird droppings. The samples are also exposed to high humidity longer than dry environment, meaning the plain side is exposed to low pH longer than the bird droppings side for the last 358 hours. That is for the assumption that the barrier properties of the bird droppings protect from the low-pH solution. Thus, the plain side closes the mass loss gap between the plain side and the bird dropping side in the last part of the experiment. Resulting in a lower difference between the plane side and the bird droppings side after 692 hours compared to samples 1 and 2. The most probable reason for the mass loss of the plain side is therefore pH decrease, which could indicate that the mass loss of samples 1 and 2 also is caused by lower pH. Corrosion rate per hour of exposure, similar to that done for the carbon steel, could not be done for the TSA samples 2 and 3. This is because of the difference in the initial area density of these samples. Still, it is assumed that the lowering of pH has accelerated the corrosion rate of the TSA for the last 358 hours when the solution was acidic.

When the exposure time increased, a thicker salt deposit was made on the TSA that also could have affected the corrosion rate. The thicker salt deposit could create a seal that may facilitate crevice corrosion in the same way as described with the bird droppings. Another effect of the salt deposits could occur in combination with drinking water. The local authority of Trondheim conducted a drinking water quality test in 2020 [44], which should be representative for the water used in the test. In this analysis, the amount of magnesium is 0.90 mg/L. This could result in the formation of $MgCl_2$ on the TSA surface, which is known as slightly acidic. During long exposure in the salt-spray chamber, the accumulation of magnesium on the TSA sample could result in a $MgCl_2$ concentration that is high enough to be of significance. Thus, the pH will be lowered around the salt deposits. However, as the mass loss of the plain side is much larger for 692 hours than 334 hours, the biggest reason for the increase in corrosion rate is believed to be mainly caused by the lower pH. This is because the magnesium accumulation is not believed to have accelerated for the last 358 hours in the chamber, and the effects of pH are therefore believed to trump the effects of magnesium.

The increased concentration of anions due to the bird droppings could also help with accelerating the corrosion of the TSA, as these could break down the oxide layer protecting the aluminium. Hence, there are three reasons believed to affect the corrosion of the aluminium-containing samples with bird droppings on the surface. Either individually, a combination of 2, or even all of these effects together. To confirm, or exclude, the crevice-like corrosion, the salt deposit underneath the bird droppings could be analysed to investigate if there are $AlCl_2$ present in the salt. This could help in understanding if there is an autocatalytic reaction occurring under the bird droppings. Nevertheless, the bird droppings are believed to be detrimental to the TSA coating.

### 5.1.6 EN AW 6082

EN AW 6082 aluminium alloy is frequently used in offshore applications. For example, the upper part of the helideck of platforms is often built with this or similar aluminium alloys. Therefore

the behaviour of this material is important for predicting the lifetime as these are often subject to bird droppings. After the salt-spray test, there were some differences between the sides with and without bird droppings. For all samples, there is a colour difference, where the side with bird droppings had a brown tint on the surface. This could be caused by some organic residues of the bird droppings that were left on the surface. Along with the colour difference, there are clear signs of localized corrosion for (b) and (c) in Figure 13. This could either be pitting or crevice corrosion that has occurred underneath the bird droppings. Some signs of localized corrosion could also be seen in (a) for the upper part of the bird droppings side. Similar to the stainless steels, the combination of the barrier properties, lower pH, and increased concentration of anions in the bird droppings are believed to have a detrimental effect on the aluminium.

For the samples removed after 692 hours, the plain side of the samples has a brighter colour than the sample removed after 334 hours. This is caused by aluminium oxide corrosion products that form a film on the surface. Figure 13c also shows some pitting on the plain side of the sample. This increase in corrosion product and pitting could be caused by both the longer exposure time and lowering of the pH solution. Although there is some visible corrosion on the samples, this is not reflected in the mass loss shown in Table 8. To investigate the reason for this, the largest pit shown for the right side in Figure 13b was measured. The mass loss in this pit was found to be in the magnitude of milligrams, which is less than the precision of the weight used. There was also some corrosion product that would not be removed from the surface after the corrosion-product removal. Thus, the mass increase due to the small amounts of corrosion product on the surface could be close to the mass lost in the pit and these would then cancel each other out. However, the visual evidence of the samples is sufficient to determine that the bird droppings introduce an environment that is harmful to the aluminium.

## 5.2 Vibrational spectroscopy

The vibrational spectroscopy was conducted on the samples that were exposed for the longest time in the salt-spray chamber for the respective material. These samples were already washed with water to remove salt deposits accumulating on the surface after the salt-spray chamber. This will also wash away different substances from the bird droppings, but substances that are hydrophobic or that have been anchored to the surface of the material were expected to stay on the surface. Any other cleaning, e.g. removal of the nail polish, was not completed until after the vibrational spectroscopy was finished. The spectroscopy was also done before the corrosion-product removal of the samples.

During the analysis of the samples with Raman spectroscopy, the laser proved to be able to burn organic compounds, as well as alter corrosion products to high-temp corrosion products. This was easily discovered by the microscope which showed darker colour where the laser had been hitting, or recognizable peaks of high-temp corrosion products in the spectrum. Through some trial and error, the laser power was adjusted to a value where the samples were not altered, but at the same time had enough power to get spectra with distinct peaks.

The main goal of these examinations was to investigate if any substances could affect the corrosion behaviour of the substrate material that was exposed to bird droppings. I.e looking after substances that occurred on the side with bird droppings, but not on the plain side of the sample. This quickly proved to not be the case for any of the samples, which will be discussed more in chapter 5.2.2 and

5.2.1. For wavenumbers above approximately 1750 $cm^{-1}$, it was often a lot of fluorescence in the Raman spectra for the steel samples. Therefore, the region from 1750 and up will not be evaluated for the Raman spectra of the steel samples.

### 5.2.1 FTIR spectra

FTIR spectra with gold mirror showed somewhat similar plots for all steel samples, where the peaks represented organic compounds not relevant for the corrosion behaviour of the samples. Some minor differences in the intensity could be observed in the various spectra shown in the appendix (A.1), but there are no peaks present on the bird droppings side that is not present on the plain side of the sample. Hence, it could be determined that there is no significant difference on the surface of the samples in terms of compounds that could alter the corrosion behaviour of the steel samples.

In the spectra where the plain side was used as the background, there was little difference for most samples. In these spectra, a minimum below zero means that the peak is for the plain side, while a peak above zero is for the side with bird droppings. The spectrum for aluminium with the plain side as the background is not included due to the differences between the two sides when a gold mirror was used. The spectra that showed the most peaks for the plain side as background, were the DSS and SDSS spectra. DSS shows minima at 1480, 1035 and 945 $cm^{-1}$ in Figure 35. At 945 it is most likely a C=C vibration occurring. The other two peaks could be caused by O-H and C-O vibrations, for 1480 and 1035 respectively. For SDSS (Figure 37) there are peaks both above and below zero. The one minimum below zero is at 1110 $cm^{-1}$, which could represent a C-O stretching vibration. The two peaks above zero are at 1000 and 920 $cm^{-1}$. Both of these could represent C=C bending.

The FTIR of aluminium 6082 in Figure 16 was different from the steel samples. Some peaks are not present for the side with bird droppings, and the whole spectra are also slightly higher in intensity. The higher intensity could lead to some of the peaks being masked, which could be the case for the three peaks at 2854, 2925, and 2959 $cm^{-1}$. These three bands are vibrations most likely caused by $CH_3$ and $CH_2$ [27][45]. The origin of these species is unclear, but a possibility is that these are from the storage where this material was found. This was stored with different metals, where some oil could have been present. This oil could have been transferred to the aluminium plate, and not been rinsed off during the sample preparation

Aside from the three peaks, traces of the peaks on the plain side could be seen on the bird droppings side. But with lower relative intensity. This could be caused by other bonds masking these sharper bonds. Another possibility is that the same bonds exist in various compounds, leading to a broader peak. These broad bands around 1500 $cm^{-1}$ are most likely due to C-O and C=C stretching. Hence, the surfaces of the two sides are most likely similar, except for an increased amount of C-O and C=C bonds for the side with bird droppings. The broad peaks at 1143, 1122, 983 $cm^{-1}$ are most likely aluminium hydrooxides or aluminium oxyhydrates, but it could also be $SO_4^-$ [27]. The peak is broader for the side with bird droppings, which could indicate that there are more bonds involving $SO_4^-$ on that surface. It could also indicate more aluminium corrosion products with more deviation in e.g. bond lengths. To better determine whether this is caused by corrosion product or $SO_4^-$, other measurements have to be done, e.g. x-ray diffraction. The peaks at 732 and 613 $cm^{-1}$ is most likely caused by aluminium oxide, $Al_2O_3$ [27].

### 5.2.2 Raman spectra

The spectrum provided in Figure 17 was the one for carbon steel without bird droppings. The peaks at 685, 556, 480, 399, 305, and 255 $cm^{-1}$ fit well with goethite peaks, presented in Table 1.This spectre was measured on the dark spot on the sample, shown in Figure 8c, which confirms that the spectre shows goethite, which indeed is a dark-brown corrosion product of iron. The side of the sample with bird droppings was shown in the appendix in Figure 40. This has peak at 330, 418, 530, 681, and 726, which corresponds well with akagenite ($\beta$-FeOOH) [46]. The peak at 1383 is believed to be caused by O-H vibrations for both spectra.

The 316 sample had few peaks in general. Both sides of the sample have three peaks close to 1500 $cm^{-1}$, which are organic compounds. There are some deviations in the position of these, but they are still believed to be caused by the same bonds. The plain side of the samples has a peak at 144 $cm^{-1}$, where the origin is not clear. Due to an error when acquiring the spectrum, the bird dropping side did not measure at these low wavenumbers. Therefore it is not known if this peak is present on the side of the sample with bird droppings.

The spectrum for DSS with bird droppings in Figure 43 has peaks at 445 and 615, which is believed to be caused by chromium oxide on the surface [47]. The side without bird droppings (Figure 44) has several peaks between 346 and 601 $cm^{-1}$. All of which are related to a chromium oxide film on the surface [47]. The sharp peak at 927 $cm^{-1}$ is believed to be caused by molybdenum oxide as these often have a band in the area around 950 [48].

The spectra of SDSS in Figure 45 and Figure 46 also has some peaks around 1500 $cm^{-1}$. Like the other samples, these peaks are also believed to be caused by different organic bonds, e.g. O-H, and C-O. The plain spectra of the plain side have peaks at 305, 401, 552, and 697 $cm^{-1}$, which point to different iron corrosion products, e.g. goethite and maghemite, along with chromium oxide.

The two spectra for TSA in Figure 47 and Figure 48 have many differences. The side with bird droppings has many more peaks, and the peaks are also much broader. Some peaks, e.g. at 2977 and 1340 are present at both spectra and could be caused by $CH_3$ or $CO_2$. The peaks present for the bird-dropping side of the sample have been investigated, and along with peaks representing corrosion products of aluminium, the peaks are organic bonds, such as O-H, C=C, $CH_2$, etc. None of the peaks has shown any sign of anions, or similar, which could have attached to the surface and originating from the bird droppings.

The aluminium spectra showed in Figure 49 and Figure 50 show somewhat similar spectra for wavenumbers above 1300 $cm^{-1}$. The peaks present above 1300 $cm^{-1}$ are evaluated to be different organic bonds, similar to those in the TSA spectra. The spectrum of the plain side (Figure 49) shows a peak at 1151, which most likely is due to a pseudo-boehmite structure [27]. Thus, no difference in organic compounds is found for the EN AW 6082.

## 5.3 Electrochemical experiments

In the following discussion, there will be referring to the two systems used for the electrochemical experiments. With and without bird droppings. For simplicity and less wordiness, the system without and with bird droppings will be referred to as systems A and B respectively. This also correlates with how the systems are organized in the figures.

### 5.3.1 Carbon steel

The polarization curves of carbon steel were presented in Figure 18, where the systems with and without bird droppings showed clear differences in the anodic behaviour. The most surprising difference was the passivating behaviour when bird droppings were present. The passive behaviour is indicated by the constant current density when the potential is around 0 mV followed by a sharp increase in current in the cell when the potential is approximately 200 mV. This sudden increase in current is most likely due to pitting occurring on the carbon steel. The blue and orange lines in Figure 18b also show some noise in the passive region. The noise could be caused by metastable pitting, where pitting is initiated but not able to propagate. What has caused the passivation of the carbon steel is difficult to determine. Based on the FTIR/Raman spectra for the carbon steel given in Figure 32, and 40, it appears that there is no substance in the bird droppings that have reacted or anchored to the carbon-steel surface. It could be possible that there is a substance that has a passivating property that was present on the surface of the material when both the salt-spray test and the electrochemical experiments were conducted. But when the samples from the salt-spray test were rinsed with water, this substance could have been washed away. Thus, the passivation could be caused by an increase in pH, which would move the system from active corrosion to passive corrosion in the porbaix diagram [49]. An increase in pH is not expected based on the literature on bird droppings, and no analysis has been done to verify the pH of the bird droppings. There could also be other substances causing passivation, which also could explain the decrease in corrosion rate in the salt-spray test for the side with bird droppings. These substances could then have been washed off when rinsing the samples and are therefore not identified.

The cathodic branch for the two plots in Figure 18 are very much the same. At a current density of $10^0$ the potential is slightly below -500 mV for both systems. For a slightly higher current density, it is clear that the current increase is lowered for a small region. This is most likely due to reaching the limiting current of ORR, due to the diffusion of oxygen being lower than the reaction speed of the ORR on the carbon steel surface. When the potential reaches approximately -750 mV it is most likely the hydrogen evolution reaction (HER) that causes the current to increase.

For a setup like this, it is useful to have some quantification that makes it easier to compare the setups. As previously mentioned, these numbers should be treated more like indicators, rather than definite answers. Based on the numbers given in Table 9, some predictions can be done on how the bird droppings can affect the carbon steel. The $E_{corr}$ increases by about 250 mV when the bird droppings are present. This could indicate that the carbon steel has become nobler in the presence of bird droppings in the system. The same increase in $E_{corr}$ is also seen in the polarization resistance shown in Figure 19.

The other parameter that has changed with the presence of bird droppings, is the corrosion current density. The corrosion current density is lowered by a factor of $10^2$ when there are bird droppings in the system. Resulting in a lower corrosion rate as long as the potential is held below the pitting potential. In some cases, this could be beneficial, but the introduction of the pitting mechanism could lead to more catastrophic failures. Rapid corrosion through the whole substrate and the creation of pinholes could occur when the pitting potential is exceeded. As carbon steel often is used as a structural material the areas close to the pinholes will experience a stress concentration, which could lead to premature failure of the carbon steel. There were no signs, however, of pitting on the surface of the samples exposed to the salt-spray chamber.

### 5.3.2 AISI 316

The AISI 316 stainless steel is the stainless steel with the lowest PREN among the selected materials. Thus, it is the stainless steel that is assumed to have the lowest pitting resistance. When looking at the polarization curves given in Figure 20 it is clear that there are significant changes to the system when bird droppings are present.

The measurements for system A are for a shorter potential range than for system B. The potential range should be higher, but it is long enough to see the potential of which the pitting initiates.

The pitting potential of the anodic curves is increased by nearly 500 mV when bird droppings are present. If the potential on the steel surface is higher than the potential measured at the reference electrode the difference would be even bigger. The 316 also shows less metastable pitting in the passive area of the curve for system B. Both of these effects are most likely related to increased resistance to pitting initiation. The metastable pits are pits that initiate but are unable to propagate. As there are fewer metastable pits in system B, it could indicate that the bird droppings make the 316 less prone to pitting initiation. A possible explanation of this could be the decreased amount of anions near the surface due to poor ion transport through the bird droppings.

If a shaded area, introduced in Figure 31, is drawn for the curves for 316, it seems like the amount of corrosion occurring up to 0 mV is the same for both systems. From then on system A suffers from pitting while system B corrodes actively at this potential. With these results, the bird droppings appear beneficial as the pitting initiates at a higher potential.

The cathodic branch of the two systems is not that easy to compare as the potential range for system A was set too low which means there is not much curve to compare. In the small section that is comparable, it seems like there is not too much difference between the two. The cathodic branch of system B shows an expected behaviour of the ORR reaching a diffusion limiting current before reaching the HER region. This is most likely the reason why the current has a shelf at about 0.1 $mA/cm^2$.

The $E_{corr}$ is different for the plots showing the polarization curves and polarization resistance (Figure 21). This could be due to the roughness or microstructure changes across the samples that could result in different $E_{corr}$ for different spots on the sample.

The corrosion current density has not changed much between the two systems. It has remained in the same order of magnitude, and the corrosion potential remains more or less unchanged. If it is assumed that the potential measured is lower than the real potential on the metal surface, it is safe to say that the effects that occur for 316 are beneficial in terms of corrosion behaviour in contact with bird droppings, based on the electrochemical experiments.

### 5.3.3 22% Cr DSS

The 22% Cr duplex stainless steel (DSS) is expected to have a higher pitting resistance than 316 based on the PREN given in the theory chapter (2.2). In addition, the DSS is not expected to pit at all in these conditions due to its critical pitting temperature being above room temperature.

The polarization curves shown in Figure 22 show some difference, especially on the anodic branch. For Figure 22a, which is system A, a typical passivating behaviour is shown. For the orange and the green curve, it is clear that the steel is initially in the active corrosion region, which is where the curve follows a smooth incline. This section of the curve also follows the Tafel Law. Then, in

the range of -250 mV and 0 mV, the current has a sudden drop and eventually stabilizes between 0.1 and 1 mA/cm$^2$. This is because the material passivates. The blue and the red area do not show this behaviour. It is not believed to be due to the differences in the austenite and ferrite phases. The size of these phases is usually in the micron region, while the opening of the syringe is in the millimetre region. The area that is exposed to the electrolyte is therefore assumed to be larger than the austenitic and ferritic phases in the steel. Thus, the differences in the two behaviours of the anodic lines are not expected to be caused by running the measurements on different phases. The differences are rather believed to originate from the surface roughness, the roughness of a sample could affect the OCP. For the blue and red curve in Figure 22a, the first measurement starts just above -250 mV, which will be the OCP of the system. If we draw a horizontal line on this potential, as shown in Figure 30, it is clear that the OCP for the blue and red lines is at the same potential as the orange line starts to passivate. Thus, the DSS could have OCP above the passivating potential for the blue and red curves. There is also a difference in the potential, of which the passivation starts, for the orange and green lines. The difference in passivating potential could be due to roughness on the surface, impurities, or small differences in the microstructure.

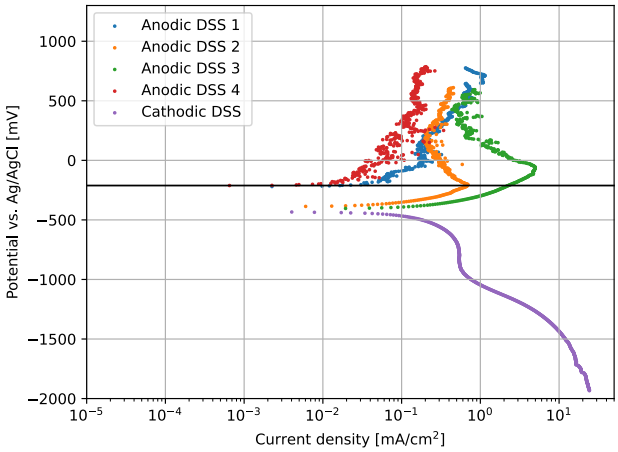


Figure 30: Polarization curve of DSS without bird droppings, with a line that compares the OCP of the red and blue line with the passivation potential for the orange line.

The polarization curves for system B shown in Figure 22b display a different behaviour than system A. One of the differences is that the measurements show no evidence of metastable pitting in system A, in contrast to system B. It also appears that the steel no longer shows a passive domain on the polarization curve. The curve changes a bit around 0 mV, to a more straight line. This could indicate that the passive region is exceeded. Meaning the steel is in the trans-passive domain, and pitting is occurring on the steel surface. If this is the case, the propagation of the pitting is slow. This could be because of the pitting initiated at an austenite/ferrite grain boundary and propagates slowly into the ferrite phase. It propagates into the ferrite phase although this is the phase that is richest in corrosion-resistant alloys, i.e. Cr and Mo [24]. As the austenite in the DSS is not yet suffering from pitting, the current density increase is not that large as the pitting propagation is slow. At the top of the blue line, the current density is starting to increase more rapidly. This could indicate that the austenite is no longer able to resist pitting, and thus, pitting is occurring on more sites. However, the measurement should be done for higher potentials to confirm this statement.

The cathodic branches for the two systems have some differences in shape. For system A, the diffusion limiting current for the ORR is below 1 $mA/cm^2$. It is also more or less vertical. System B does not show a vertical line. This could be due to differences in the roughness of the examined area, which could give different abilities to adsorb oxygen on the surface. It could also be different concentrations of oxygen in the electrolytes during the measurements.

The corrosion current density has been lowered by the addition of bird droppings. The effect is also relatively high, with a lowering by a factor of 100. However, the corrosion current density of system A is higher than 316, which is not as expected. This could be related to the suspected chemical composition across the DSS plate. The corrosion potential of system B is in the same range as the corrosion potential of the blue and red lines for system A. The orange, green and purple line for system A has a corrosion potential that is about 250 mV below the others. Based on the statistics related to this, one could assume that the corrosion potential has increased somewhat when bird droppings are added.

Whether the bird droppings are beneficial or not for the DSS is difficult to determine based on the experiments done. The electrochemical experiments suggest that there could be pitting occurring on the surface when bird droppings are present. On the other hand, the results of the salt-spray test suggest that the bird droppings act like a barrier which is beneficial in terms of corrosion resistance. The salt-spray test also raised suspicion about the chemical composition and microstructure of the samples. Thus, there should be more experiments conducted on this material to better determine the corrosion behaviour. Especially in terms of the described hypothesis on pitting in the ferrite phase. For example, polishing of the sample before polarization and post-examination in a scanning electron microscope (SEM) could be utilized to understand if pitting is occurring in the ferrite phase. The uncertainties related to the chemical composition of the samples should also be addressed as described in the discussion for the salt-spray test.

### 5.3.4 25% Cr SDSS

The 25% Cr super duplex stainless steel is the steel, among those tested, that has the highest PREN and thus, the steel with the highest expected pitting resistance. This is reflected in the polarization curves provided in, only small signs of metastable pitting for the two systems.

This steel is the one that shows the least change in the corrosion behaviour, as presented in Figure 24, in both the anodic and cathodic branches. This could be due to the high corrosion resistance of the material which makes the eventual positive and negative effects less prominent. In the salt-spray test, it was slightly less corrosion on the side that was exposed to bird droppings based on the colour difference. If anything, the material could have been nobler in system B. The measurements indicate that there is little change, but with the assumption that the measured potential is lower than the real, the SDSS could have become nobler.

The anodic branches of systems A and B have a similar shape as the anodic branches for system B with DSS. For SDSS in system B, there is a passive region when the potential is kept below approximately 100 mV. After this, it appears that there is pitting that slowly propagates in the ferrite. This proceeds until about 750 mV where the current stops to increase, before an increase above 1000 mV. The current increase is believed to be caused by pitting in both the austenite and ferrite phases. [50]

The cathodic branch of the two systems has almost the same slope until 0.1 $mA/cm^2$ is reached. At

this point, there are some differences in the transition from ORR to HER as dominant reactions. But when the transition is done, it seems like the curves are somewhat similar in the short section of the curve which is comparable.

The corrosion current density in both systems is in the same order of magnitude but a slight increase for system B, unlike the other steels. There is a slight difference, but as this is in the same domain it could be errors related to the measurements that are bigger than the differences in the corrosion behaviour. The corrosion potential has altered a bit, whereas system B has a corrosion potential of about 250 mV lower. This could be caused by a difference in the roughness of the examined areas of the sample, acidity of the bird droppings, or microstructure differences.

### 5.3.5 Thermally sprayed aluminium

TSA is a metallic coating that is widely used due to its corrosion resistance. The substrate material for the experiments was chosen to be carbon steel both because it is a combination that is commonly used in the offshore industry, and the substrate material is assumed to not affect the electrochemical reactions occurring on the surface of the TSA.

The polarization curves presented in Figure 26 give us information on the corrosion behaviour of the TSA. Aluminium is expected to have a passive film on the surface which leads to pitting at a given potential. Passive behaviour is recognized both when bird droppings are present and not present. The pitting potential is seen to increase when the bird droppings are present with 250-500 mV. The increase in pitting potential could be caused by fewer anions near the surface due to poor ion transport or substances that contribute to passivity. Unlike carbon steel, the OCP does not seem to increase significantly when bird droppings are present. This may indicate that the material has not become nobler, but the pitting potential of the TSA has increased. Both variables could also have increased due to the difference in measured and real potential.

The corrosion current density is given for both systems in Table 9. For the TSA, the bird droppings cause the corrosion current density to increase by a factor of 10. In the potential region where the aluminium is passive, there is also a difference between the two systems. The slope of the passive region in system A is steeper than in system B. The increased corrosion current density along with the more shallow slopes gives a bigger area to the left of the curves as Figure 31 highlights. The shaded area is related to the number of charges that are received from the TSA which again can be related to how many atoms have reacted and dissolved from the substrate material. The area for system A is larger than the area given by system A. Thus, more atoms get dissolved in system A, resulting in a greater corrosion rate. Based on these two polarization curves, the corrosion rate of the uniform corrosion is greater when bird droppings are present. But if the pitting potential is taken into consideration the evaluation of this case changes.

For a material that is used in a corrosive environment, one would most often desire a material that is as slowly corroding as possible. But at the same time, the occurrence of pitting could also have an effect. As discussed in the chapter on carbon steel, pitting is not desired e.g. structural parts in the installation. Thus, the increase in the pitting potential could be more beneficial than the uniform corrosion rate increase when there are bird droppings in the system, as uniform corrosion could be managed through e.g. adding a thicker coating along with frequent inspections. However, pitting is not necessarily as consequential for this coating compared to the other materials tested. If pitting occurs on this coating, the substrate material could be exposed after a short period. The substrate material used in combination with TSA is often carbon steel, which has a higher

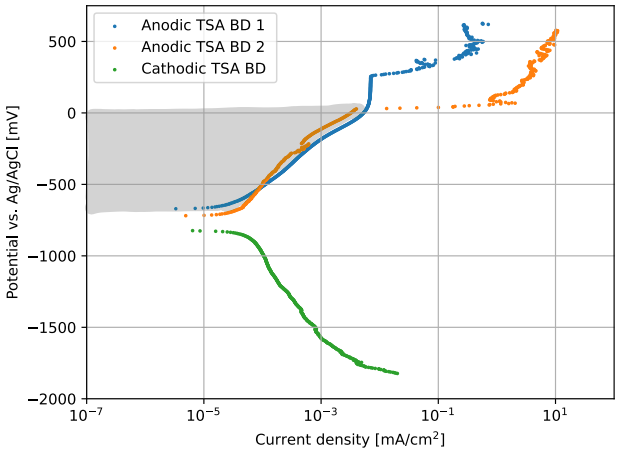


Figure 31: Polarization curves of TSA with bird droppings where the shaded area is related to the amount of dissolved metal ions.

reversible potential than the TSA, which in this case is aluminium. The effect then is that the substrate steel is protected by the TSA through cathodic protection. This will cause the TSA to corrode quicker and expose more of the substrate steel. However, the mechanical properties of the substrate steel will remain as long as it is protected by the TSA.

The two anodic branches for system A show some differences. Mainly in the OCP of the two curves, and that the slope is steeper for the blue curve. The pitting potential, however, is near identical. The reason behind the differences in the OCP could be due to local differences in the roughness of the measured area, impurities in the microstructure for the TSA, or impurities from the application of the TSA. It could also be because the sealer that is on top of the TSA is different for the two areas used for the measurements. When the polarization resistance is taken into account, there are still an equal amount of $E_{corr}$ potentials in the range of -700 mV as -900 mV. Which of these regions is most reliable is therefore not possible to determine.

The pitting of the two anodic curves for system B initiates at different potentials, one being around 0 mV and the other at about 250 mV. After the pitting has been initiated, the current density of the orange curve is increasing more than for the blue curve and also maintains a higher current density. This could also be because of local differences in the roughness of the sample surface, and the possibility of impurities in the microstructure. The anion concentration in the bird droppings could also be different for the two measurements.

The cathodic branch of the two plots has some differences. The slope is different for the two, as well as the cathodic branch of Figure 26a shows an increase in current at approximately -1250 mV. The curve for system B is somewhat choppy, which is a characteristic experienced to be related to bird droppings that are too dry. The cathodic curve for system B should therefore have been run again with more water in the bird droppings. This was discovered after concluding the experimental part and has therefore not been done.

Based on these aspects, the electrochemical results are not enough to evaluate if the presence of bird droppings is beneficial or not. Thus, the results from the salt-spray test can be used to get a better understanding of the behaviour.

### 5.3.6 EN AW 6082

Before the experiments started, the TSA and 6082 were expected to have more or less the same properties as the main component in both materials is aluminium. There are some similarities in the polarization curves of the two materials, but also some differences.

The anodic branch of system A is showing a corrosion behaviour which is as expected for this material. For both the blue and orange curves the material has a pitting potential at about -550 mV. The passive domain is not visible which could be related to the chloride content in the solution, as the chloride content makes the passive region less visible [33]. In comparison, the passive region for system B is much more visible, and following this is a pitting potential that is raised to around 0 mV. The increase could be caused by a lower concentration of anions near the surface or substances that could strengthen the passive film. For system B the aluminium shows a more distinct Tafel-slope in the region around $10^{-3}$ mA/cm$^2$ compared to system A. When the potential increases further, system B shows a clear passivation behaviour. After the pitting has been initiated, the current density for both systems A and B is somewhat similar around 10 mA/cm$^2$.

A similarity of the TSA and 6082 is that the difference in current density between the start and the end of the experiments is larger than that of the different steel alloys examined. For the 6082 in system A, this is mainly because of the large increase of current density when the pitting propagates, but in system B the current density is changing by 3 orders of magnitude for the anodic part before the pitting potential. There are differences in the OCP of the TSA and 6082. The 6082 had a much smoother surface than the TSA because of the differences in how these materials are produced. The rougher surface of the TSA should, as discussed earlier, raise the OCP of the material. However, Figure 26 and Figure 28 show that the TSA has a lower OCP. An explanation of this could be that the microstructure of the two materials is different, which makes the OCP differ. The additional alloying elements in 6082 could also precipitate towards the metal surface which also could change the OCP of this material.

The cathodic branches of the two 6082 systems are similar in terms of the shape of the curve, but the curve for system B is shifted up and left in the diagram. The starting position of the measurement for system B is also above those for the anodic branches. This could be because of some local differences between the spots where the measurements were done, i.e. local roughness difference or impurities in the microstructure. Based on this observation, the cathodic branch of system B was considered an outlier in terms of OCP and shape. The result of this was that the anodic branches were used to establish the values presented in Table 9 for system B.

The corrosion current density of the two systems is different, where the corrosion current density was lowered by a factor of about 10 with the presence of bird droppings. Based on the electrochemical experiments, the addition of bird droppings to the 6082 alloys appears to be beneficial due to the increased pitting potential and lowered corrosion current density.

## 5.4 Summary

The two analyzing methods have provided a lot of information on the topic, but the results from the methods seem to be conflicting. Results from the salt-chamber test suggest that the effect of bird droppings is detrimental for most materials, with more localized corrosion for the passive materials

when bird droppings were present. The results from the electrochemical experiments suggest beneficial effects for most materials, where the pitting potential was increased for most materials when bird droppings were present. Corrosion current density was lowered for most materials when bird droppings were present. The conflicting results could indicate that the main reason for the corrosion in the salt-spray chamber could be caused by the pH drop during the drying of the bird droppings, and the barrier properties. The lowered ion transport due to the bird droppings could have lowered the concentration of anions on the metal surface, which could explain the beneficial effects seen in the electrochemical experiments. The pH and barrier properties are assumed to not make a significant difference in the electrochemical measurements. The results from the salt-spray chamber are believed to be caused by mainly the pH and barrier properties of the bird droppings. These effects are evaluated to trump the beneficial effects seen in the electrochemical measurements, thus, weighing more in the overall evaluation. In addition, the passivation seen for the carbon steel could have been caused by an increase in the pH, but this is not confirmed. Increased pH would also confirm most of the beneficial effects seen in the electrochemical experiments. Thus, the barrier properties of the bird droppings could be the reason for the localized corrosion seen in the salt-spray chamber.

For stainless steels and EN AW 6082, the addition of bird droppings led to an increased possibility of localized corrosion, leading to a less desirable corrosion behaviour. The TSA coating proved to suffer from corrosion reminding of crevice corrosion underneath the bird droppings, where the rapid dissolving of the TSA is suspected as a possible reaction in service. The TSA also proved to be negatively affected by the bird droppings in the electrochemical experiments, with a higher corrosion current density. The carbon steel appeared to benefit from the bird droppings' presence, where the barrier properties led to less dissolving of the iron oxide and ultimately less mass loss due to corrosion. The carbon steel also showed passivating properties when bird droppings were present. The SDSS seem somewhat unaffected by the bird droppings by the tests done.

## 5.5 Review of methods

### 5.5.1 Review of salt-spray method

When the experiment was planned, it stood between two standard methods for salt-spray testing. One of which was the cyclic ASTM G85 standard, and the other where ASTM B117, which is a constant spraying test. There were two main reasons why the G85 was chosen. The first is that the cycles of rain, drying, and high humidity meant that the samples would be exposed to environments that they will be exposed to in real life. The other reason is that the G85 was assumed to make the samples corrode faster because the salt concentration of the solution present on the sample surface will be very high when the solution is drying up. The samples' corrosion rate will be largest for the limiting case where the amount of water on the surface reaches zero, both during wetting and drying. The pH of the bird droppings is also believed to become lower when it is dry. Hence, by using the cyclic program, there will be both a lowering in pH and an increase in salt concentration in the chamber. To produce the solution used in the test, drinking water was used instead of distilled water because of the large volume needed to run the test for nearly 700 hours.

The sample preparation was done to remove the majority of contamination on the surface, as well as remove the edge effects that could change the corrosion behaviour. This was done by applying

clear nail polish to the sides of the samples, even though this could facilitate crevice corrosion around the edges. No nail polish was applied to the back of the samples, as this was presumed to not corrode significantly as there would be low amounts of water on the backside during the exposure. But, with high humidity in the chamber, there will be a thin film of water on the backside that could cause the backside to corrode. For the stainless steels, the effect proved to not be significant, but the carbon steel showed some corrosion on the backside. The TSA samples also showed some corrosion on the backside as the substrate material for these was carbon steel. In the real-world scenario, the bird droppings will most likely be present on e.g. a spool or other closed equipment, where only the externals are exposed to the environment, and the internals are exposed to e.g. water. For the best understanding of the corrosion behaviour of the externals, the backside of the samples should, with the best effort, be protected from the environment in the chamber. In this way, the samples would ideally corrode only on the upper side, and the material loss over time would be easier to establish without error. Thus, the material loss in Table 8 will have some errors, especially for carbon steel and TSA samples. The surfaces of the samples were not polished or altered in any way to have a surface similar to what the materials would have in service. However, EN AW 6082 is often anodized to increase its corrosion resistance. This was not done for the samples in the test, which means there could be slight differences between the corrosion behaviour of these samples and the parts used in offshore, and onshore applications.

Regarding the placement of the bird droppings on the samples, there were two options. One of which was to have quadratic samples where one was with bird droppings and the other was without. Resulting in double the amounts of samples, but each sample being smaller than the rectangular ones used. This option was not used because it would not give the intersection between bird droppings and no bird droppings. Rectangular samples with bird droppings spread across half of the topside surface were therefore the preferred method.

### 5.5.2 Review of electrochemical method

The method used in the electrochemical experiments was an unconventional setup with both positive and negative sides. The positive side of this method is that it is quick to use. It is also beneficial that the tip of the syringe could be moved around on different spots of the metal surface. Thus, the measurements could be done in a new spot for each experiment. Another positive to this method is that the syringe is small, which leads to a low volume of electrolyte needed for each experiment. Decreased consumption of electrolyte both lowers the amount of time spent for creating different solutions and reduced costs related to chemicals that are needed for the respective solution. The ability to fill the syringe tip with bird droppings is probably the biggest advantage of this setup, which makes it possible to run electrochemical experiments on a metal surface covered by bird droppings.

The first negative side of the method is that the electrolyte could dry out during the experiments, which caused a loss of electric contact. This could be mitigated by not having the setup in a fume hood as the airflow would be lower. This would not be possible as the odour caused by the bird droppings would be unpleasant without a fume hood. For other types of experiments, the setup could be moved out of the fume hood to lower the airflow. It was experienced that a lower distance between syringe tip and metal sample mitigated the problem. A similar problem existed for the bird droppings, which could dry out during experiments and cause high resistance or loss of contact. Both of these problems were possible to manage after some practice of the method, i.e. having the syringe as low to the sample as possible without it touching and having the right initial consistency

of the bird droppings. Along with the practical difficulties, there are also some challenges related to mechanics happening in the syringe. Without bird droppings, the dissolved metal ions will have limited transport in the tip of the syringe and the ions could accumulate in the lower part of the syringe, especially the syringe tip. For the experiments that were run with bird droppings, the flow of dissolved iron ions would be even lower. Thus, the charge around the reference electrode will be different from the potential at the metal surface and therefore the potential measured is not the same as the true potential at the surface of the metal. However, as there is no reason to think that the ion transport is increased when bird droppings are present in the syringe tip, it is safe to assume that the measured potential is lower than the real potential of the metal surface. Low ion transport could lead to an IR-drop when there is an electrical current in the system. As the resistance of the systems is not measured, there has not been done IR-drop correction on the curves provided in the results. The decreased ion transport could also affect the number of anions present near the surface of the respective material. The initial anion concentration in the bird droppings is 4%, while the seawater solution has an ion concentration of 3.5%. But during the experiment, the concentration for system A could decrease and change the corrosion behaviour of the system.

Along with the challenges related to the setup, there are also some aspects of the procedure that proved to give challenges in analyzing the data. Comparison of the corrosion behaviour of the materials would probably be easier if the surfaces were polished. The thought behind this decision was that the roughness of the samples was uniform over the whole sample surface and that the surface roughness for the samples would be similar to the materials used in service. This is also something stressed by Sendriks [19], who states that the sample to be tested should have the same surface properties as it would have in service. The fact that the increase in surface roughness would lead to a bigger statistical deviation of the result was not taken into account. The increased statistical deviation is because the roughness of the samples could help passive materials to initiate the pitting process easier as the electrolyte would be close to stagnant in the microscopical pits that are present on the surface. The OCP of the passive samples would also fluctuate more due to the roughness, as there is a bigger chance of meta-stable pitting occurring in these already-existing pits. The increase in deviation due to the surface roughness would again lead to less reliable data, and more challenging to suggest a solid conclusion. If the samples were polished it would be easier to compare the corrosion behaviour of the different materials, with and without bird droppings. Corrosion behaviour across materials would also be easier. The deviation in the polarization resistance measurements may have been mitigated if the surface of the samples were smoother. Polarization resistance measurements with less deviation could give the electrochemical experiments more credibility.

The pH of the electrolyte solution was a bit higher (8.9) than 8.2 as the standard, used for the solution, suggested. According to the introduced theory, an increase in pH will lead to an increase in the potential of pit initiation for stainless steels. However, some change in the pH will also lead to a change in which region of the Porbaix-diagram the system is representing. The effect is unknown, as the activity of the metal ions is not estimated, but we can assume that for an activity near 1 there will only be a minor change for both iron and aluminium.

As discussed in the chapter on the salt spray chamber, the pH of the bird droppings drops as the droppings dry out. This effect is something that is not possible to investigate in the electrochemical experiments, as moisture in the bird droppings is crucial for keeping electrical contact in the cell. Therefore, the effect of the pH change the bird droppings introduce is not represented in these

results. A small lowering in pH for system A could, however, be assumed. The barrier properties of the droppings would not be possible to determine with the electrochemical measurements done.

Having discussed some of the challenges the method and procedure give to the interpretation of the results, it is clear that there are aspects of the experiments that should have been done differently. Thus, the results achieved in the experiments should be considered thereafter. Most of the polarisation resistance curves give a very high resistance, which again gives a very low corrosion current density when using the Stern-Geary equation. The deviation of the resistance was also very high. For example, the resistance of DSS ranged from 90M$\Omega$cm$^2$ to 6k$\Omega$cm$^2$ when bird droppings were present. This deviation is higher than tolerated. Thus, these plots will not be discussed with a focus on the current density. The corrosion potential will be used in some of the discussions. The reason why the current for the polarization resistance is very low for most of the curves, and why the deviation is so high, is not fully understood. It could be due to the small currents as the exposed area is small. Thus, the currents could be smaller than the precision of the potentiostat. The surface of the samples could also introduce statistical differences.

# 6 Conclusion & further work

The corrosion behavior of different materials used in offshore applications has been investigated in the presence of bird droppings. Two parallel testing methods have been used to understand the corrosion behaviour of these materials. These methods were salt-spray tests and electrochemical experiments. A proposal for an electrochemical testing method for bird droppings on the surface of a material has also been given. The results from the electrochemical method were conflicting with the salt-spray test. The conclusions of the corrosion behaviour of the metals based on the experiments that have been conducted are:

- Carbon steel benefits from the presence of bird droppings with a lower mass loss and dense corrosion product due to the barrier capabilities of the bird droppings. In electrochemical measurements, the material showed passivating behaviour with the presence of bird droppings.
- AISI 316 has an increased amount of localized corrosion underneath the bird droppings in the salt-spray chamber, which could lead to more catastrophic failures than uniform corrosion. Electrochemical experiments showed an increase in pitting potential when bird droppings were present.
- 22% Cr duplex stainless steel had some deviation between the samples which introduced an uncertainty related to the corrosion behavior. The steel has either similar behavior as AISI 316 or more corrosion resistance that leads to less localized corrosion resistance. For the latter, the steel is not significantly affected by the bird droppings.
- 25% Cr super duplex stainless steel shows a behaviour that is nearly unaffected by the bird droppings. Both the salt-spray testing electrochemical experiments prove little change in the behavior of the steel.
- Thermally sprayed aluminium (TSA) on steel also suffers from localized corrosion under the bird droppings. This could be caused by a crevice-like reaction that occurs due to barrier properties of the bird droppings in a combination of lower pH. TSA is evaluated to be one of the materials that suffer the most, of those tested, with the presence of bird droppings.
- EN AW 6082 suffers from localized corrosion underneath the bird droppings. The effect was more severe than for the AISI 316, where relatively large pits were made during the salt spray test. Bird droppings are evaluated to be detrimental to the aluminium alloy despite the increase in pitting potential shown in the electrochemical experiments.

To better understand how the bird droppings affect the corrosion of different materials, and open opportunities to mitigate the effect there are some suggestions on how to achieve this.

- Electrochemical impedance spectroscopy (EIS) to establish knowledge of the barrier capabilities of the bird droppings.
- Analyse the duplex stainless steel samples to investigate if there is a difference in chemical composition across the samples.
- Analyse the composition of the salt deposits accumulating on the surface of the TSA. This could help to determine if the TSA corrodes due to corrosion mechanism reminding of crevice corrosion or not.

- An improved and more sophisticated method to perform electrochemical measurements which has fewer uncertainties attached, such as Kelvin probe measurements that could show proof of crevice-like effects.
- Polished surface of the samples to better isolate the corrosion behavior of the different materials and eliminate statistical deviations.
- Investigate different coatings, metallic, or organic, to test if any coatings can withstand the bird droppings better than TSA.
- A real-life experiment that spans over, at least, one year to investigate the real-life effects and determine the different material losses with and without bird droppings.
- New experiments with sea-bird droppings to understand if its effect is the same as the droppings from chicken.
- Thorough investigation of the passivation of the carbon steel, to determine if the pH is increasing or if substances in the bird droppings passivates the material.

# Bibliography


[1] H. Yari, M. Mohseni and B. Ramezanzadeh, 'A mechanistic study of degradation of a typical automotive clearcoat caused by bird droppings', *Journal of Coatings Technology and Research*, vol. 8, no. 1, pp. 83–95, 1st Jan. 2011, ISSN: 1935-3804. DOI: 10.1007/s11998-010-9273-2. (visited on 15th Sep. 2021).

[2] H. Yari, M. Mohseni, B. Ramezanzadeh and N. Naderi, 'Use of analytical techniques to reveal the influence of chemical structure of clearcoat on its biological degradation caused by bird-droppings', *Progress in Organic Coatings*, vol. 66, no. 3, pp. 281–290, Nov. 2009, ISSN: 03009440. DOI: 10.1016/j.porgcoat.2009.08.003. (visited on 30th Aug. 2021).

[3] B. Ramezanzadeh, M. Mohseni, H. Yari and S. Sabbaghian, 'An evaluation of an automotive clear coat performance exposed to bird droppings under different testing approaches', *Progress in Organic Coatings*, vol. 66, no. 2, pp. 149–160, 1st Oct. 2009, ISSN: 0300-9440. DOI: 10.1016/j.porgcoat.2009.06.010. (visited on 30th Aug. 2021).

[4] E. Bernardi, D. J. Bowden, P. Brimblecombe, H. Kenneally and L. Morselli, 'The effect of uric acid on outdoor copper and bronze', *Science of The Total Environment*, vol. 407, no. 7, pp. 2383–2389, 15th Mar. 2009, ISSN: 0048-9697. DOI: 10.1016/j.scitotenv.2008.12.014. (visited on 27th May 2022).

[5] K. Balogh, Z. Slížková and K. Kreislová, 'Research on effects of bird excrement on metal materials copper and bronze', vol. 2017, p. 13, 2017.

[6] C. P. Huang and G. Lavenburg, 'Impacts of bird droppings and deicing salts on highway structures: Monitoring, diagnosis, prevention', p. 24, 2011.

[7] P. Tiano, 'Biodegradation of cultural heritage: Decay mechanisms and control methods', *Biodegradation of Cultural Heritage: Decay Mechanisms and Control Methods*, pp. 7–12, 2002.

[8] M. Gömez-Heras, D. Benavente, M. Á. De Buergo and R. Fort, 'Soluble salt minerals from pigeon droppings as potential contributors to the decay of stone based cultural heritage', *European Journal of Mineralogy*, vol. 16, no. 3, pp. 505–509, 1st May 2004, ISSN: 0935-1221. DOI: 10.1127/0935-1221/2004/0016-0505. (visited on 30th May 2022).

[9] S. Christensen-Dalsgaard, N. Dehnhard, B. Moe, G. H. R. Systad and A. Follestad, *Unmanned installations and birds. A desktop study on how to minimize area of conflict*. Norwegian Institute for Nature Research., 2019, Accepted: 2019-11-27T14:48:05Z ISSN: 1504-3312 Publication Title: 47, ISBN: 978-82-426-3485-6. (visited on 30th Aug. 2021).

[10] P. Szpak, J.-F. Millaire, C. D. White and F. J. Longstaffe, 'Influence of seabird guano and camelid dung fertilization on the nitrogen isotopic composition of field-grown maize (zea mays)', *Journal of Archaeological Science*, vol. 39, no. 12, pp. 3721–3740, 1st Dec. 2012, ISSN: 0305-4403. DOI: 10.1016/j.jas.2012.06.035. (visited on 22nd Oct. 2021).

[11] S. De La Peña-Lastra, 'Seabird droppings: Effects on a global and local level', *Science of The Total Environment*, vol. 754, p. 142 148, 1st Feb. 2021, ISSN: 0048-9697. DOI: 10.1016/j.scitotenv.2020.142148. (visited on 22nd Nov. 2021).

[12] D. H. R. Spennemann and M. J. Watson, 'Experimental studies on the impact of bird excreta on architectural metals', *APT Bulletin: The Journal of Preservation Technology*, vol. 49, no. 1, pp. 19–28, 2018, Publisher: Association for Preservation Technology International (APT), ISSN: 0848-8525. (visited on 27th May 2022).

[13] R. Shahack-Gross, F. Berna, P. Karkanas and S. Weiner, 'Bat guano and preservation of archaeological remains in cave sites', *Journal of Archaeological Science*, vol. 31, no. 9, pp. 1259–1272, 1st Sep. 2004, ISSN: 0305-4403. DOI: 10.1016/j.jas.2004.02.004. (visited on 29th May 2022).

[14] C. M. Wurster, N. Munksgaard, C. Zwart and M. Bird, 'The biogeochemistry of insectivorous cave guano: A case study from insular southeast asia', *Biogeochemistry*, vol. 124, no. 1, pp. 163–175, 1st May 2015, ISSN: 1573-515X. DOI: 10.1007/s10533-015-0089-0. (visited on 22nd Nov. 2021).

[15] B. Cámara, M. De Buergo, R. Fort *et al.*, 'Anthropic effect on the lichen colonization in building stones from cultural heritage', *Periodico di Mineralogia*, vol. 84, no. 3, pp. 539–552, 2015, ISSN: 0369-8963. DOI: 10.2451/2015PM0030.

[16] 'NORSOK standard m-001: Material selection', NTS, Oslo, Norway, 2002.

[17] 'NORSOK standadrd m-121: Aluminium structural material', NTS, Oslo, Norway, 2015.

[18] C. Holager, R. Johnsen and K. Nisancioglu, 'Corrosion of thermally sprayed aluminum in flowing seawater', presented at the Corrosion 2015, OnePetro, 15th Mar. 2015. (visited on 29th May 2022).

[19] J. A. Sendriks, *Corrosion of Stainless Steels, 2nd Edition — Wiley*, 2nd ed. John Wiley & Sons, 1996, ISBN: 978-0-471-00792-0. (visited on 26th May 2022).

[20] H. Bhadeshia and R. Honeycombe, 'Stainless steel', in *Steels: Microstructures and properties*, Fourth edition, Elsevier Ltd., 2017, pp. 343–376, ISBN: 978-0-08-100270-4.

[21] M. Stratman and G. Frankel, *Encyclopedia of Electrochemistry. Volume 4. Corrosion and Oxide Films*, in collab. with A. J. Bard. Wiley-VCH GmbH & Co. KGaA, 2003, ISBN: 3-527-30396-0.

[22] Z. A. Foroulis and M. J. Thubrikar, 'A contribution to the study of the critical pitting potential of oxide covered aluminum in aqueous chloride solutions', *Materials and Corrosion*, vol. 26, no. 5, pp. 350–355, 1975, ISSN: 1521-4176. DOI: 10.1002/maco.19750260505. (visited on 9th Jun. 2022).

[23] H. Bhadeshia and R. Honeycombe, 'Duplex and ferritic stainless steels', in *Steels: Microstructures and properties*, Fourth edition, Elsevier Ltd., 2017, pp. 362–366, ISBN: 978-0-08-100270-4.

[24] K. Siow, T. Song and J. Qiu, 'Pitting corrosion of duplex stainless steels', *Anti-Corrosion Methods and Materials*, vol. 48, no. 1, pp. 31–37, 1st Jan. 2001, Publisher: MCB UP Ltd, ISSN: 0003-5599. DOI: 10.1108/00035590110365309. (visited on 28th May 2022).

[25] 'Introduction to thermal spray coatings', in *Future Development of Thermal Spray Coatings*, N. Espallargas, Ed., Woodhead Publishing, 1st Jan. 2015, pp. 1–13, ISBN: 978-0-85709-769-9. DOI: 10.1016/B978-0-85709-769-9.00001-4. (visited on 30th May 2022).

[26] P. V. Thomas, V. Ramakrishnan and V. K. Vaidyan, 'Oxidation studies of aluminum thin films by raman spectroscopy', *Thin Solid Films*, vol. 170, no. 1, pp. 35–40, 1st Mar. 1989, ISSN: 0040-6090. DOI: 10.1016/0040-6090(89)90619-6. (visited on 30th May 2022).

[27] F. Fondeur and J. L. Koenig, 'FT-IR characterization of the surface of aluminum as a result of chemical treatment', *The Journal of Adhesion*, vol. 40, no. 2, pp. 189–205, 1st May 1993, ISSN: 0021-8464. DOI: 10.1080/00218469308031284. (visited on 29th May 2022).

[28] K. B. Oldman, *Electrochemical Science and Technology - Fundamentals and Applications*, in collab. with J. C. Myland and A. M. Bond. John Wiley & Sons, 2012, ISBN: 978-0-470-71085-2.

[29] E. Bardal, *Corrosion and protection*. London ; New York: Springer, 2004, 315 pp., ISBN: 978-1-85233-758-2.

[30] O. Ø. Knudsen, T. Rogne and T. Rossland, 'Rapid degradation of painted TSA', presented at the Corrosion 2004, OnePetro, 28th Mar. 2004. [Online]. Available: https://onepetro.org/NACECORR/proceedings/CORR04/All-CORR04/NACE-04023/114949 (visited on 18th Mar. 2022).

[31] B. Zaid, D. Saidi, A. Benzaid and S. Hadji, 'Effects of pH and chloride concentration on pitting corrosion of AA6061 aluminum alloy', *Corrosion Science*, vol. 50, no. 7, pp. 1841–1847, 1st Jul. 2008, ISSN: 0010-938X. DOI: 10.1016/j.corsci.2008.03.006. (visited on 26th May 2022).

[32] C. Dong, H. Luo, K. Xiao, T. Sun, Q. Liu and X. Li, 'Effect of temperature and cl-concentration on pitting of 2205 duplex stainless steel', *Journal of Wuhan University of Technology-Mater. Sci. Ed.*, vol. 26, no. 4, pp. 641–647, 1st Aug. 2011, ISSN: 1993-0437. DOI: 10.1007/s11595-011-0283-4. (visited on 26th May 2022).

[33] D. Cicolin, M. Trueba and S. P. Trasatti, 'Effect of chloride concentration, pH and dissolved oxygen, on the repassivation of 6082-t6 al alloy', *Electrochimica Acta*, vol. 124, pp. 27–35, 1st Apr. 2014, ISSN: 0013-4686. DOI: 10.1016/j.electacta.2013.09.003. (visited on 26th May 2022).

[34] Y. Yi, P. Cho, A. Al Zaabi, Y. Addad and C. Jang, 'Potentiodynamic polarization behaviour of AISI type 316 stainless steel in NaCl solution', *Corrosion Science*, vol. 74, pp. 92–97, 1st Sep. 2013, ISSN: 0010-938X. DOI: 10.1016/j.corsci.2013.04.028. (visited on 29th May 2022).

[35] P. Vandenabeele, *Practical Raman Spectroscopy – An Introduction*, 1st ed. John Wiley & Sons, Ltd, 2013, ISBN: 1-119-96129-7. [Online]. Available: https://onlinelibrary.wiley.com/doi/10.1002/9781119961284 (visited on 12th Jun. 2022).

[36] 'How an FTIR spectrometer operates', Chemistry LibreTexts. (2nd Oct. 2013), [Online]. Available: https://chem.libretexts.org/Bookshelves/Physical_and_Theoretical_Chemistry_Textbook_Maps/Supplemental_Modules_(Physical_and_Theoretical_Chemistry)/Spectroscopy/Vibrational_Spectroscopy/Infrared_Spectroscopy/How_an_FTIR_Spectrometer_Operates (visited on 12th Jun. 2022).

[37] M. Hanesch, 'Raman spectroscopy of iron oxides and (oxy)hydroxides at low laser power and possible applications in environmental magnetic studies', *Geophysical Journal International*, vol. 177, no. 3, pp. 941–948, 2009, ISSN: 1365-246X. DOI: 10.1111/j.1365-246X.2009.04122.x. (visited on 26th May 2022).

[38] G. Genchev and A. Erbe, 'Raman spectroscopy of mackinawite FeS in anodic iron sulfide corrosion products', *Journal of The Electrochemical Society*, vol. 163, no. 6, p. C333, 25th Mar. 2016, Publisher: IOP Publishing, ISSN: 1945-7111. DOI: 10.1149/2.1151606jes. (visited on 29th May 2022).

[39] 'Aluminium alloy 6082'. (), [Online]. Available: https://www.aalco.co.uk/datasheets/Aluminium-Alloy_6082-T6~T651_148.ashx (visited on 26th May 2022).

[40] 'ASTM g85-19, standard practice for modified salt spray (fog) testing.', ASTM International, West Conshohocken, 2019.

[41] 'ASTM g1-03, standard practice for preparing, cleaning, and evaluating corrosion test specimens', ASTM International, West Conshohocken, 2017.

[42] 'ASTM standard d1141-98, standard practice for the preparation of substitute ocean water', ASTM International, West Conshohocken, 1998.

[43] O. Ø. Knudsen and A. Forsgren, 'Protection mechanisms of organic coatings', in *Corrosion Control Through Organic Coatings*, 2nd ed., CRC Press, 2017, ISBN: 978-1-4987-6072-0.

[44] 'Drikkevannskvalitet', Trondheim kommune. (2020), [Online]. Available: https://www.trondheim.kommune.no/tema/veg-vann-og-avlop/vann-og-avlop/om-vann-og-avlop/drikkevannskvalitet/ (visited on 28th May 2022).

[45] W. Durnie, B. Kinsella, R. de Marco and A. Jefferson, 'A study of the adsorption properties of commercial carbon dioxide corrosion inhibitor formulations', *Journal of Applied Electrochemistry*, vol. 31, no. 11, pp. 1221–1226, 1st Nov. 2001, ISSN: 1572-8838. DOI: 10.1023/A:1012716911305. (visited on 28th May 2022).

[46] S. J. Oh, D. Cook and H. Townsend, 'Characterization of iron oxides commonly formed as corrosion products on steel', *Hyperfine Interactions*, vol. 112, no. 1, pp. 59–66, 1st Dec. 1998, ISSN: 1572-9540. DOI: 10.1023/A:1011076308501. (visited on 31st May 2022).

[47] R. L. Farrow, P. L. Mattern and A. S. Nagelberg, 'Characterization of surface oxides by raman spectroscopy', *Applied Physics Letters*, vol. 36, no. 3, pp. 212–214, Feb. 1980, Publisher: American Institute of Physics, ISSN: 0003-6951. DOI: 10.1063/1.91429. (visited on 31st May 2022).

[48] G. Mestl and T. K. K. Srinivasan, 'Raman spectroscopy of monolayer-type catalysts: Supported molybdenum oxides', *Catalysis Reviews*, vol. 40, no. 4, pp. 451–570, 1st Nov. 1998, ISSN: 0161-4940. DOI: 10.1080/01614949808007114. (visited on 31st May 2022).

[49] *Pourbaix diagram*, in *Wikipedia*, Page Version ID: 1071998418, 15th Feb. 2022. [Online]. Available: https://en.wikipedia.org/w/index.php?title=Pourbaix_diagram&oldid=1071998418 (visited on 12th Jun. 2022).

[50] H. Luo, X. G. Li, C. F. Dong and K. Xiao, 'Effect of solution treatment on pitting behavior of 2205 duplex stainless steel', *Arabian Journal of Chemistry*, vol. 10, S90–S94, 1st Feb. 2017, ISSN: 1878-5352. DOI: 10.1016/j.arabjc.2012.06.011. (visited on 4th Jun. 2022).

# A Appendix

## A.1 Spectra from FTIR spectroscopy

In this section, the rest of the FTIR spectra is found. All of which shows that there are small differences between the sides with and without bird droppings.

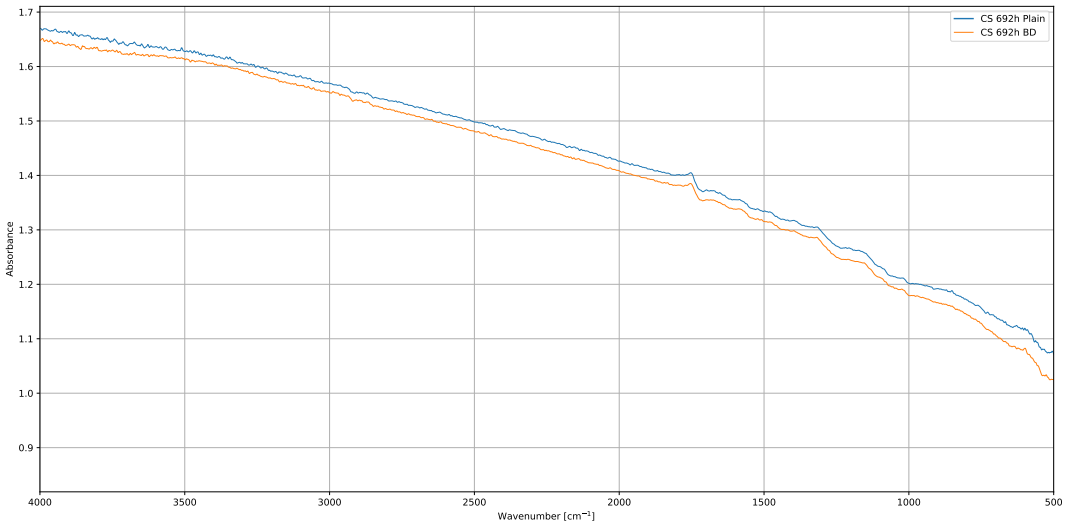


Figure 32: Comparison of the FTIR spectra for the carbon steel sample, with and without bird droppings, that was in the salt spray test for 592h. The background for these spectra is gold mirror.

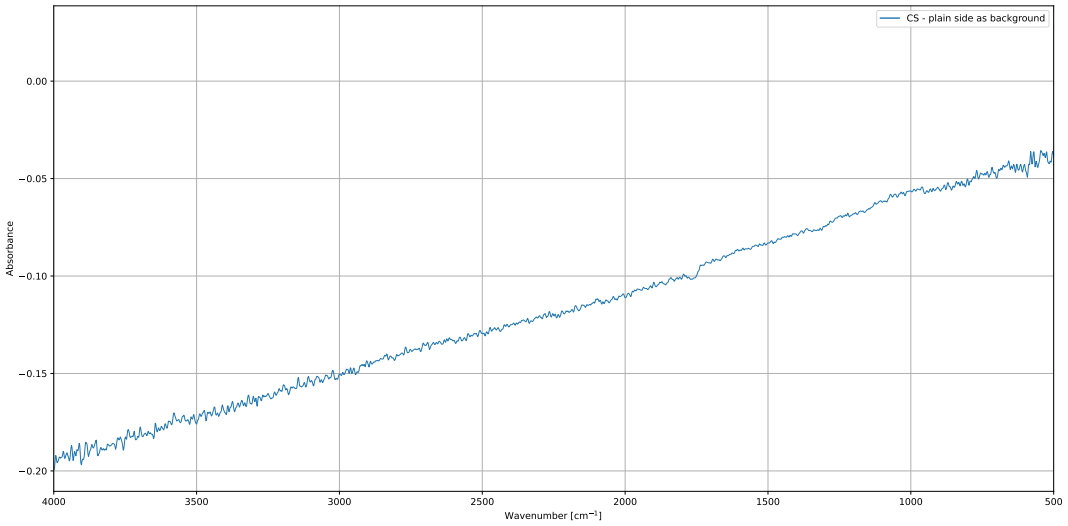


Figure 33: Spectra of the carbon steel when the plain side of the sample was used as background

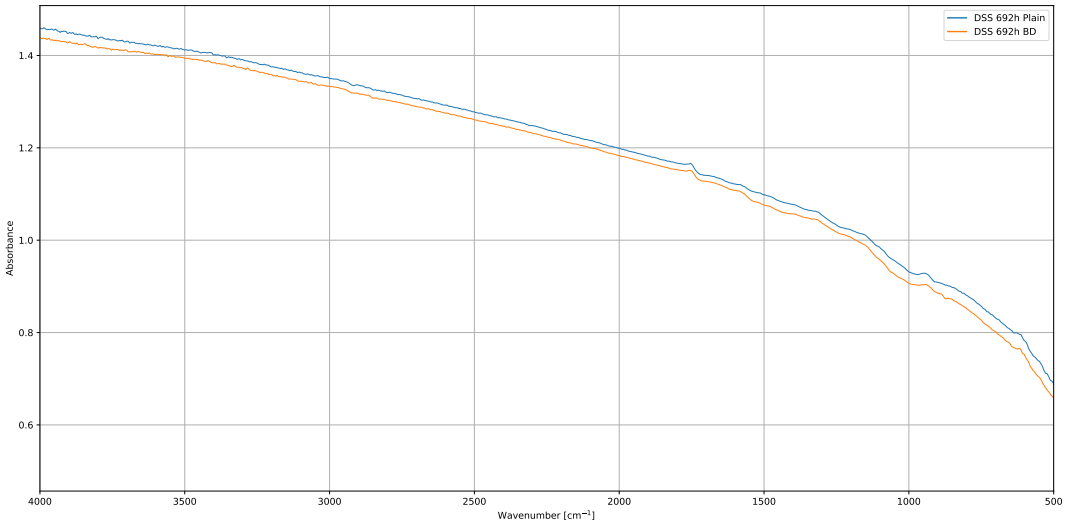


Figure 34: Comparison of the FTIR spectra for the DSS sample, with and without bird droppings, that was in the salt spray test for 692h

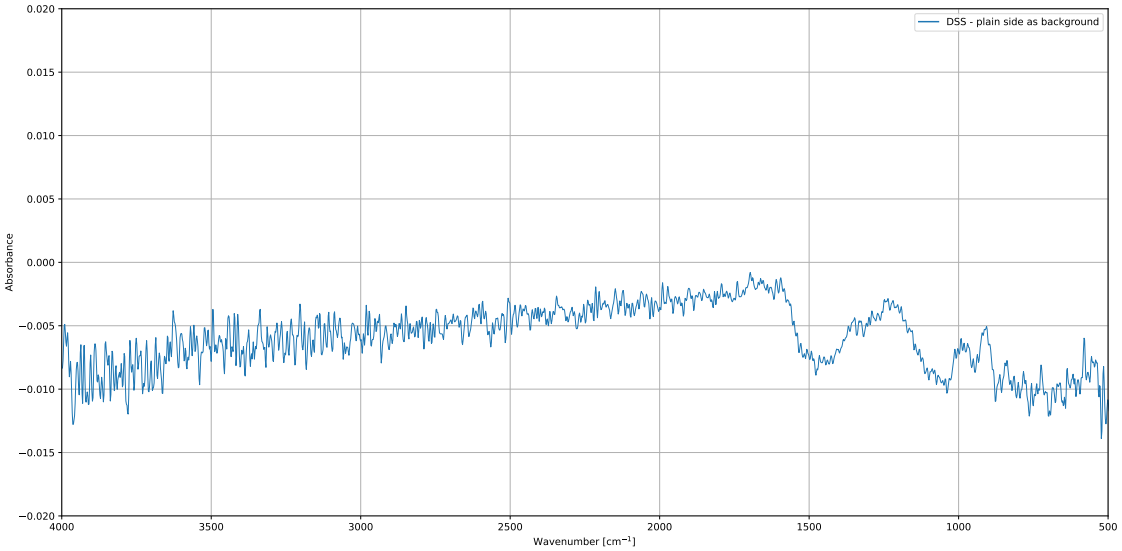


Figure 35: Spectra of the DSS when the plain side of the sample was used as background

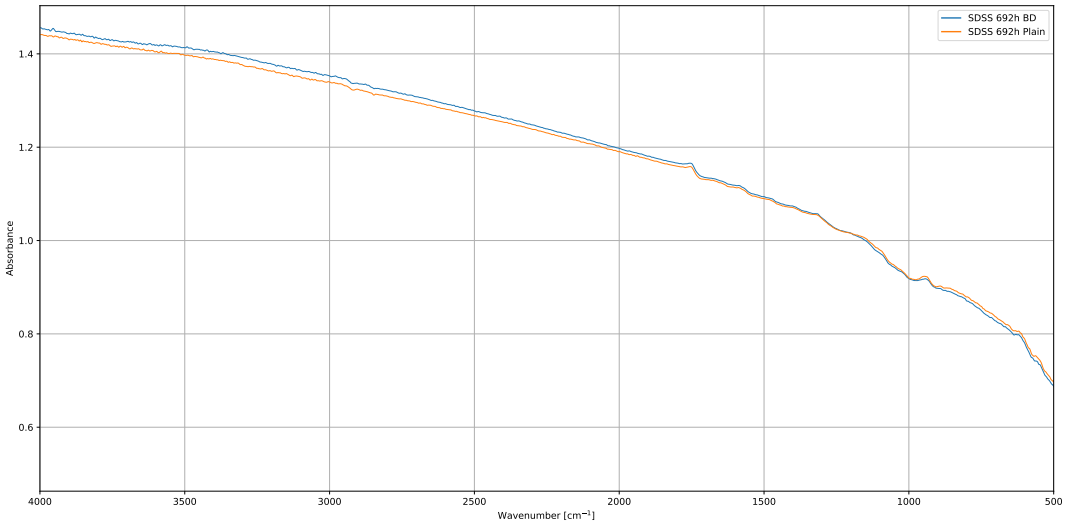


Figure 36: Comparison of the FTIR spectra for the SDSS sample with and without bird droppings that was in the salt spray test for 692h

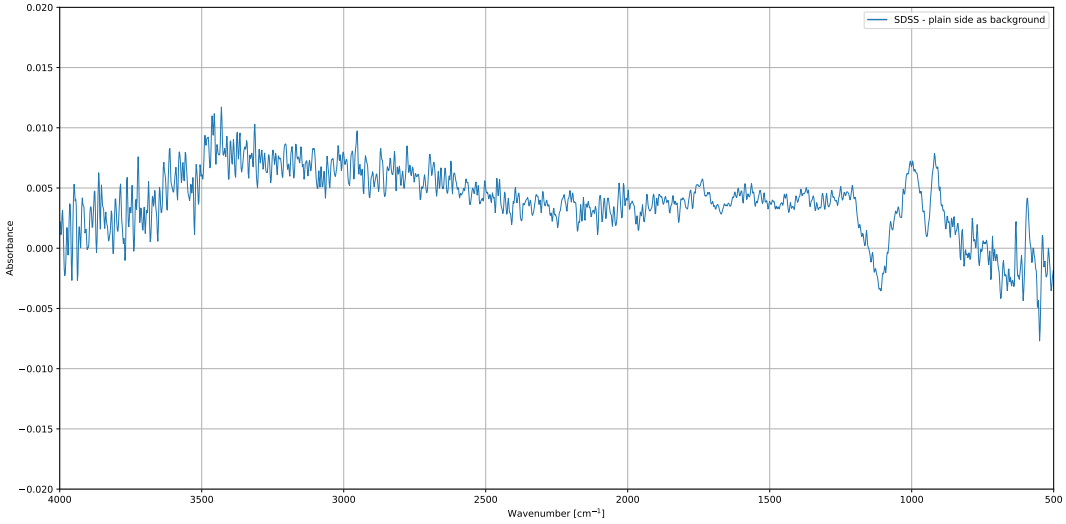


Figure 37: Spectra of the SDSS when the plain side of the sample was used as background

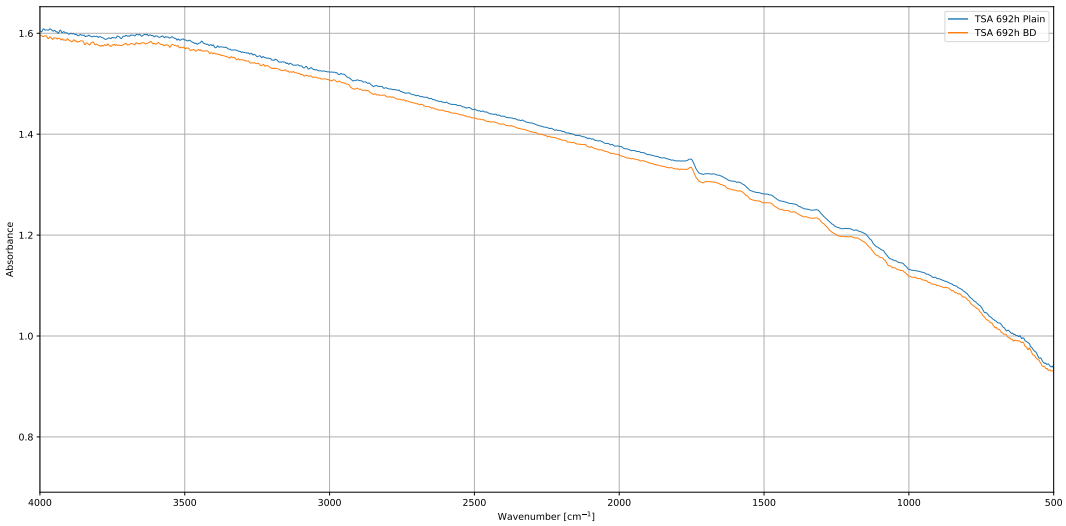


Figure 38: Comparison of the FTIR spectra for the carbon steel with TSA sample, with and without bird droppings, that was in the salt spray test for 692h

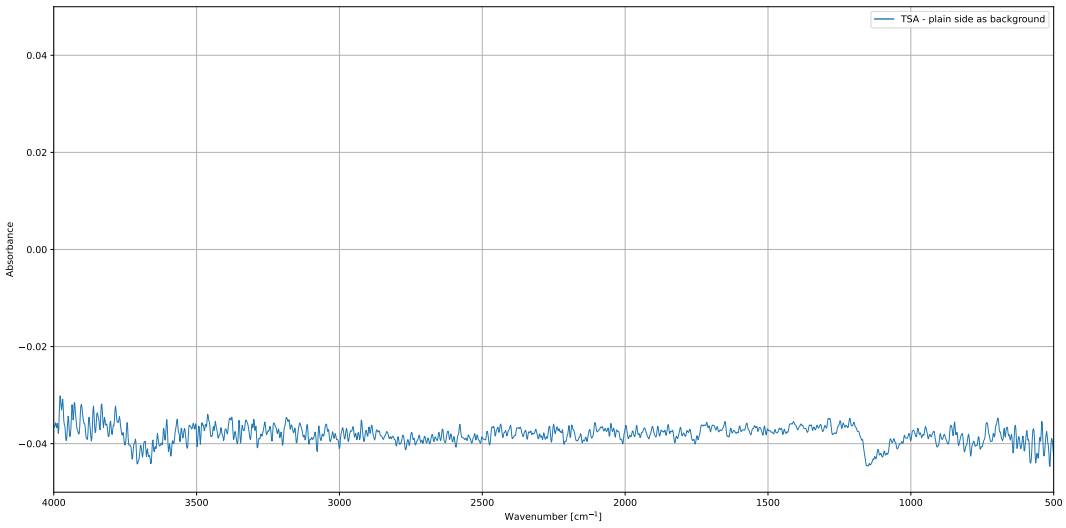


Figure 39: Spectra of the carbon steel with TSA when the plain side of the sample was used as background

## A.2 Spectra from Raman spectroscopy

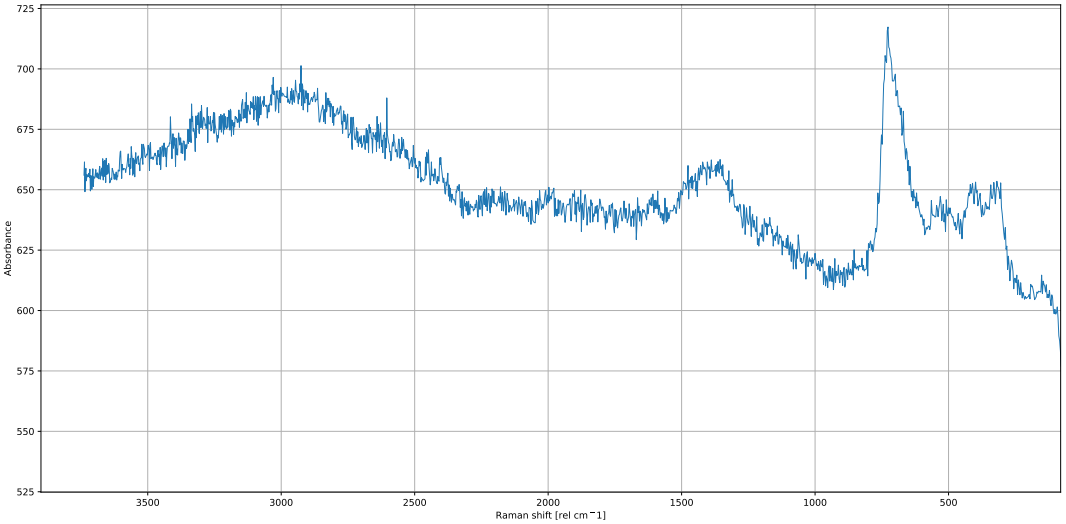


Figure 40: Raman spectra of the bird-dropping side of carbon steel, exposed to the salt-spray chamber for 692h

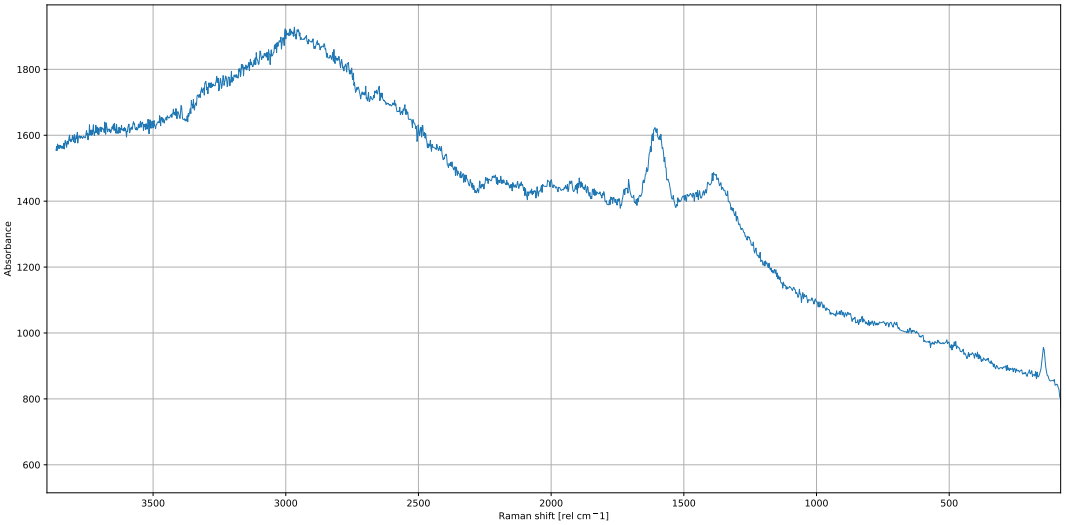


Figure 41: Raman spectra of the plain side of AISI 316, exposed to the salt-spray chamber for 692h

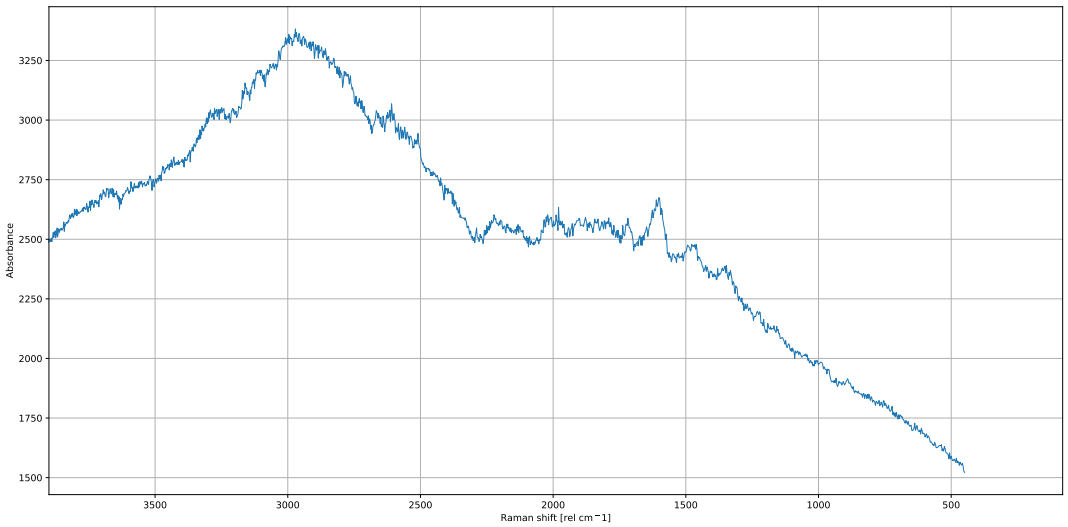


Figure 42: Raman spectra of the bird-dropping side of AISI 316, exposed to the salt-spray chamber for 692h

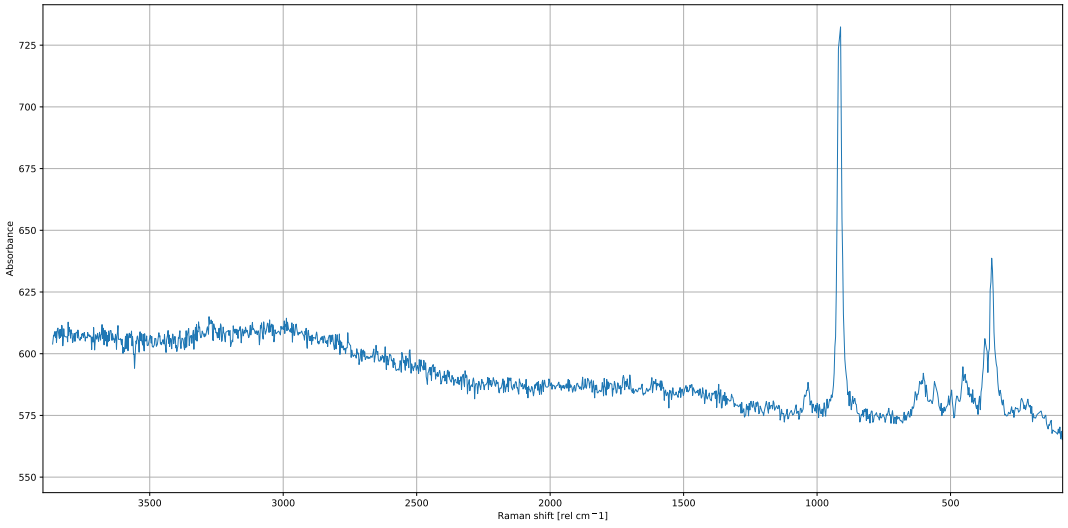


Figure 43: Raman spectra of the plain side of 22% Cr DSS, exposed to the salt-spray chamber for 692h

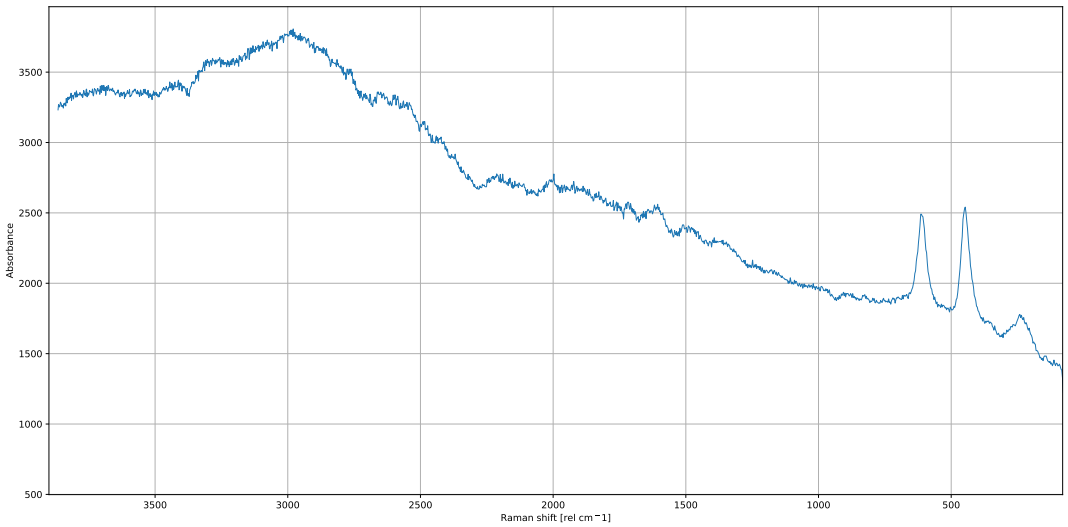


Figure 44: Raman spectra of the bird-dropping side of 22% Cr DSS, exposed to the salt-spray chamber for 692h

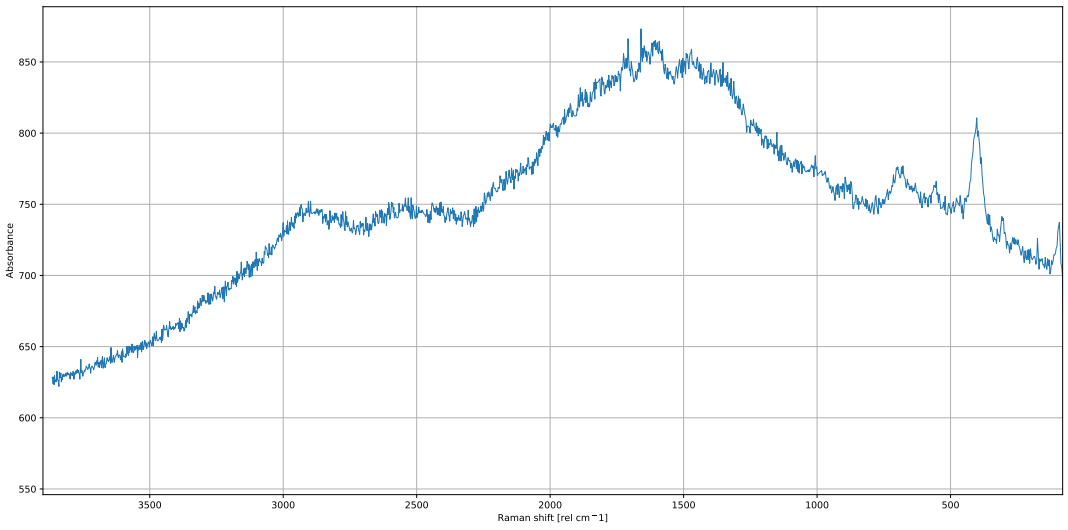


Figure 45: Raman spectra of the plain side of 25% Cr SDSS, exposed to the salt-spray chamber for 692h

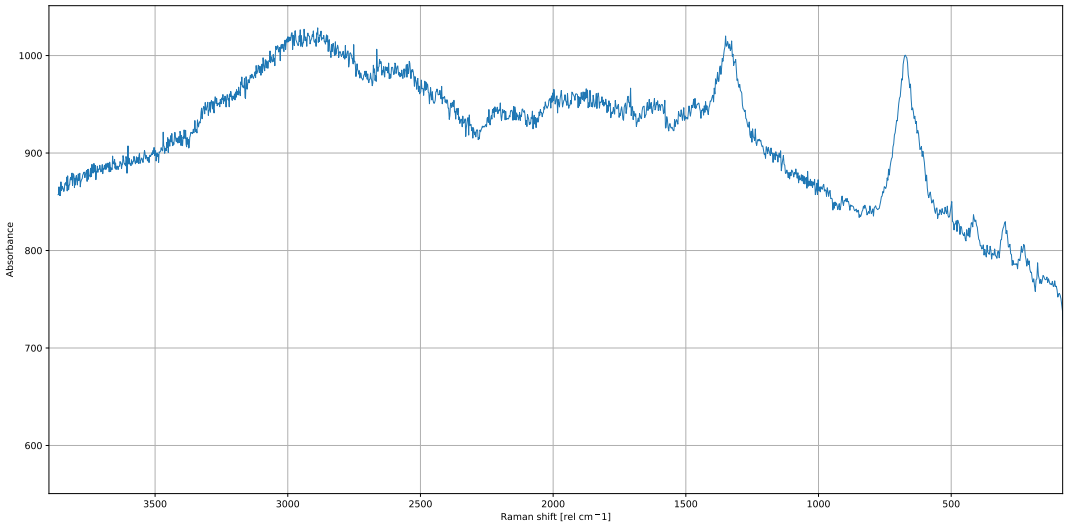


Figure 46: Raman spectra of the bird-dropping side of 25% Cr SDSS, exposed to the salt-spray chamber for 692h

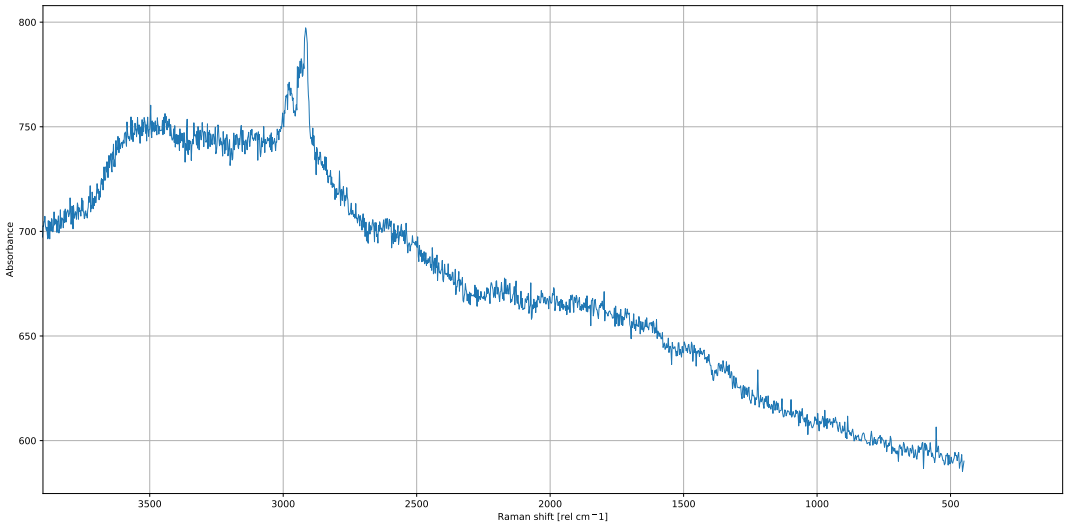


Figure 47: Raman spectra of the plain side of TSA, exposed to the salt-spray chamber for 692h

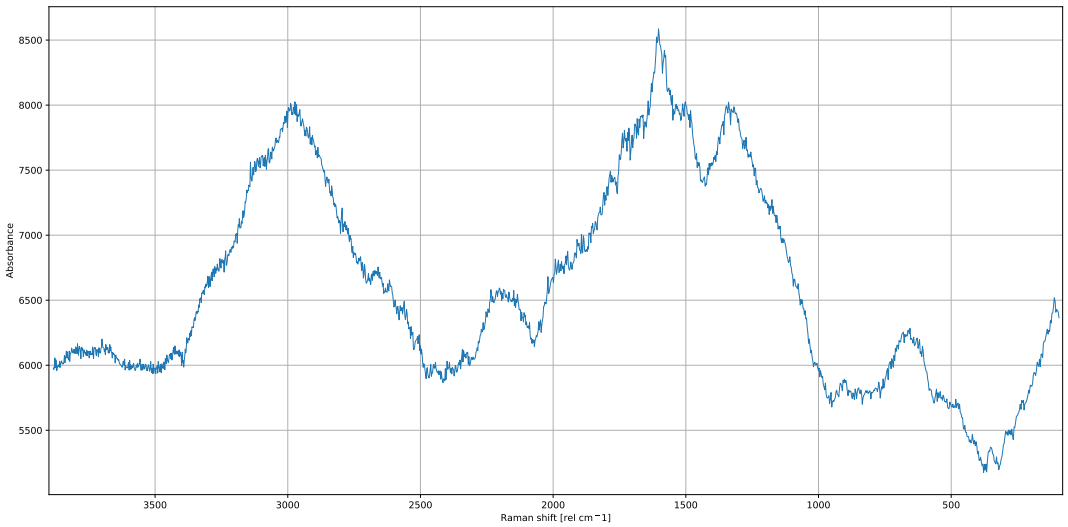


Figure 48: Raman spectra of the bird-dropping side of TSA, exposed to the salt-spray chamber for 692h

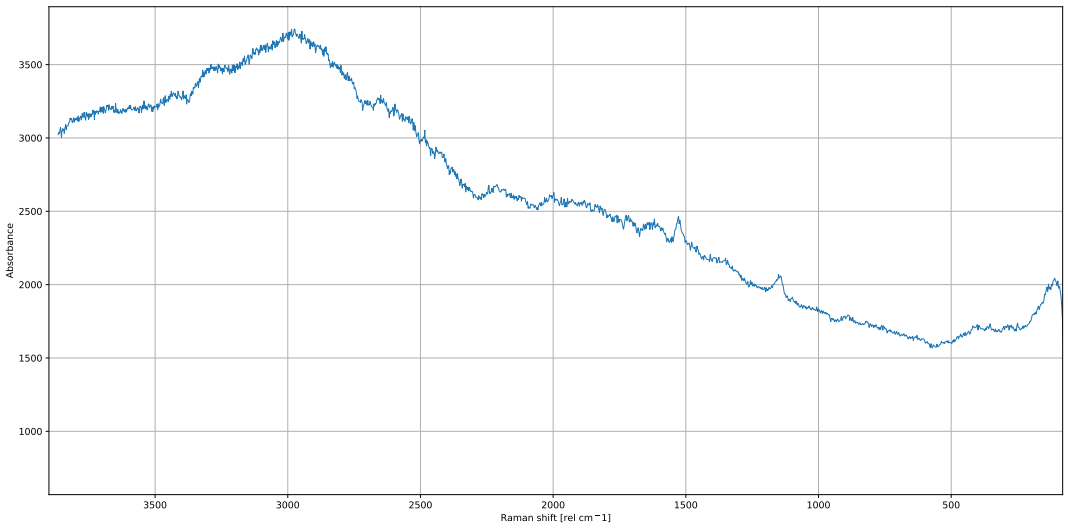


Figure 49: Raman spectra of the plain side of EN AW 6082, exposed to the salt-spray chamber for 692h

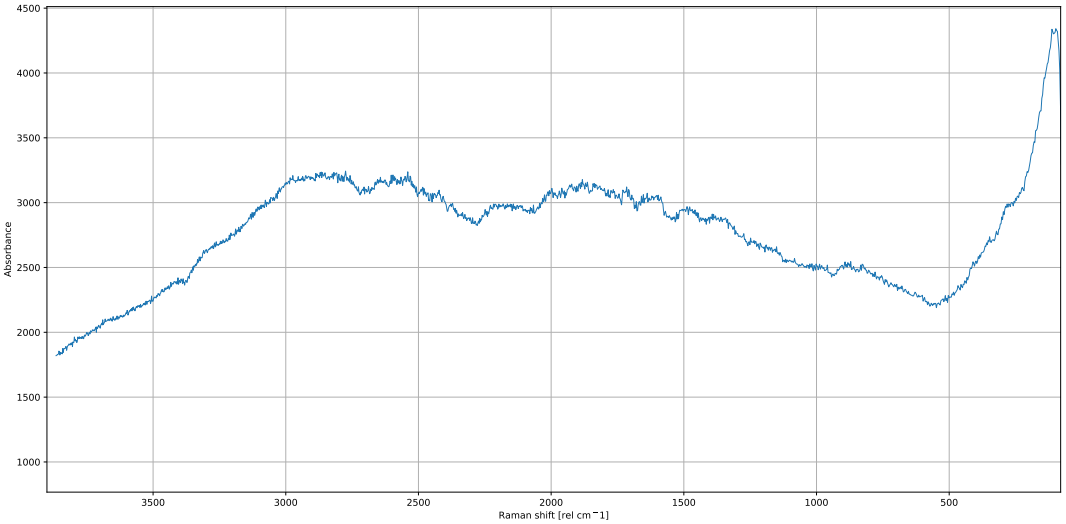


Figure 50: Raman spectra of the bird-dropping side of EN AW 6082, exposed to the salt-spray chamber for 692h

## A.3 Raw data for mass loss

The calculations for the area density listed in Table 7 and Table 8 were done based on this raw data. Table 10 lists raw data *before* removal of the corrosion products, while Table 11 lists raw data *after* corrosion removal.

Table 10: Raw data for the area density given for the mass loss *before* removal of the corrosion products.

| | | Initial conditions | | Without bird droppings | | With bird droppings | |
|---|---|---|---|---|---|---|---|
| Material | Sample | Dimensions [cm] | Mass [g] | Dimensions [cm] | Mass [g] | Dimensions [cm] | Mass [g] |
| Carbon steel | 1 | 4.00×8.00 | 143.20 | 4.00×4.00 | 69.90 | 4.00×4.00 | 71.30 |
| | 2 | 4.00×8.00 | 141.35 | 4.00×4.04 | 71.42 | 4.00×3.96 | 69.88 |
| | 3 | 4.00×8.00 | 140.94 | 4.00×4.08 | 72.39 | 4.00×3.88 | 70.38 |
| AISI 316 | 1 | 4.00×8.00 | 143.11 | 4.00×3.98 | 71.22 | 4.00×3.92 | 69.92 |
| | 2 | 4.00×8.00 | 143.44 | 4.00×4.00 | 70.97 | 4.00×3.94 | 70.36 |
| | 3 | 4.00×8.00 | 143.03 | 4.00×4.00 | 71.38 | 4.00×3.94 | 69.63 |
| 22% Cr DSS | 1 | 4.00×8.00 | 147.39 | 4.00×3.85 | 70.63 | 4.00×4.06 | 74.58 |
| | 2 | 4.00×8.00 | 149.45 | 4.00×3.98 | 74.50 | 4.00×3.94 | 73.11 |
| | 3 | 4.00×8.00 | 147.66 | 4.00×3.93 | 72.38 | 4.00×4.00 | 73.13 |
| 25% Cr SDSS | 1 | 4.00×8.00 | 165.62 | 4.00×3.95 | 81.21 | 4.00×3.98 | 81.85 |
| | 2 | 4.00×8.00 | 167.35 | 4.00×4.01 | 83.19 | 4.00×3.91 | 81.49 |
| | 3 | 4.00×8.00 | 165.67 | 4.00×3.97 | 81.73 | 4.00×3.98 | 81.98 |
| TSA | 1 | 4.00×8.00 | 147.85 | 4.00×3.94 | 72.47 | 4.00×3.99 | 73.01 |
| | 2 | 4.00×8.00 | 148.41 | 4.00×3.97 | 73.55 | 4.00×3.93 | 71.84 |
| | 3 | 4.00×8.00 | 145.52 | 4.00×3.95 | 71.2 | 4.00×4.00 | 71.65 |
| EN AW 6082 | 1 | 4.00×8.00 | 12.68 | 4.00×3.87 | 6.01 | 4.00×4.01 | 6.37 |
| | 2 | 4.00×8.00 | 12.54 | 4.00×3.78 | 6.20 | 4.00×3.99 | 6.72 |
| | 3 | 4.00×8.00 | 12.54 | 4.00×3.98 | 6.51 | 4.00×3.94 | 6.45 |

Table 11: Raw data for the area density given for the mass loss *after* removal of the corrosion products.

| | | Initial conditions | | Without bird droppings | | With bird droppings | |
|---|---|---|---|---|---|---|---|
| Material | Sample | Dimensions [cm] | Mass [g] | Dimensions [cm] | Mass [g] | Dimensions [cm] | Mass [g] |
| Carbon steel | 1 | 4.00×8.00 | 143.20 | 4.00×4.00 | 69.60 | 4.00×4.00 | 70.99 |
| | 2 | 4.00×8.00 | 141.35 | 4.00×4.04 | 67.25 | 4.00×3.96 | 66.54 |
| | 3 | 4.00×8.00 | 140.94 | 4.00×4.08 | 61.09 | 4.00×3.88 | 63.38 |
| AISI 316 | 1 | 4.00×8.00 | 143.11 | 4.00×3.98 | 71.10 | 4.00×3.92 | 69.77 |
| | 2 | 4.00×8.00 | 143.44 | 4.00×4.00 | 70.97 | 4.00×3.94 | 70.26 |
| | 3 | 4.00×8.00 | 143.03 | 4.00×4.00 | 71.30 | 4.00×3.94 | 69.52 |
| 22% Cr DSS | 1 | 4.00×8.00 | 147.39 | 4.00×3.85 | 70.66 | 4.00×4.06 | 74.59 |
| | 2 | 4.00×8.00 | 149.45 | 4.00×3.98 | 74.09 | 4.00×3.94 | 72.72 |
| | 3 | 4.00×8.00 | 147.66 | 4.00×3.93 | 72.33 | 4.00×4.00 | 73.07 |
| 25% Cr SDSS | 1 | 4.00×8.00 | 165.62 | 4.00×3.95 | 81.19 | 4.00×3.98 | 81.86 |
| | 2 | 4.00×8.00 | 167.35 | 4.00×4.01 | 83.11 | 4.00×3.91 | 81.45 |
| | 3 | 4.00×8.00 | 165.67 | 4.00×3.97 | 81.44 | 4.00×3.98 | 81.66 |
| TSA | 1 | 4.00×8.00 | 147.85 | 4.00×3.94 | 72.51 | 4.00×3.99 | 73.00 |
| | 2 | 4.00×8.00 | 148.41 | 4.00×3.97 | 73.32 | 4.00×3.93 | 71.81 |
| | 3 | 4.00×8.00 | 145.52 | 4.00×3.95 | 70.76 | 4.00×4.00 | 71.26 |
| EN AW 6082 | 1 | 4.00×8.00 | 12.68 | 4.00×3.87 | 6.07 | 4.00×4.01 | 6.42 |
| | 2 | 4.00×8.00 | 12.54 | 4.00×3.78 | 5.93 | 4.00×3.99 | 6.43 |
| | 3 | 4.00×8.00 | 12.54 | 4.00×3.98 | 6.22 | 4.00×3.94 | 6.15 |

## A.4 Test certificate EN AW 1050

# GUTMANN ALUMINIUM DRAHT GMBH

*zertifiziert nach / certified to*

*DIN EN ISO 9001 : 2015 / DIN EN ISO 14001 : 2004 + Cor 1 : 2009*
*IATF 16949 : 2016 / DIN EN ISO 22000 : 2005 / DIN EN ISO 50001 : 2011*

we wire the world

## Abnahmeprüfzeugnis 3.1 / Test Certificate 3.1

nach/ based on EN 10204 (DIN 50049)

**WAZ-Nummer / doc.-number: 57657**

**Datum / date:** 31. März 2020

**Kunde / customer:**
Norspray As
Maskinveien 10
4033 Stavanger
Norwegen

**Kundenartikelnummer / customer code:**
1000418

**Spezifikation / specification code:**

**Werkstoff u. Lieferzustand / Quality & condition:**
EN AW 1050//F15/BLANK

**Auftragsnummer / confirmation number:**
818859
**Bestellnummer / order number:**
13284

**Zusammensetzung nach / chemical composition to DIN EN 573-3:2019-10**
Istwert gem. Angabe des Vordrahtlieferanten; Messverfahren gem. DIN EN 1715-1:2008-07
actual value according to rod supplier; measurement according to DIN EN 1715-1:2008-07

| Werte in % values in % | Si | Fe | Cu | Mn | Mg | Cr | Zn | Ga | B | Al | Pb | Ti |
|---|---|---|---|---|---|---|---|---|---|---|---|---|
| Sollwerte target values | max. 0.25 | max. 0.4 | max. 0.05 | max. 0.05 | max. 0.05 | max. - | max. 0.07 | max. - | max. - | max. - | max. - | max. 0.05 |
| Istwert / actual value Charge/batch W60025561 | 0.035 | 0.08 | 0.003 | 0.001 | 0.001 | 0.001 | 0.004 | 0.005 | 0.0010 | 99.88 | 0.0015 | - |

**mechanische Werte / mechanical values**

| | Toleranz/Abmessung tolerance/dimension mm | Zugfestigkeit tensile strength $R_m$ N/mm$^2$ | Dehngrenze yield strength $R_{p\,0,2}$ N/mm$^2$ | Bruchdehnung% elongation% A100MM | Härte hardness HB |
|---|---|---|---|---|---|
| Vorgabewerte target values | 2.40-2.45 | min 140 | - | - | - |
| Istwert / actual value Charge/batch W60025561 | 2.44 | 171 | 156 | 2,0 | - |

**Bemerkungen / notes:** We confirm a delivery according to DIN EN ISO 14919:2015-04

Dieses Dokument wurde elektronisch erstellt und ist auch ohne Unterschrift gültig.
This document was generated electronically and is valid without signature.

**GUTMANN ALUMINIUM DRAHT GMBH**
Am Sand 2
91781 Weißenburg
Germany
Tel. +49 (9141) 9975 - 0
Fax. +49 (9141) 9975 - 222

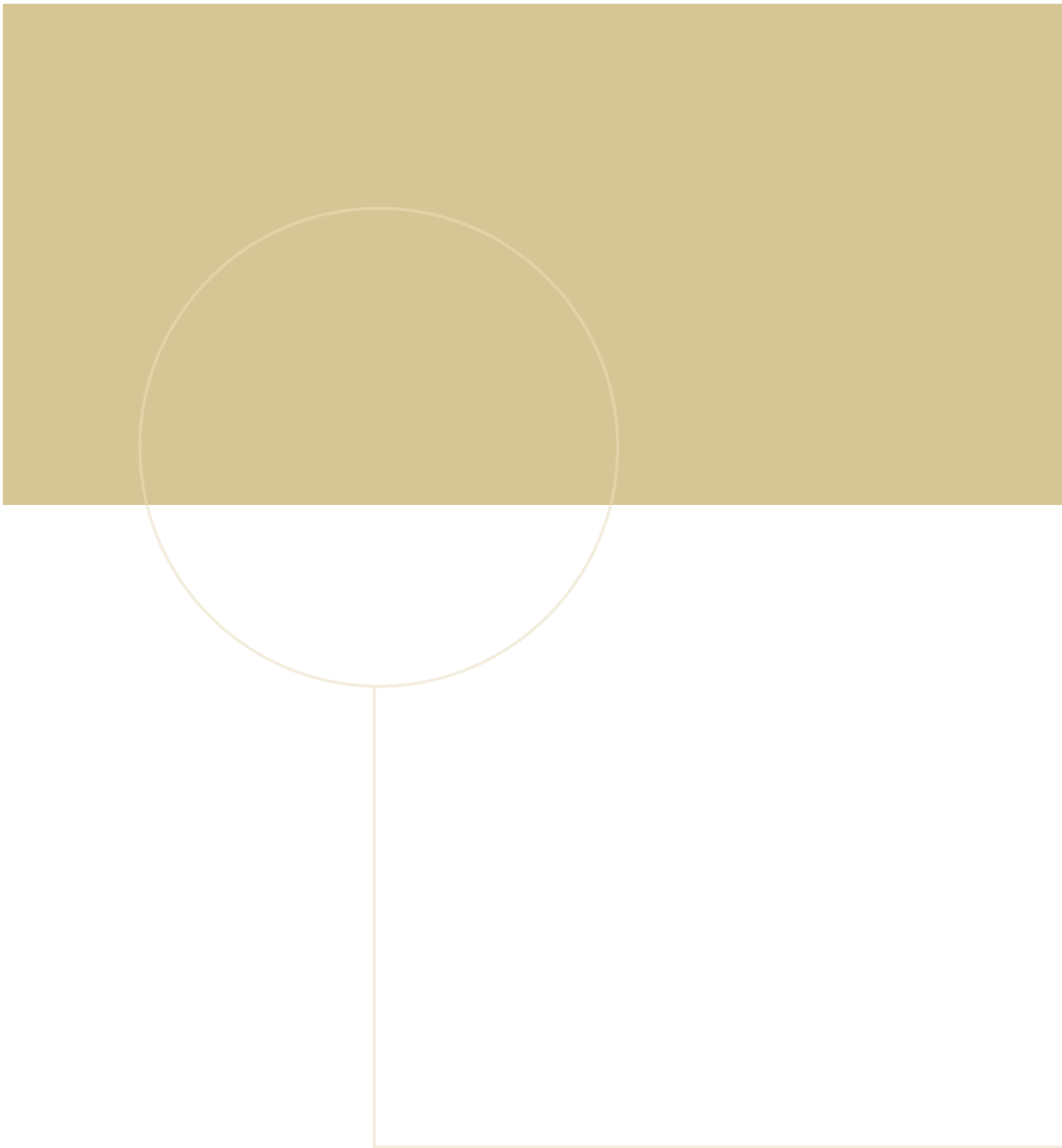

NTNU

Norwegian University of
Science and Technology